ORIENTATION, MICROSTRUCTURE AND PILE-UP EFFECTS

ON NANOINDENTATION MEASUREMENTS OF

FCC AND BCC METALS

Ashish Kumar Srivastava, B.E.

Thesis Prepared for the Degree of

MASTER OF SCIENCE

UNIVERSITY OF NORTH TEXAS

May 2008

APPROVED:

Reza A. Mirshams, Major Advisor
Rajarshi Banerjee, Committee Member
Thomas Scharf, Committee Member
Michael Kaufman, Chair of the Department of
      Materials Science and Engineering
Oscar Garcia, Dean of the College of
      Engineering
Sandra L. Terrell, Dean of the Robert B.
      Toulouse School of Graduate Studies

Srivastava, Ashish Kumar. <u>Orientation, Microstructure and Pile-Up Effects on Nanoindentation Measurements of FCC and BCC Metals</u>. Master of Science (Material Science and Engineering), May 2008, 113 pp., 16 tables, 83 illustrations, references, 28 titles.

This study deals with crystal orientation effect along with the effects of microstructure on the pile-ups which affect the nanoindentation measurements. Two metal classes, face centered cubic (FCC) and body centered cubic (BCC, are dealt with in the present study. The objective of this study was to find out the degree of inaccuracy induced in nanoindentation measurements by the inherent pile-ups and sink-ins. Also, it was the intention to find out how the formation of pile-ups is dependant upon the crystal structure and orientation of the plane of indentation.

Nanoindentation, Nanovision, scanning electron microscopy, electron dispersive spectroscopy and electron backscattered diffraction techniques were used to determine the sample composition and crystal orientation. Surface topographical features like indentation pile-ups and sink-ins were measured and the effect of crystal orientation on them was studied. The results show that pile-up formation is not a random phenomenon, but is quite characteristic of the material. It depends on the type of stress imposed by a specific indenter, the depth of penetration, the microstructure and orientation of the plane of indentation. Pile-ups are formed along specific directions on a plane and this formation as well as the pile-up height and the contact radii with the indenter is dependant on the aforesaid parameters. These pile-ups affect the mechanical properties like elastic modulus and hardness measurements which are pivotal variables for specific applications in micro and nano scale devices.

ACKNOWLEDGEMENTS

Finally, I thank the almighty for steering me through everything in life. He has been with me always and it is His blessings that have made this work possible.

TABLE OF CONTENTS

LIST OF TABLES

LIST OF ILLUSTRATIONS

Page

CHAPTER 1

INTRODUCTION

Indentation testing is a simple method that consists essentially of touching the material of interest whose mechanical properties such as elastic modulus and hardness which are unknown, with another material whose properties are known [1]. As the devices continue to shrink in size, there is an urgency to probe more for their properties at micro and nano levels. This need has fueled the reduction of scale of study, from meters to microns and nanometers. Nanoindentation is simply an indentation test where the scale is in nanometers instead of microns or millimeters.

Nanoindentation tests are now commonly used for the study of Mechanical properties of materials at a nano level. The nanoindentation tests derive their support from various disciplines because of the fact that they are enormously flexible and could be used to measure a majority of mechanical properties. Coupled with development in electronic instrumentation and advanced video techniques, nanoindentation is now the universal tool for mechanical property characterization. It is no longer necessary to image the indent as was the practice for determination of the indent size. Indenters have specific geometries and together with the known depth of indentation, a relation between the area of contact and the depth of indentation can be devised. It is for this reason, nanoindentation testing can be considered to be a sub section of the larger group of depth sensing indentation (DSI) or instrumented indentation testing (IIT). The load displacement curves generated from the indentation testing are a huge source of information. These can be used to determine the mechanical properties of small volumes of material at large.
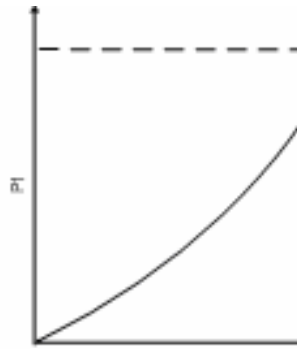
Figure 1: Typical load displacement curves for different types of material behavior in indentation [1].

The polycrystalline material is often used is based on the bulk properties of the material and those are used as a design parameter even to this date. Research, however, has shown that the properties vary significantly as the scale of study changes. As the scale decreases, the hardness and elastic modulus values of the material increase. This effect has been rationalized as the indentation size effect (ISE). With the continued usage and constant need for improvement in material properties, it is now necessary to know the properties of material at an atomic level. The wafers in the semiconductor industry use specific orientations depending on their usage.

Polycrystalline material differs from the single crystal material in many ways. However, it is possible to study single crystal orientation effects on the material properties by nanoindentation on polycrystalline materials with reasonable grain size. This is possible because the indent size is too small compared to the grain and for a particular indent sitting in middle of a grain, it can be assumed that the behavior of the material for that particular indent is not influenced by the adjoining grains. It is possible to get an array of mechanical properties by indenting across a wide range of crystal orientations, which is a simple way to forecast or study trends in mechanical properties.

If all the parameters are the same, the behavior seen is representative of the orientation effects of the material on the mechanical properties obtained by nanoindentation . This facilitates the correlation of mechanical properties of material with the more fundamental aspects like the crystal structure and orientation. With this information at hand, it can be further extrapolated to predict or estimate material properties at the nano level at large.

Studies have been done on conical indentations as the conical indenters have minimum variation of the applied stress, while the material is being indented [2]. The stress variations in real life indentations are quite complex. Although, the conical indentations give a basic idea of the crystal orientation on mechanical properties [2], the area of real indenters, which are being used for characterization, the pyramidal indenters is still unexplored. The chief tool of mechanical surface characterization through nanoindentation is the Berkovich indenter. The Berkovich indenter is the principal representative of the family of pyramidal indenters and is widely used for determination of mechanical properties at a nano level. In this study, we have used the Berkovich indenter to observe the orientation effect on the material properties and have tried to correlate it with the theories on elasticity derived from Hooke's three dimensional elasticity laws. The observations here were used for further determination of other mechanical properties and their integration with the basic crystal structure and orientation of the material. Comparisons have been made with all three indenters and their effects on a wide variety of materials, spanning three metals in two classes, the face centered cubic (FCC) and the body centered cubic (BCC). This study as a whole, is

an investigation of mechanical properties at a nano level and its integration with the

most fundamental arrangement of atoms in the three dimensional crystal space.

CHAPTER 2

LITERATURE REVIEW

2.1   Oliver-Pharr Method

Young's modulus can be obtained from the elastic displacement data obtained during unloading of the indentation [3]. Since hardness is representative of the plastic deformation potential of the material, elastic contributions of the nanoindentation test should be removed from total displacement in order to calculate hardness.

Depth sensing indentations were introduced to avoid errors due to direct imaging of indents in micro hardness tests and also to study mechanical properties in very small volumes of material. They also provide information about the elastic and time dependant properties of the material.   Nanoindenter was first introduced, in order to fulfill this need. Although, first used as a lab specific instrument, the nanoindenter gradually evolved as standard equipment used to commonly characterize the mechanical properties in small volumes of materials. The position of the indenter is determined by a capacitance displacement gauge. A coil and magnet assembly located at the top of the loading column is used to drive the indenter towards the sample. The force on the indenter is controlled by varying the current in the coil. The loading column is suspended by flexible springs and the motion is damped by air flow around the center plate of the capacitor, which is attached to the loading column.

Hardness is the equivalent of average pressure under the indenter, calculated as the applied load divided by the projected area of contact between the indenter and the sample. However, since the depth measured is a combination of both elastic and plastic displacements, the elastic contribution should be removed from the total to

calculate hardness of the sample. This is done by using the plastic depth in

calculations. Plastic depth is found by drawing a tangent at the initial unloading curve of

the load displacement graph. This tangent when extrapolated to zero load at the

displacement axis, gives the plastic depth. This method assumes that during initial

unloading the area in contact with the indenter remains constant. Constant contact area

is obtained for metals for most of their unloading range. However, for materials with

higher ratios of hardness to elastic modulus, more curvature is obtained in the

unloading curve. The loss of contact with the indenter is a result of the change in shape

of the indentation due to elastic recovery.

The slope of the unloading curve can be used to measure the elastic property.

This initial unloading slope is known as the stiffness. Its reciprocal is defined as the

compliance of the system. If the area of contact is constant during initial unloading, the

elastic behavior can be modeled as a blunt punch indenting an elastic solid. By equating

the projected area of the indenter to the area of the punch, stiffness is given as,

$$\frac{dP}{dh} = \left(\frac{2}{\pi}\right)^{1/2} DE_r$$

and

$$\frac{1}{E_r} = \frac{1-v^2}{E} + \frac{1-v_0^2}{E_0}$$

where D is the Vickers diagonal length, E_r, E, E_0 and v, v_0 are the reduced elastic

modulus of the system, indenter and sample respectively.

Now if the indenter is assumed to have a pyramidal geometry and plastic depth is

used instead of diagonal length we get,

6

$$\frac{dh}{dp} = \frac{1}{2h_p} \left(\frac{\pi}{24.5}\right)^{1/2} \frac{1}{E_r}$$

In addition, the y intercept of the compliance vs the reciprocal of the plastic depth should give any additional compliance which is independent of the contact area. This includes the compliance which is independent of the contact area and also includes the compliance of the loading column along with any additional compliance associated with mounting of the sample.

Indenter shape calibration is very important. Corrected hardness values show that the values are independent of depth of indentation. Effective depth is defined as the depth needed for a pyramid of ideal geometry to obtain a projected contact area equivalent to that of the real pyramid.

Mathematically, it is given as,

$$h_{eff} = \left(\frac{Area}{24.5}\right)^{1/2}$$

where area is obtained from shape calibration and true plastic depth of the indentation.

2.2   Indentation Size Effect (ISE)

The indentation size effect (ISE) plays an important role and is seen in all the curves which portray the mechanical behavior with respect to the displacement into the surface. Indentation size effect is the phenomenon of increasing hardness with the depth of penetration. This effect is rationalized by the concept of geometrically necessary dislocations and work hardening. The behavior varies for the pyramidal, conical and spherical indenters. Initially proposed for conical indenters [4] the result is extended for spherical and pyramidal indenters. For pyramidal indenters, the hardness

measured in crystalline materials increases with decreasing depth of indentation. For spherical indenters, however, this increase in hardness is related to decreasing sphere radius. [4] This effect becomes quite prominent in cases of analysis of thin films and studies where small volumes of materials are to be characterized. This effect generally approaches a constant value as this depth of penetration is increased. The visualization of this formation of geometrically necessary dislocations can be further aided by the following figure.
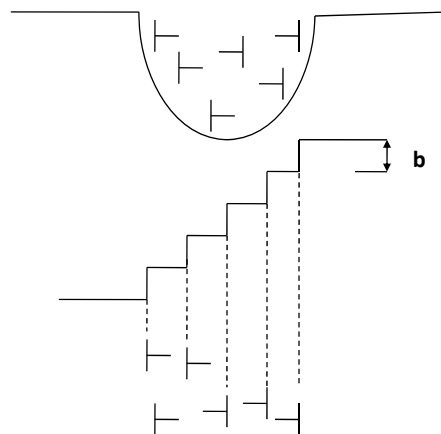
Figure 2: Schematic showing the formation of dislocations beneath indenter tips [3].

2.3   Crystal Orientation Effects

Berkovich indenter is commonly used for the investigation of mechanical behavior of materials. Most of these investigations in past were based on the premise assuming the tip to be spherical. However, the actual tip geometries are much more complex. Efforts in past have been made to quantify this behavior and relate the mechanical properties with orientation [2]. The work which has been done is mostly on conical indenter. This is due to the fact that the conical indenter has a symmetrical

stress distribution and hence the anisotropy due to the structure is revealed while assuming uniform stress distribution in the material.

2.4   Pile-Up Behavior

The pile-up behavior is given due attention in the literature and it was pointed out earlier on that the mechanical properties measured by the Oliver and Pharr approach lead to inaccurate values for elastic modulus and hardness [5]. It has been pointed out that the pile-up behavior and sink-in behavior is dependant on other mechanical properties of the material as well as its processing history. The major factors affecting the pile-up and/or sink-in are the work hardening rate, the ratio of the elastic modulus to the yield strength (E/σ_y) and the ratio of contact depth to the maximum depth of indentation (h_c/h_{max}). It has been pointed out that the critical h_c/h_{max} ratio or strain hardening exponent for no piling up or sink-in is a function of E/σ_y. Finite element simulation has been carried to authenticate this claim and it is sometimes possible to predict a pile-up vs a sink-in observation if the parameters are known[6].

2.4.1 Pile-Up Effects

The criticality of pile-ups and sink-ins in measurement of elastic modulus and hardness is pointed out in previous works [5,7-8]. It has been said that the pile-ups occur in materials with large Eeff/Y ratio. The occurrence of pile-ups and or sink-ins is also interpreted in terms of the strain or work hardening of the material under consideration. Pile-ups are formed when the indented surface is heavily pre-strained.

The localized plastic deformation forces the material upwards thus forms pile-ups. On the other hand, when the sample is not work hardened or pre-strained, the localized plastic zone tends to shift away resulting in a sink-in pattern [9-12]. Orientation effect has been studied for the case of conical indentations with respect to single crystals. It has been pointed out that the pile-up formation is along specific directions around the indent depending on the crystallographic orientation of the crystal [13-18]. However, studies on indenters other than spherical and conical are still rare and the present study is an effort to reduce that gap.

2.4.2   The Mechanics of Pile-Up Formation

The pile-up behavior is typified by the kinematics and dynamics of the process [2]. Kinematics of the indentation process dictates the dominance of primary slip in the local deformation around the indent to such an extent that the intersection of primary slip direction and the indented surface gives rise to characteristic pile-up for a specific crystallographic orientation of the crystal. Dynamics of the process dictates the activation of small set of slip systems around the indentation which carries most of the material without seeing much interaction with secondary slip systems, which results in rather little strain hardening of the system. Formation of two, three and four fold symmetry has been observed for cases of conical indenters and   has been rationalized on the concept discussed above [2].

2.5   Energy Methods

As the indentation progresses, the initial elastic response of the material

gradually changes to plastic deformation when the applied stress exceeds the theoretical shear stress of the material. There is a formation of a plastic zone beneath the indenter tip, which is directly related to the depth of indentation. This relation has been devised by energy methods in literature [19]. For our purposes, we like to avoid the plastic zone interference of two successive indents as that might affect their pile-up behavior, which is the prime area of interest of this study. In this context, we have kept a distance of 50 microns between every two consecutive indents for both the X and Y axis respectively.

2.6   Pile-Up Measurement Methods

Pile-up formation is an important physical phenomenon. Ignorance of pile-ups lead to underestimation and/or overestimation of the contact area of the indenter with the material which leads to inaccuracies in the calculated elastic modulus and hardness, which render the data unusable for practical purposes. There are various methods to estimate the pile-up area which are devised over the years. The holy grail in this section of analysis is to obviate the imaging of the indent and hence to reduce the factor of human error. However, till date, we still rely on some form of imaging or the other viz. atomic force microscopy, scanning electron microscopy. In the present study, we have used the Nanovision™ method which works akin to the atomic force microscope, the only difference being in the fact that it has a very low compliance of the shaft profiling the topography, as the indenter shaft itself is used to create three dimensional profile of the indents. Discussed below are some methods used to estimate the pile-up or sink-in area in literature.

2.6.1 The Work of Indentation Method

This method is less sensitive to the effects of pile-ups. Elastic modulus and hardness values can be estimated through the load-unload curves and hence the contact area overestimation can be found out. This method essentially utilizes the information on the energy dissipated during the indentation.
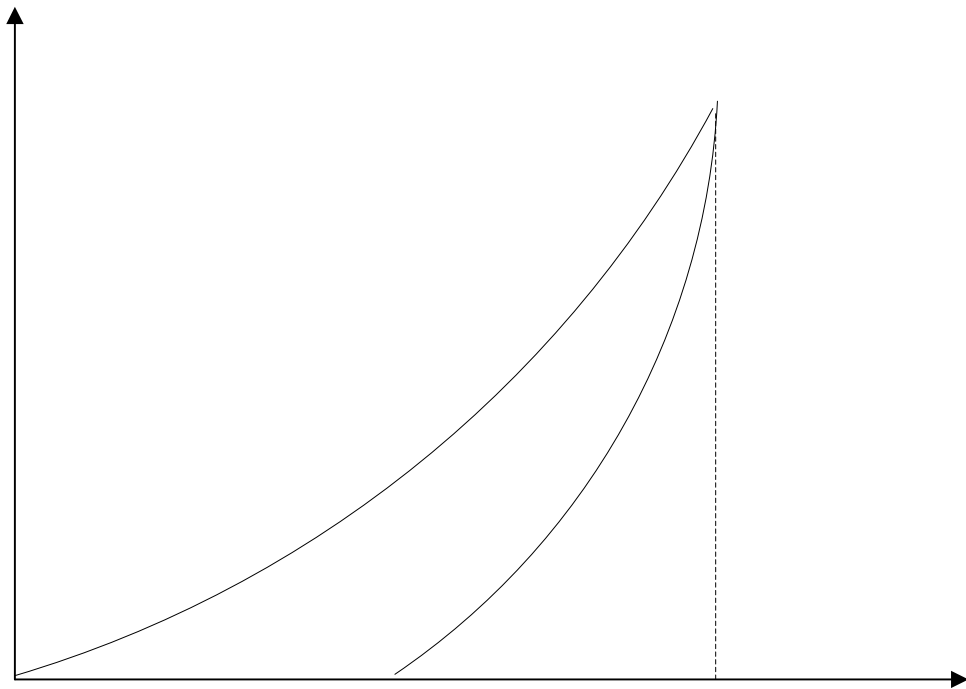
Figure 3: Load displace curve outlining the plastic and elastic works of indentation [20].

Total work (W_t) is given by the area of curve under loading while elastic work (W_e) is given by the area of curve under unload. Plastic work is then defined as (W_p) = Wt - W_e

Conventional hardness is now equated to plastic work divided by the volume of indent which could be found by software help, but then again requires imaging of the indent.

The hardness is now defined as

Ω

$$\frac{P}{A_p} = \frac{W_p}{V_p}$$

$$H = \frac{W_p}{V_p}$$

Once hardness is known, elastic modulus can be estimated. Since total energy dissipated is concerned, we come up with hardness and elastic modulus numbers which are quite accurate [20].

2.6.2 Hertzian Loading Analysis Method

This method is used to calculate the corrected hardness and elastic modulus values [21]. This approach explains indentation as a contact between a sphere and a flat surface. It derives it validity because most of the indenters have a tip rounding effect as perfect point apexes are a physical impossibility. Another factor that induces tip rounding is the excessive wear of the tip over the period of its usage. The elastic contact assumption leads to the determination of elastic modulus, which by the virtue of assumption, includes the pile-up contribution to the indent. By routing it backwards, we can find out the contact area over/under estimation. The pile-up corrected area can be calculated through the reduced modulus formulation experimentally with the help of the relation below.

$$A_c = \frac{\pi S^2}{4E_r^2}$$

The reduced modulus in the above expression is found by the Hertzian loading equation as follows,

Difference in area is thus given by A_c-A_c^{O-P}, where the Oliver Pharr area can be found out from the typical unloading curves of the indentation.

$$P = \frac{4}{3} E_r \sqrt{R_{eq} h^3}$$

These methods being discussed, however are still not effective as there is the underlying assumption of elastic contact for the Hertzian loading case while there is a necessity for imaging for the work of indentation approach.

2.6.3   Semi Ellipse Method

Imaging is also required for the semi-ellipse approximation used extensively in literature. However, when surface topography is plotted against well defined experimental parameters, the inaccuracies are minimized. Work has been done to devise the semi-ellipse approximation for the pile-up projected area [22]. This method images the pile-up contact area by relating it to the contact depth of the indentation and the contact radii. While the contact depth is an experimentally determinable quantity, the determination of contact radii for indentations requires imaging. Once this empirical relation using above mentioned two parameters is established between the contact area, the contact depth and the contact radii respectively, the excess contact area can be found out from the measurable parameters by simple calculations. In this study, I extrapolated this relation for cube corner indentations, which is again a pyramidal indenter and the basics that are

used for the Berkovich indentations could be easily used here too. However, I used a typical traceline method in Nanovision™ which gives more accurate values because of the inherent low compliance of the system. I went a step further for conical indentations and proposed not a semi ellipse area, but an elliptical contact, as the pile-ups formed in this case have a different geometry than the ones which are formed while doing pyramidal indentations. I arrived at an empirical relation for this case using the same fundamental characteristics of an indentation, namely the contact radii and the contact depth respectively. This method along with the extrapolation and the proposition for conical indenter is discussed in much more detail in chapters 4 and 5.

CHAPTER 3

EXPERIMENTAL METHODS AND MATERIALS

3.1   Materials

The materials used in the study were chosen in such a way to cover a fundamental study of a majority of metals and thus indicate a general trend. Two types of face centered cubic (FCC) metals, nickel and copper, were chosen because copper has a lower elastic modulus, stacking fault energy, work hardening index and it is expected to see better pile-ups compared in case of copper [2]. Also, both these would indicate the effect of other parameters as the stacking fault energy on other mechanical properties as hardness and elastic modulus. The results can thus be extrapolated to predict behavior in other FCC metals. Well defined slip systems in FCC metals also give us a better insight in the deformation mechanisms involved while indentation. Iron is the most widely used body centered cubic (BCC) metal and was chosen as a representative for their behavior.

The material used for calibration of the tips was fused silica which was chosen because of its isotropic properties and amorphous structure. The negligible time dependence on plastic properties of this material makes it ideal to be used as the standard calibration material. It also shows no oxidation and has a smooth surface. The elastic modulus of fused silica is 72 GPa and the calibration of three different tips was based on the premise that this should not change with changing tips as the structure is amorphous. A material property table is shown below.

Table 1: Material Bulk Mechanical Properties [29]

Material	Elastic Mod.	Hardness	Poisson's Ratio	Strain Hardening Coeff
Nickel	200 GPa	700 MPa(Brinell) 638 MPa(Vickers)	0.31	Not Available
Iron	211 GPa	490 MPa(Brinell) 608 MPa(Vickers)	0.29	0.3
Copper	130 GPa	874 MPa(Brinell) 369 MPa(Vickers)	0.34	0.54

3.2   Sample Preparation and Purity

Fused silica used for calibration was provided by the manufacturer and is intended for calibration purposes only. It was used as standard always.

All three materials used in the study namely, copper, microcrystalline nickel and iron were 99.5% pure. Purity of copper was verified using EDX, while iron and nickel purity certificates were provided by the vendors and those have been reported [7,13]. All three metals were mechanically polished through SiC disc on grit size starting from 120, 240, 320, 400, 600, 800 and 1200 respectively. They were finally polished on velvet cloth through 1, 0.5, 0.03 micron colloidal silica suspension solutions respectively.

The specimen thus prepared has a mirror finish and can be used for indentation as well as examination using scanning electron microscopy (SEM) and electron backscattered diffraction technique (EBSD).

3.3   Nanoindenter XP

All experiments were done using the Nano XP system (MTS Systems

Corporation, USA) at the nanoindentation laboratory at University of North Texas. It has

a force and load resolution of 50 nN and 0.1 nm respectively

Figure 4a: Nano XP system (Nanoindenter™ manual, MTS Corporation [24]).

Figure 4b: The CSM control unit for the Nanoindenter™ [24].

The major component of the Nano XP system is the indenter load column, two

types of sample try, one for nanoindentation and other one for Nanovision™

experiments, 10X and 40X microscope and the continuous stiffness measurement (CSM) unit.

Care should be taken while changing the indenter tips and locking pins should be placed on the indenter head while the transition is in process. Sample tray holds the samples and these should be mounted only on the perfectly horizontal slab provided by the manufacturer. The samples should be correctly mounted at proper height for the indentation data to be authentic and reproducible. The video system links the microscope which is next to the indenter head to the computer screen, from which the sample surface could be seen and a specific location for the indent can be decided by manipulation of the mouse as it is linked to the movement of the microscope relative to the mounting stage. I used the 40X microscope for this study. The maximum load that can be applied through the indenter shaft is 650 mN.

The Nano XP system works through the depth sensing mechanism. The indenter shaft is attached to the capacitance gauge as well as the coil magnet assembly. When it goes inside the surface by changing the current in the coil, the relative displacement or change in vertical displacement is recorded in terms of volts as the distance between the capacitance plate's changes.

3.4   Continuous Stiffness Measurement (CSM)

Continuous stiffness measurement (CSM) has evolved and has proved to be the essential part of the nanoindentation measurements. CSM measures the stiffness of the sample continuously during the indentation and the mechanical properties are being measured throughout the indentation.
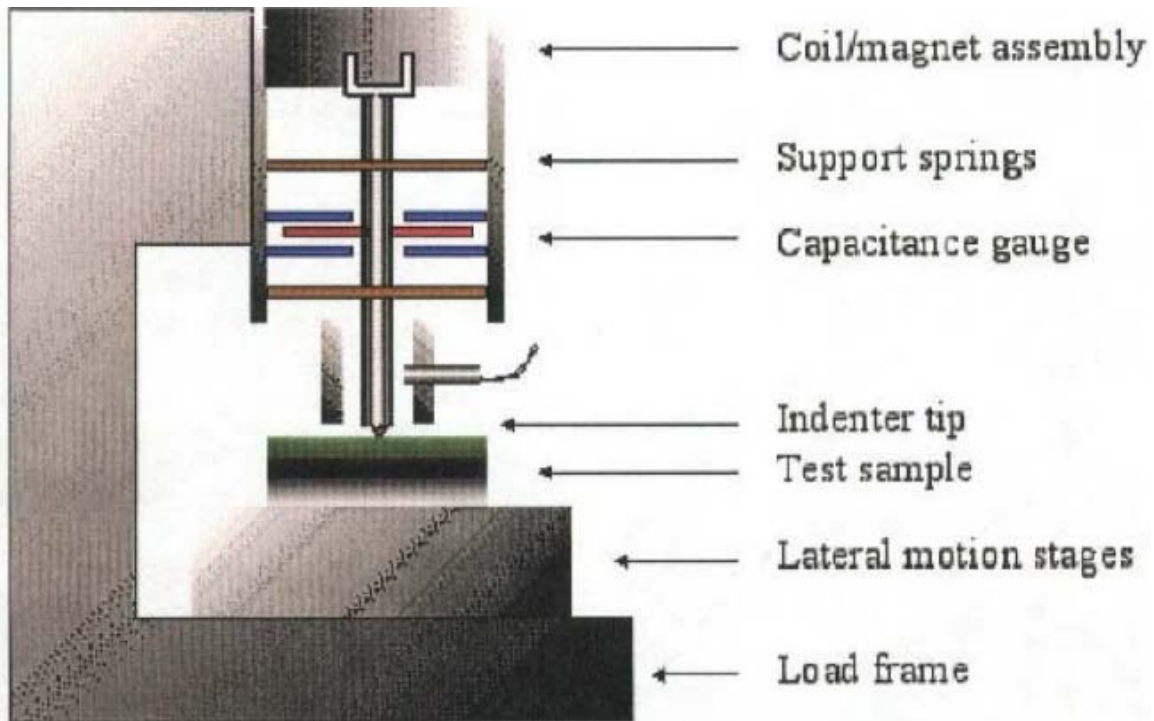
Figure 5: A schematic of the Nanoindenter (Nanoindenter™manual, MTS Corporation [24]).
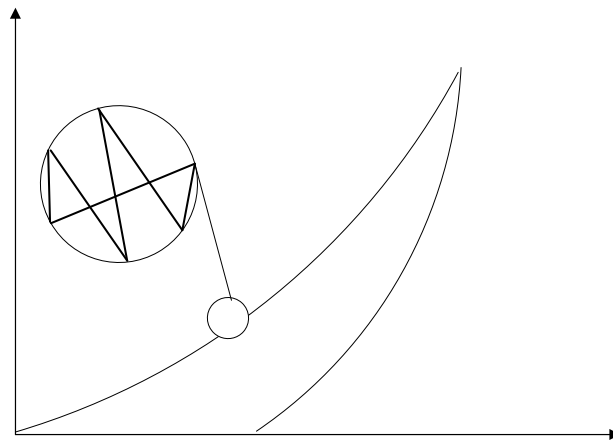
Figure 6: A schematic of CSM on the load displacement curve on a typical nanoindentation curve [9].

At every point, a load displacement data point is taken and stiffness calculated.

This is done by imposing a sinusoidal pulse on the load signal. While unload of this,

data point is taken for calculation of stiffness. This facilitates a much better and reliable averaged value for stiffness which is then used for calculation of elastic modulus with the help of Oliver-Pharr area. This data is further used to calculate the hardness of the system. CSM method has an additional benefit of being especially useful for visco-elastic systems where the phase difference between the force and displacement signals can be used for estimation of storage and loss moduli of the specimen. In the Nano XP system, this CSM unit is an additional box which works on a closed loop feedback thus minimizing any kind of errors.

3.5   Nanoindentation Method

Indentation was done at room temperature. These experiments are sensitive to vibrations; therefore tests were generally done during the night. Because the purpose in this study was to find out the effect of various extrinsically imposed stresses on different crystal orientations in a polycrystalline material, I used three different tips, namely Berkovich, cube corner and conical [Appendix A]. The first two are pyramidal in geometry and give us a very neat idea of pile-up variation with changing angles of various planes in the pyramid and crystal orientation. The third has a perfectly symmetric stress distribution and can be used to see the effect on pile-up by crystal orientations alone. The indents were scanned by the indenter tip using a nominal load utilizing a unique feature in Nanoindenter XP called Nanovision. It utilizes a special stage operated by piezoelectric and can be used to measure surface topography with nanometer precision because of

low compliance of the system. The pile-up height measured in this way was used for further analysis in the study.

All the tests were done in the continuous stiffness measurement (CSM) mode on Nanovision stage. Most indentations were performed using indent load and scan method; peak load was fixed at 500 mN for indentation while only a nominal fraction of this load was used for scanning the indent. The allowable drift rate was fixed at 0.05 nm/s. All the tests were done at one strain rate of 0.05 nm/s

Each material was indented with all three indenters on 3X3 matrix. Each indentation was separated by approximately 50 microns. Pile-ups were measured for all these indentations through Nanovision.

As the indenter is driven into the surface of the material, the material resists. This resistance is characteristic for every material and is known as the stiffness of the material. It is further used to calculate the elastic modulus and the hardness of the material. As the indenter leaves the material during unloading, there is some recovery of the material. This is known as the elastic recovery and is reflected in the unloading curves of the material. The slope of this unloading curve gives the stiffness of the material.
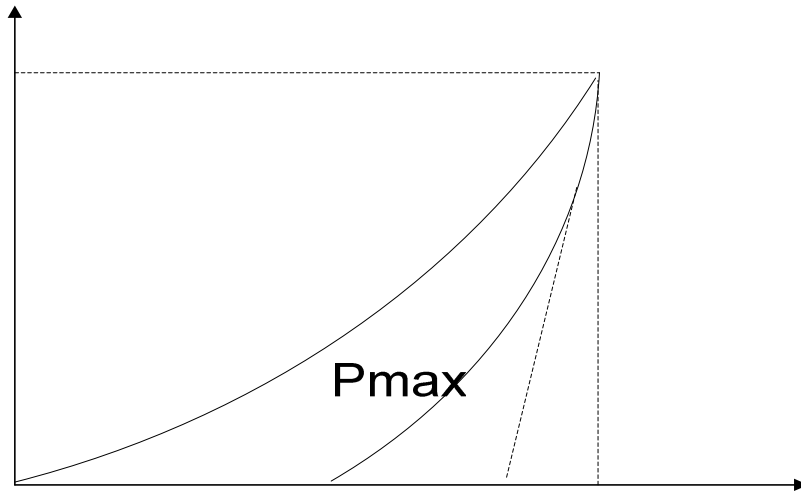
Figure 7: A schematic of a typical nanoindentation load vs displacement curve [3].

The important parameters to be calculated experimentally here are the maximum load, P_{max}, the contact depth, h_c, stiffness (S) which is the slope of the unloading curve or dP/dh. With these parameters known, one can proceed to find out the basic mechanical properties of the material like the elastic modulus and the hardness. Contact depth is given by:

$$h_c = h_{max} - \varepsilon \frac{p_{max}}{S}$$

Stiffness is defined as:

$$S = dP/dh$$

hc

Reduced elastic modulus and hardness is given by the following relation:

$$\frac{1}{E_{eff}} = \frac{1 - \nu^2}{E} + \frac{1 - \nu_i^2}{E_i}$$

$$and$$

$$H = \frac{P_{max}}{A}$$

The effective modulus of elasticity is thus defined as:

$$E_{eff} = \frac{\sqrt{\pi}}{2\beta} \frac{S}{\sqrt{A}}$$

3.5.1 Area Function and Calibration Procedure

For an indenter with known geometry, the contact area is a function of contact depth. However, the pyramidal geometries are not perfect and they change with time. There is also tip rounding of the indenter with continued usage. Berkovich has a tip radius of around 200 nm, followed by cube corner and conical indenters, which have gradually reducing tip radii respectively [7]. The half angle enclosed by these indenters defines the plastic deformation capability of these indenters. The half angle is inversely proportional to this deformation producing capability. The tip radius of Berkovich, cube corner and conical indenters are in an descending order and detail specifications for each tip have been provided in Appendix A and B and reference [7].

The generalized area as a function of contact depth for all three indenters is given as

$$A(h_c) = C_0 h_c^2 + C_1 h_c + C_2 h_c^{1/2} + C_3 h_c^{1/4} + C_4 h_c^{1/8} ......$$

The coefficients C_0, C_1 etc are found by the calibration method. Therefore, calibration should be done regularly. Fused silica is the standard for calibration for all the above stated reasons. If the value of elastic modulus and hardness differs from the standard value while calibrations indent, the area coefficients should be recalculated. The test on silica done again should match with the standard values. Calibration can be

done in many ways and depending on the type of indentation in question, weightage is decided. However, it is generally safe to give an even weightage for the data points occurring after the initial spike due to indentation size effect. Calibration area coefficients thus calculated are used in the experiments in the present study.

Table 2: Area Coefficients for the Indenter Tips Used in the Study

	Berkovich	Conical	Cube Corner
C0	23.8	9.1	2.57
C1	1080.49	6790.39	183.48
C2	6172.9	-25126.7	21758.8
C3	-1131.28	33610.8	-63685
C4	-7848.9	21044.4	-25345.1
C5	0	1722.7	2065.53
C6	0	-11635.8	17854.5
C7	0	-19292	26278.6
C8	0	23370.5	30626.9

3.6   Nanovision

Nanovision works akin to the atomic force microscope (AFM). The indenter shaft scans the indenter profile along the area specified by the user. The vertical fluctuation of the indenter shaft due to the topographical fluctuations is recorded by the change in capacitance as the displacement of the indenter plate changes with respect to the capacitor. This change is recorded as voltage and the three dimensional plot of the indentation is formed. This three dimensional plot can be manipulated by the user. There are specific methods in Nanovision which can be used to analyze different material properties. As we are interested in the pile-up effects of the material on mechanical properties, the Nanovision method used was the indent and scan

displacement limit method. The specialty of this method is that the maximum displacement or the displacement into the surface is limited by the user. We can fix the depth of indentation and thus create a common background for all the indentations in study. The indenter first indents and then scans the surface of the indentation, giving the hardness and elastic modulus values as well as the three dimensional plot of the indent.

3.6.1 Traceline Method for Nanovision

This method is a specially designed adds on for the indent and scan displacement limit method for Nanovision. The traceline is a 0.2 micron thin line enveloping the surface of the scan. It can be shifted throughout the surface of indentation by the user by changing the profile number on the input editable dashboard of the method. Once we reach the point of interest on the three dimensional topography, we can shift to a cross sectional view by changing to two dimension option. The two dimensional option gives a chart of the profile number vs the z of the figure. We can thus measure the height of the surface feature. It can also be used to find out the contact radii or the x axis projection of the portion of the pile-up which is in contact with the indenter and which contributes towards the overestimation of the area of contact for the indentation.

3.7 Scanning Electron Microscopy (SEM)

In SEM, a fine probe of electrons defined by the spot size and the excitation voltage. The excitation voltage is dependant on the material properties. For my cases, I relied on 25 or 30 KeV. A schematic of the SEM is give below.
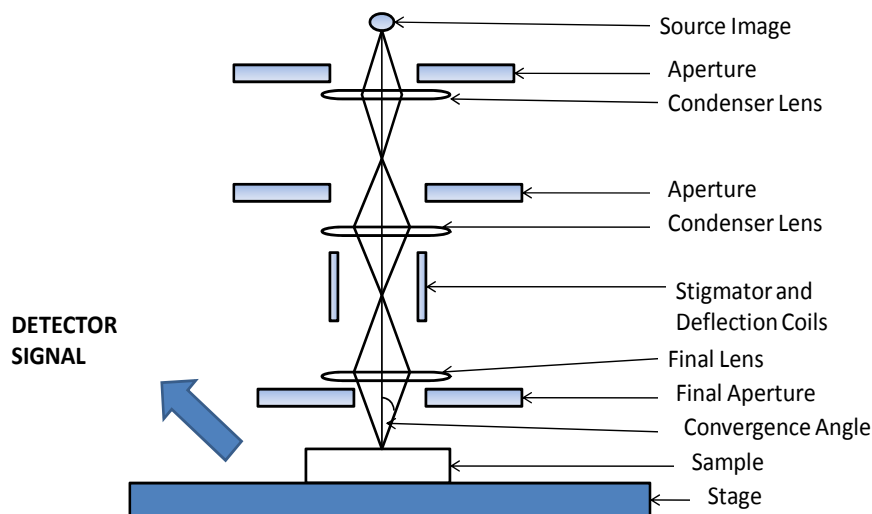
Figure 8: A schematic of the scanning electron microscope (ESEM Manual, FEI QUANTA [30]).

When electron beam hits the surface of the sample, elastic as well as inelastic collisions take place. The elastic collisions give rise to the primary electrons which are used for the imaging. The secondary electrons emitted are collected by other detectors and are characteristic of the material under study. For electron backscattered diffraction (EBSD) data, these electrons are used and give the orientation of the surface.

3.8   Electron Backscattered Diffraction (EBSD)

The mirror polished sample is mounted on a special mount which is inclined to the horizontal surface by 45 degrees. This is done in order to get the maximum number of secondary electrons to the EBSD detector as possible. The electrons collected here are used to create the orientation map of the sample. A schematic of the EBSD setup is shown below.
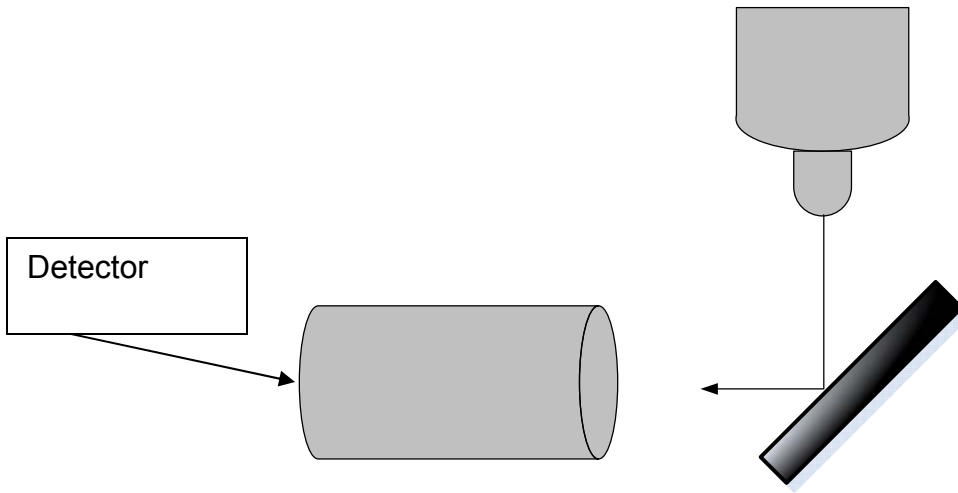
Figure 9: Schematic of electron back scattered diffraction (EDAX Manual, FEI QUANTA [30]).

SEM Va

CHAPTER 4

RESULTS

Hardness and elastic modulus values as generated from the nanoindenter are based on the Oliver and Pharr approach, discussed earlier. Continuous stiffness measurement (CSM) was used in addition to the approach for the Nanovision™ methods employed to accomplish this. However, as presented in the following discussion, the actual values for hardness and elastic modulus differ quite significantly because of the inherent plastic properties of the metals. The traceline method discussed in the previous chapter was used to measure the pile-up and sink-in heights.

4.1   Berkovich Indenter

Berkovich indenter is universally used for mechanical characterization standardization. Following results are structured as per the three metals used for the present study. A matrix of 3X3 indentations was used amounting to a total of 9 indentations for all the metals indented with the Berkovich indenter as shown in Figure 10.

4.1.1   Berkovich Indentations on Copper

A typical data set obtained from Berkovich indentations is shown in Figure 10. It can be seen that the values for elastic modulus and hardness are increasing during the initial period of indentation. This can be explained by the

indentation size effect [4], which states that the hardness values differ with different

indentation depths.

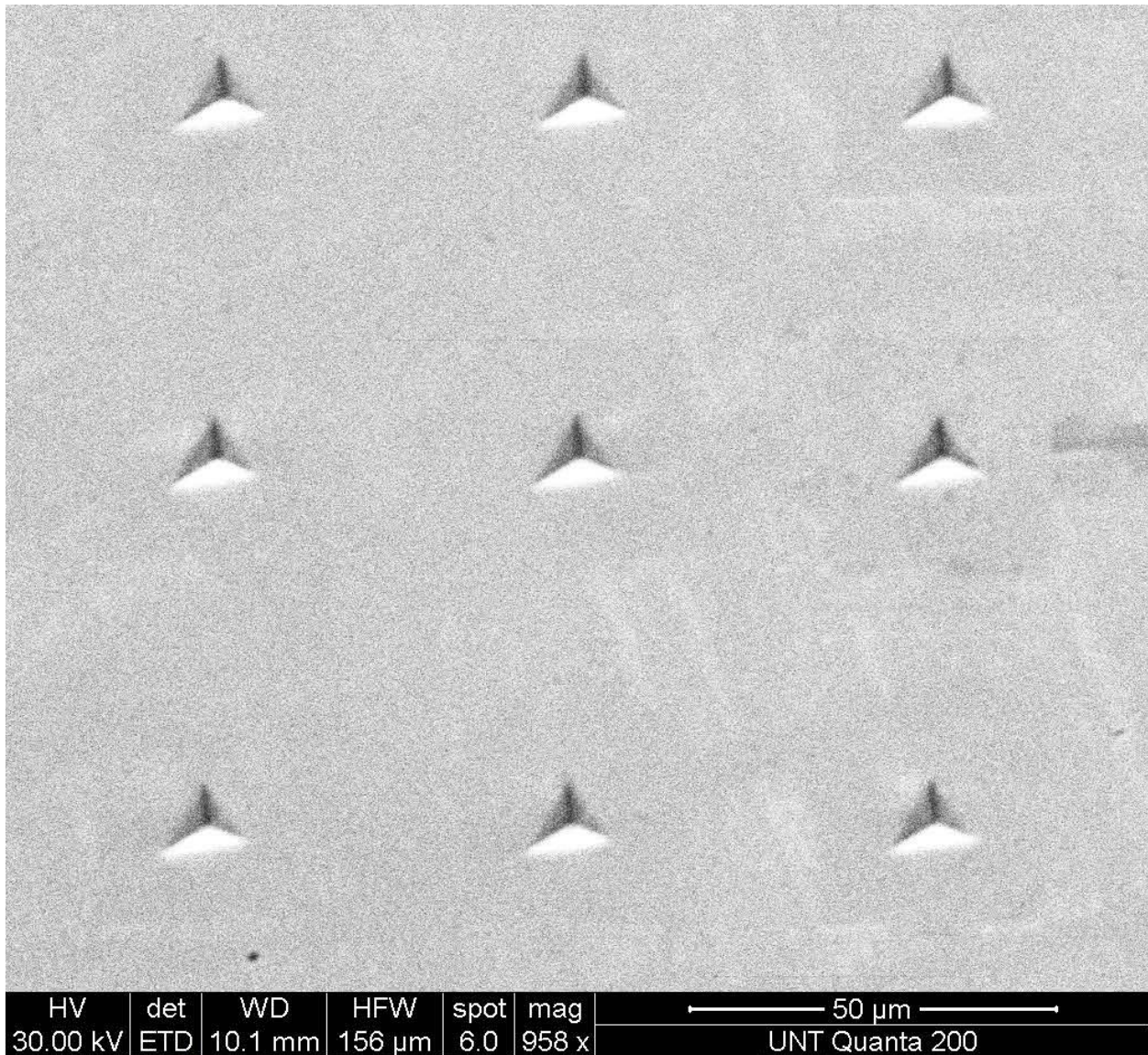| HV	det	WD	HFW	spot	mag	50 μm
30.00 kV	ETD	10.1 mm	156 μm	6.0	958 x	UNT Quanta 200

Figure 10: Scanning electron micrograph of a typical 3X3 Berkovich indentation matrix used in the study. The spacing in the X and Y directions is 50 microns respectively.

When indentation depth is low, in the range of 50-100 nm and comparable with the tip radius of the indenter, the hardness values are high. They gradually attain a constant value with increasing depth of penetration. In the present case, however, the

depth of indentation is 1000 nm. Tip rounding is not important here as the depth of

indentation is much more than that. However, this effect can still be seen at small

indentation depths. For the later part, they remain fairly constant with displacement, as

is to be expected. The values obtained for Berkovich indents on face centered cubic

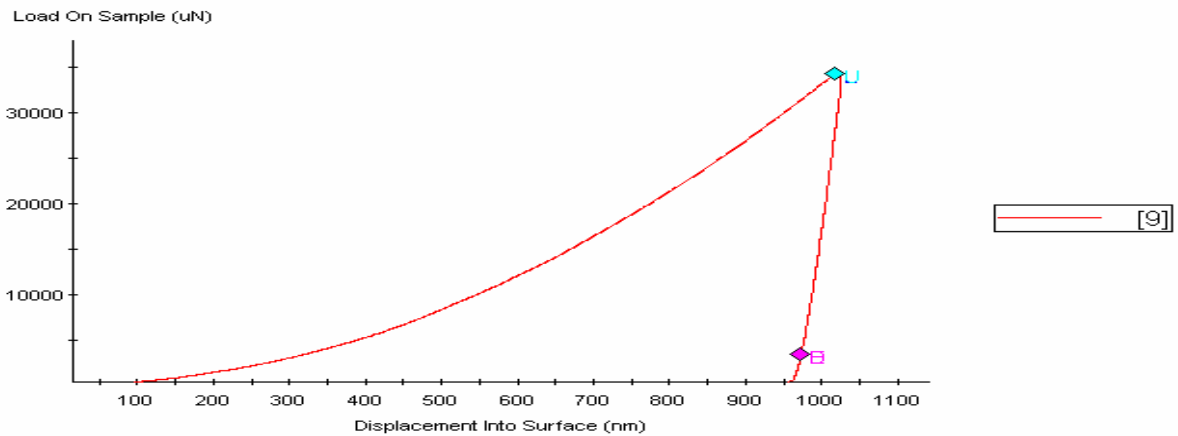(FCC) copper are in accordance with the literature.

Figure 11a: Representative load vs displacement for Berkovich copper.
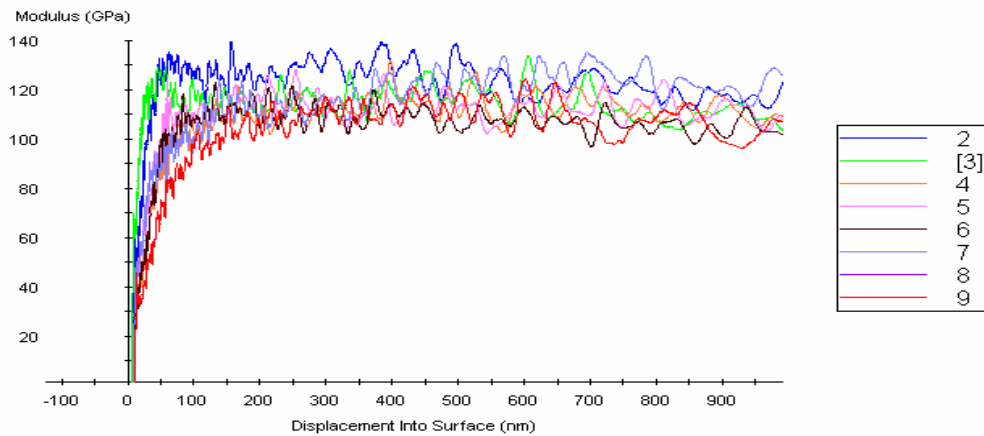

Figure 11b: Elastic modulus vs displacement into the surface for Berkovich
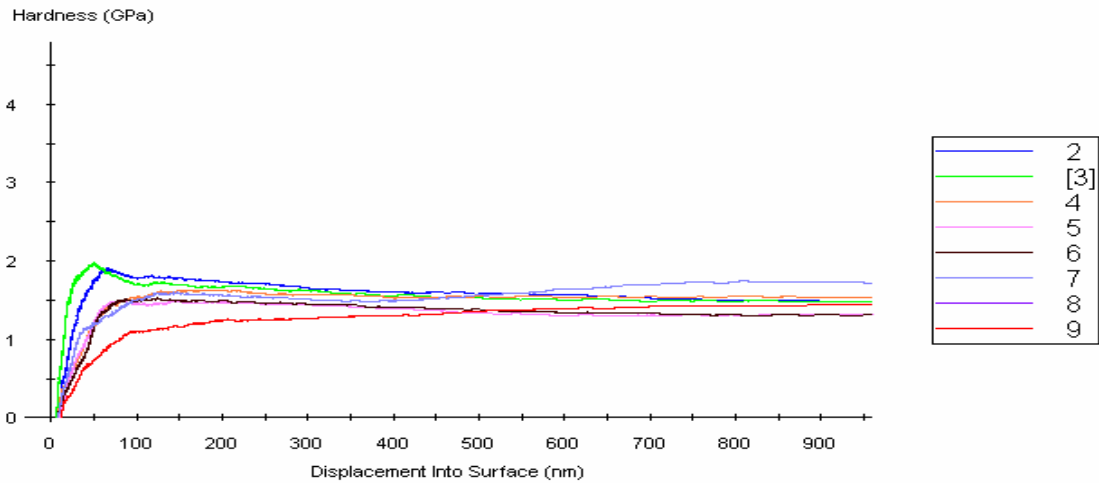indentations on copper.

Figure 12: Hardness vs displacement into the surface for Berkovich indentations on copper.

4.1.2 Berkovich Indentations on Nickel

Above data set is a representative of nine indentations on nickel by Berkovich indenter. As can be seen, elastic modulus and hardness values attain constant values after the initial spike in the values. That can be explained with the help of indentation size effect. The data values obtained are in accordance with the literature [7].
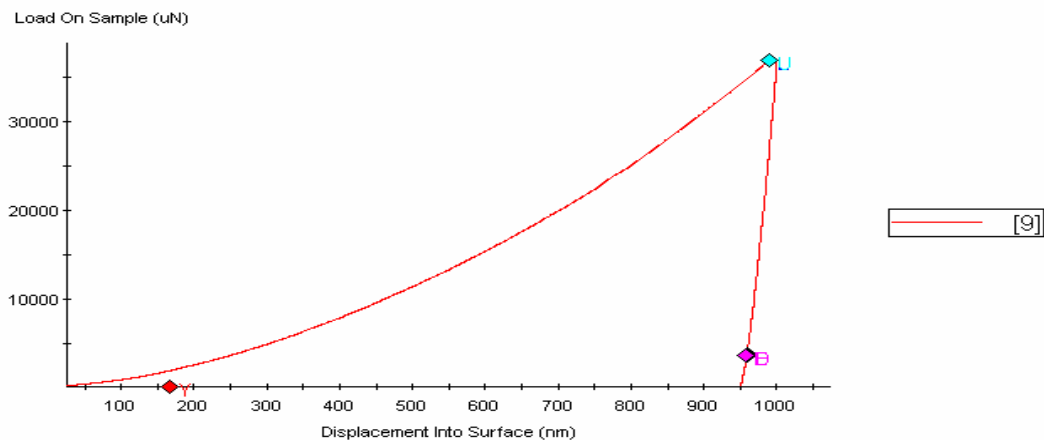

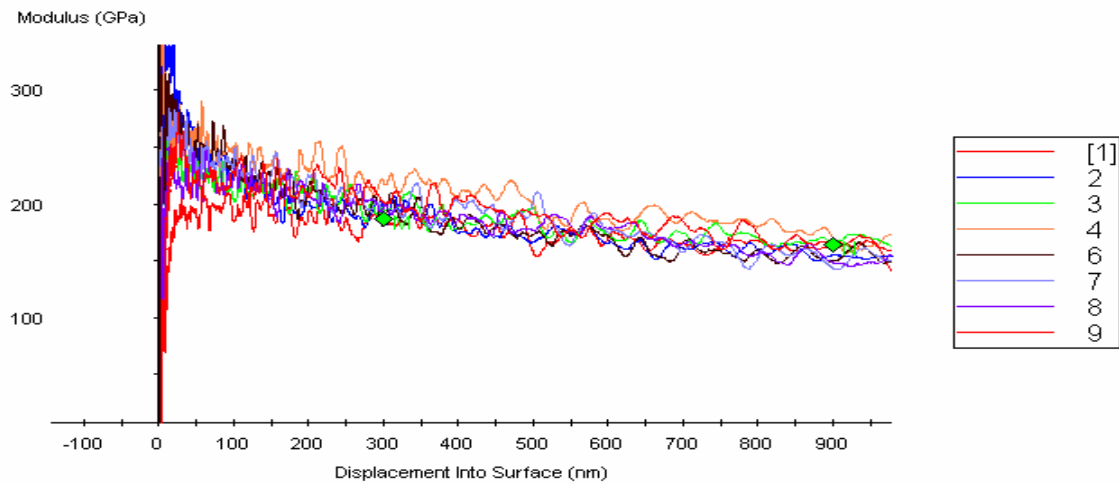Figure 13a: Representative load vs. displacement for Berkovich nickel.

Figure 13b: Elastic modulus vs displacement into surface for Berkovich indentations on nickel.
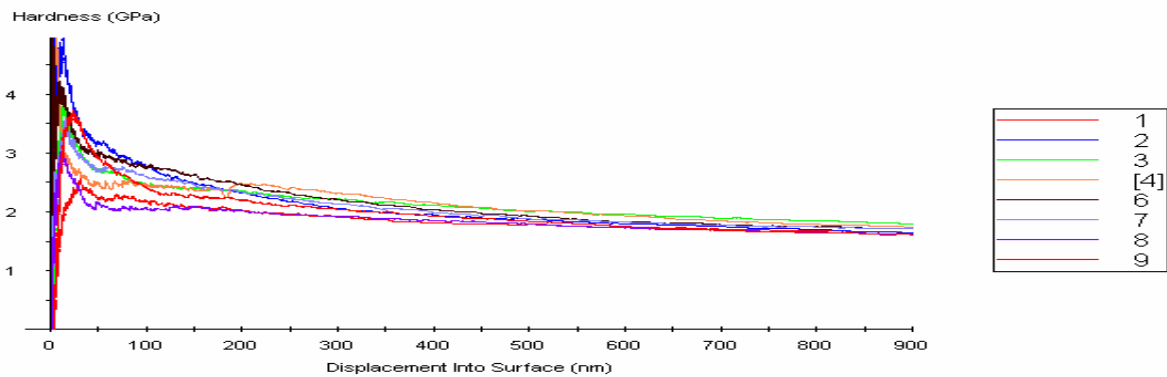

Figure 14: Hardness vs displacement into surface for Berkovich indentations on nickel.

4.1.3 Berkovich Indentations on Iron

Above are the hardness and elastic modulus values for Berkovich indentations on a 3X3 matrix for iron. It was observed that hardness attains constant value after the initial sharp rise in values for hardness and elastic modulus values. The values obtained are in accordance with the values in literature [7].
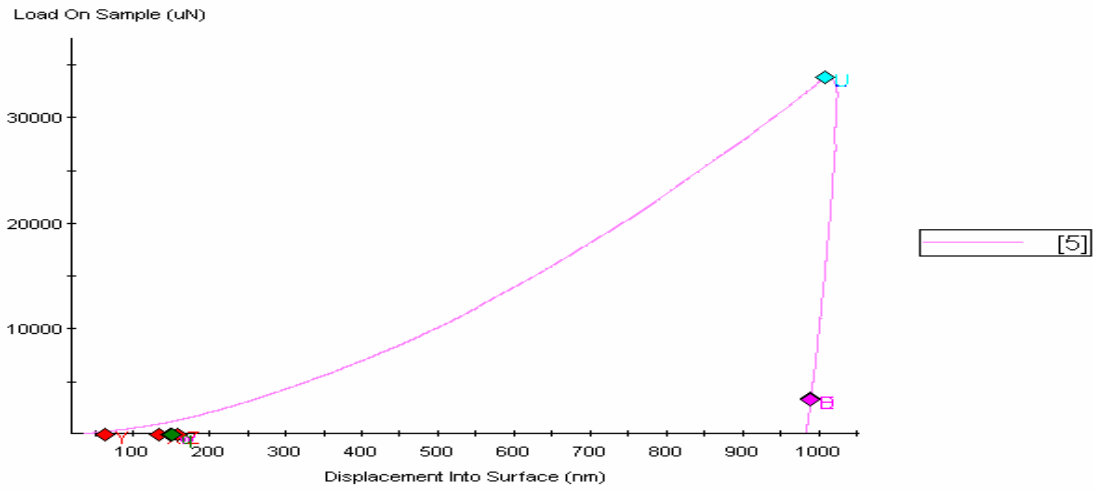
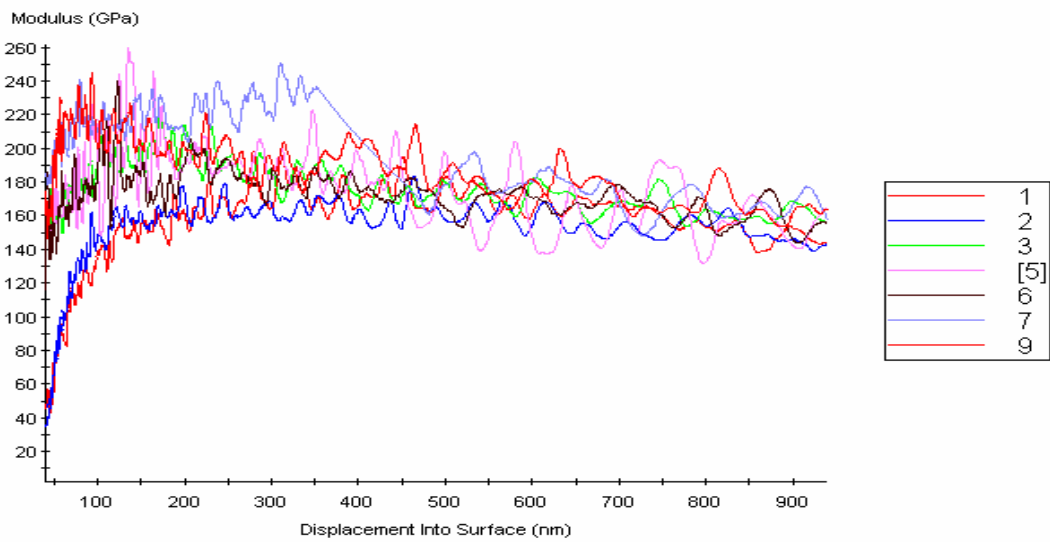Figure 15a: Representative load vs displacement for Berkovich iron.

Figure 15b: Elastic modulus vs displacement into surface for Berkovich indentations on iron.
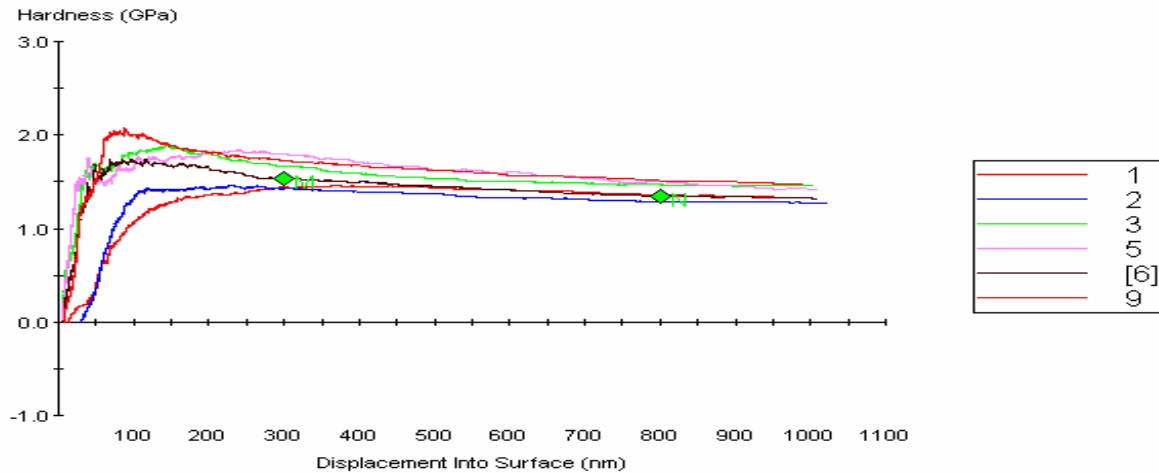
Figure 16: Hardness vs displacement into surface for Berkovich indentations on iron.

4.2   Cube Corner Indenter

Cube corner indenter is universally used for measuring the mechanical properties when sharpness and low loads are required to produce plastic deformation. It is being increasingly used to characterize thin films and low depth indentations. Following results are structured as per the three metals used for the present study.   A matrix of 3X3 indentations was used amounting to a total of 9 indentations for all the metals indented with the cube corner   indenter as shown below.

4.2.1 Cube Corner Indentations on Copper

A typical data set obtained from cube corner indentations is shown above. It can be seen that the values for elastic modulus and hardness are increasing during the initial period of indentation. For the later part, they remain fairly constant with displacement.
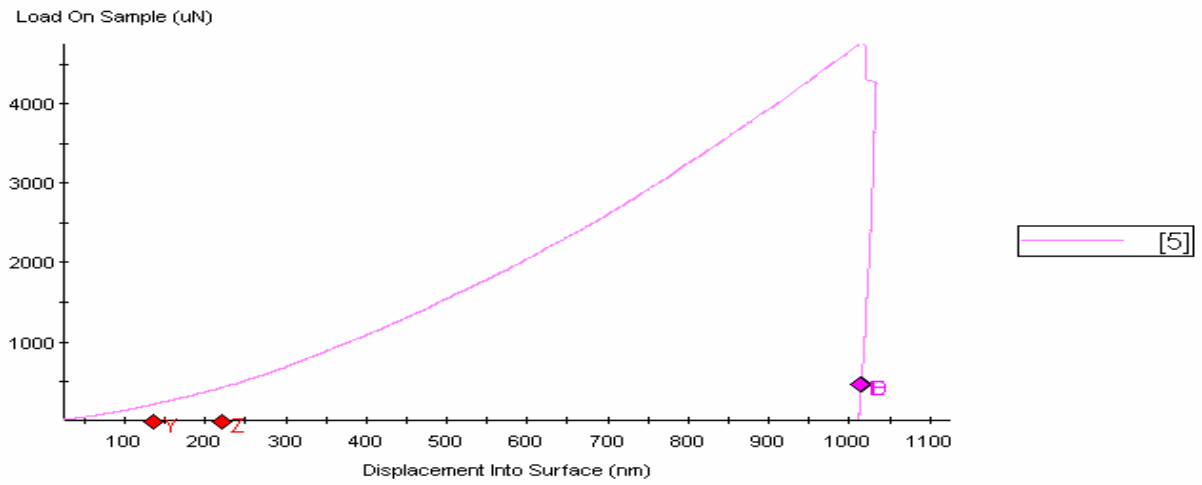
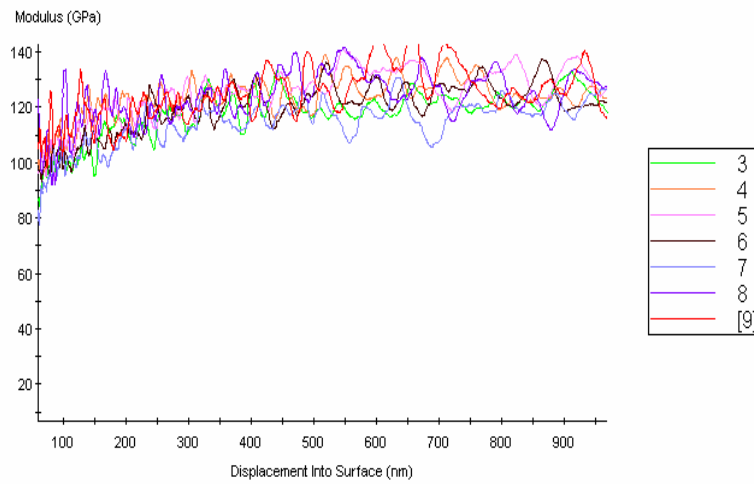Figure 17a: Representative load vs displacement for cube corner copper.

Figure 17b: Elastic modulus vs displacement into surface for cube corner indentations on copper.
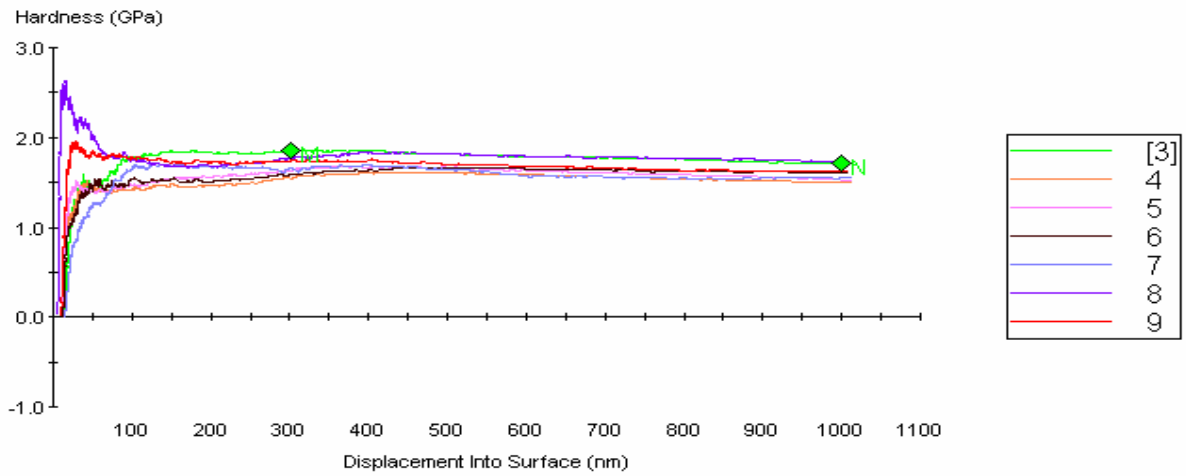
Figure 18: Hardness vs displacement into surface for cube corner indentations on copper.

4.2.2 Cube Corner Indentations on Iron

A typical data set obtained from nine cube corner indentations on iron is shown above. Elastic modulus and hardness attain a constant value with increasing penetration into the surface after the initial rise.
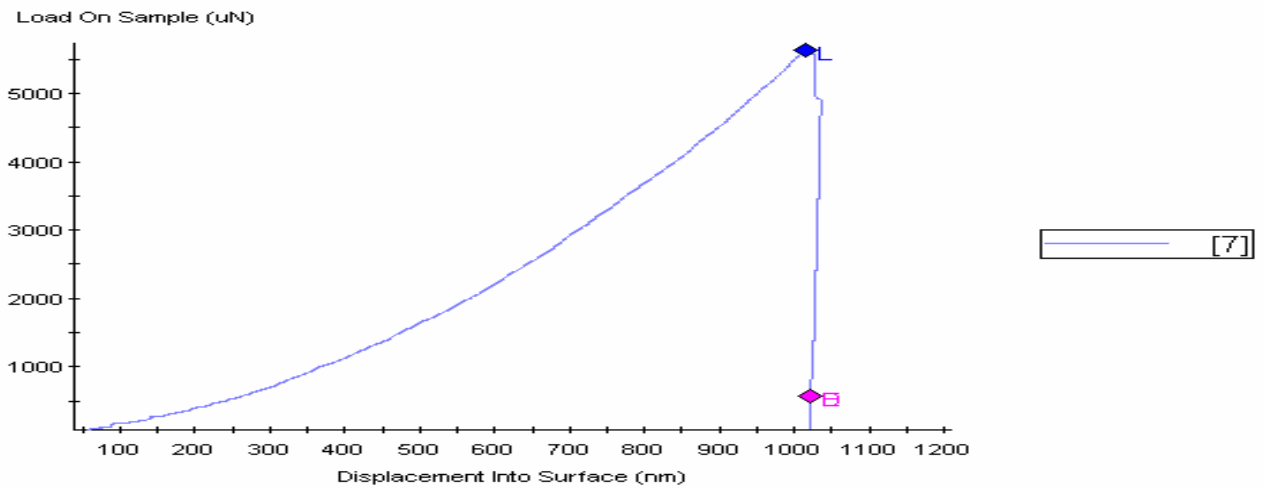

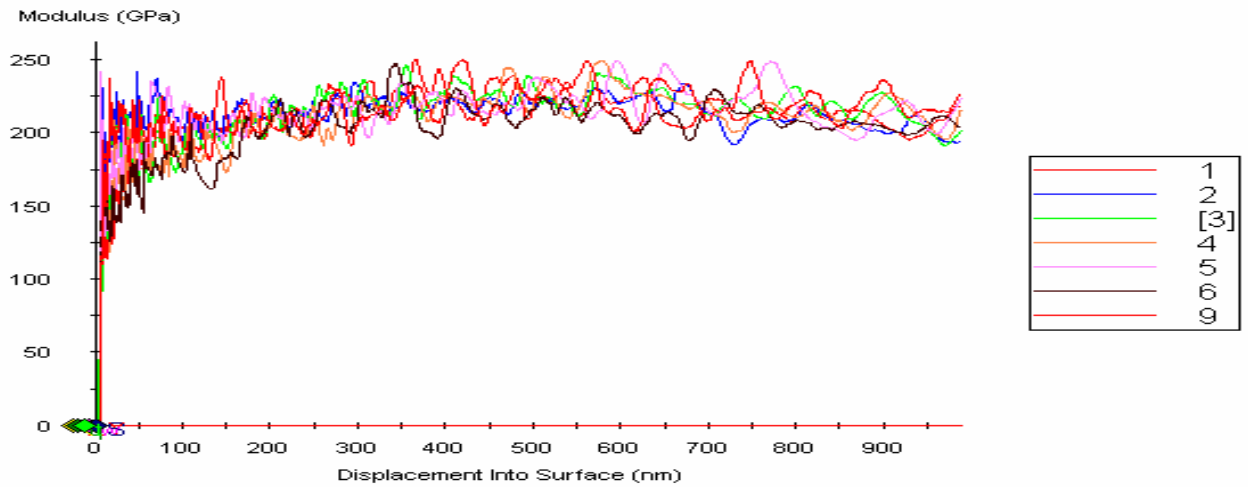Figure 19a: Representative load vs displacement for cube corner iron.

Figure 19b: Elastic modulus vs displacement into surface for cube corner indentations on iron.
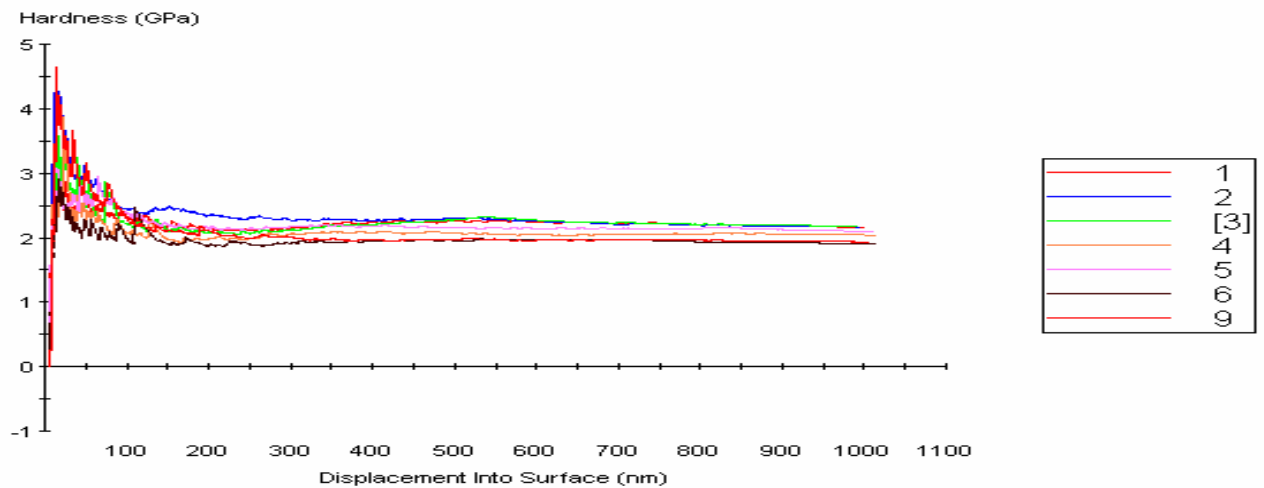

Figure 20: Hardness vs displacement into surface for cube corner indentations on iron.

4.2.3 Cube Corner Indentations on Nickel

A typical data set obtained from nine cube corner indentations on nickel is shown above. Elastic modulus and hardness attain a constant value with increasing penetration into the surface after the initial rise.
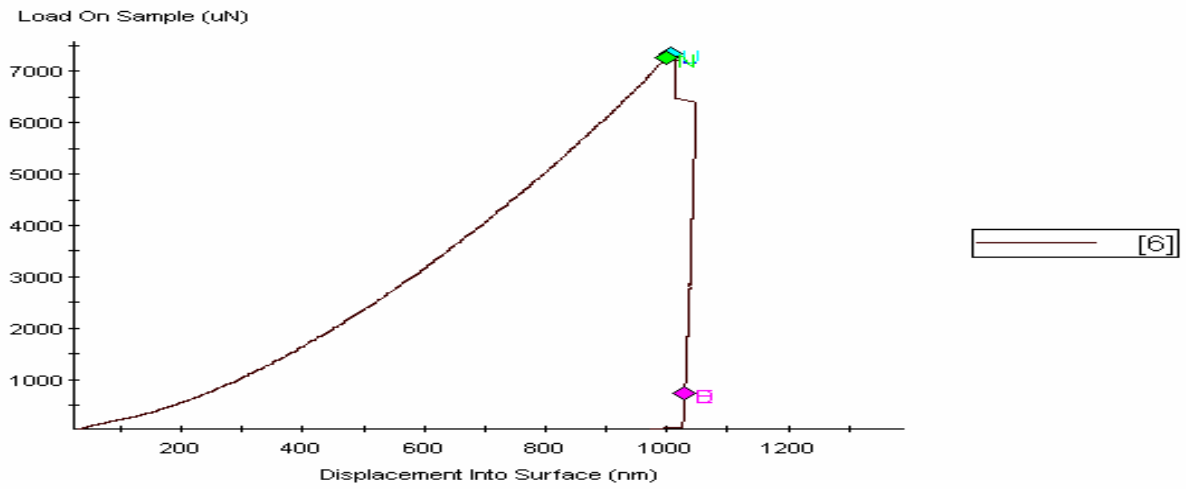
38

Figure 21a: Representative load vs displacement for cube corner nickel.
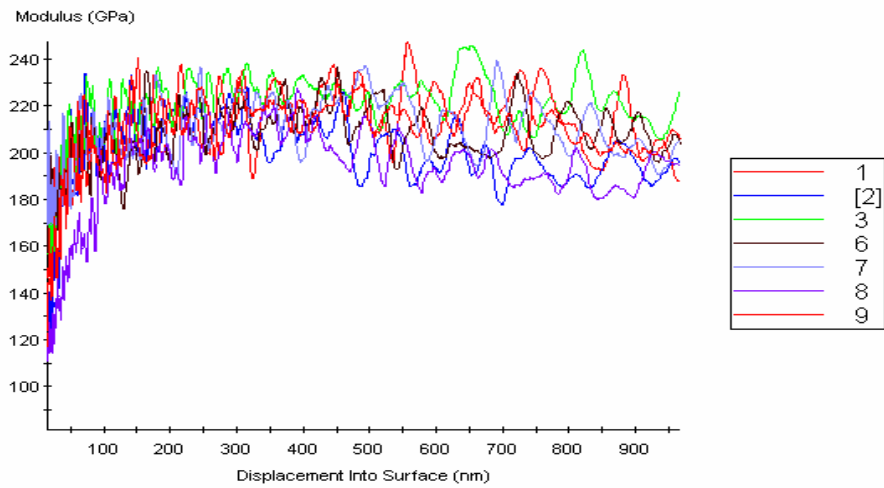

Figure 21b: Elastic modulus vs displacement into surface for cube corner indentations on nickel.
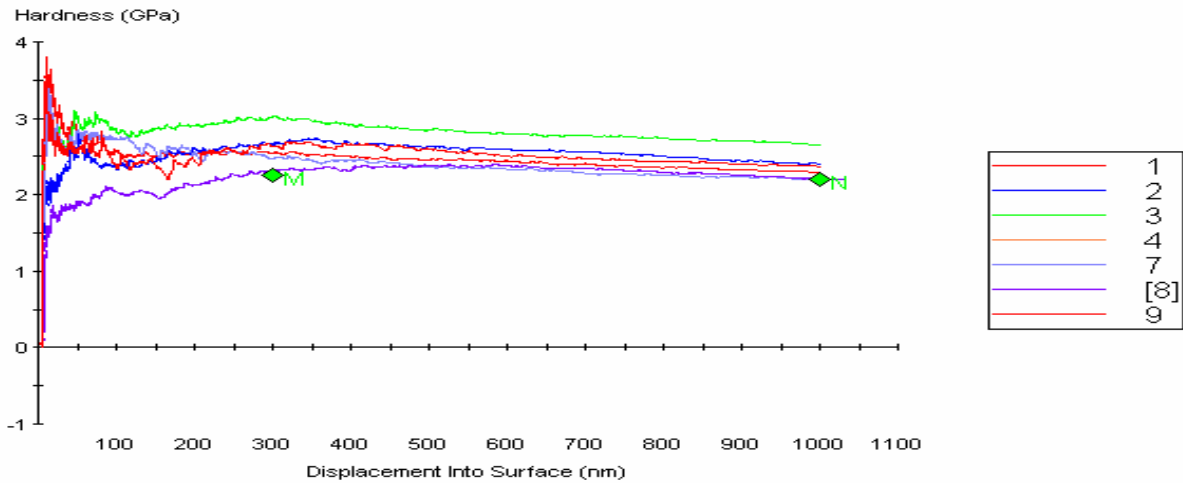
Figure 22: Hardness vs displacement into surface for cube corner indentations on nickel.

4.3   Conical Indenter

Conical indenter is one of the major indenters used for measuring the mechanical properties when material properties are to be studied and less attention is to be paid on indenter geometry. It is also useful when plasticity is to be produced at low loads due to its sharpness and symmetry. It is being increasingly used for studying orientation effects. Following results are structured as per the three metals used for the present study.   A matrix of 3X3 indentations was used amounting to a total of 9 indentations for all the metals indented with the conical   indenter as shown in later sections.

4.3.1 Conical Indentations on Copper

A typical data set obtained on a 3X3 matrix of nine conical   indentations on copper is shown above. Elastic modulus and hardness attain a constant value

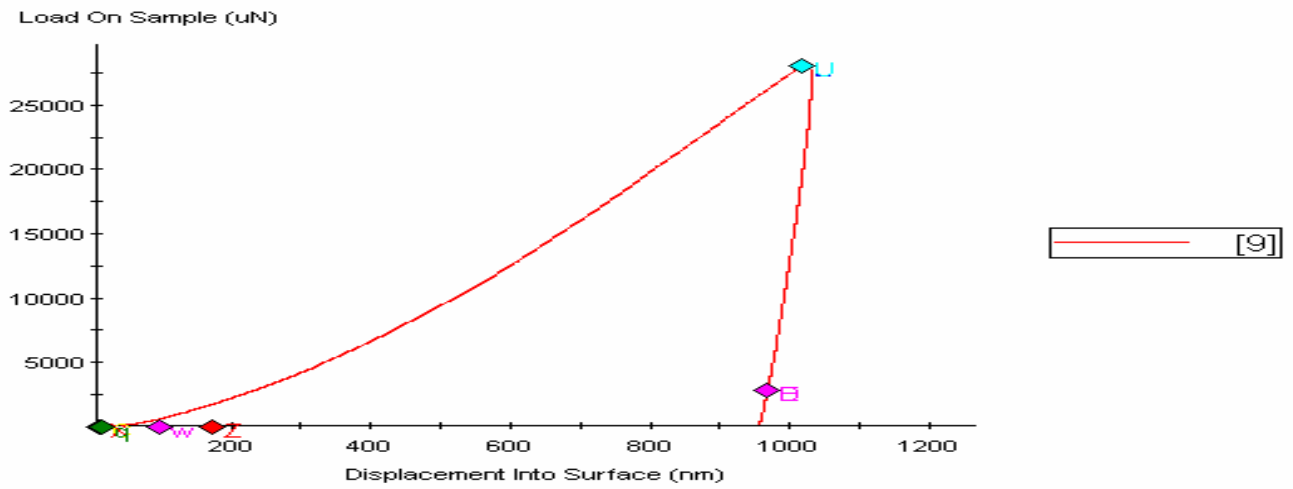with increasing penetration into the surface after the initial rise.

Figure 23a : Representative load vs displacement for conical copper.
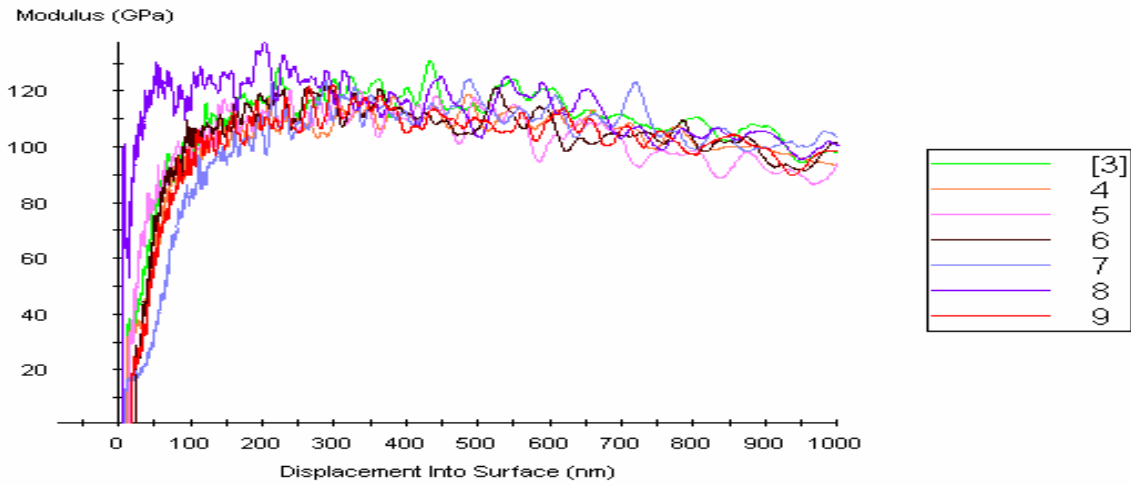

Figure 23b: Elastic modulus vs displacement into surface for conical indentations on copper.
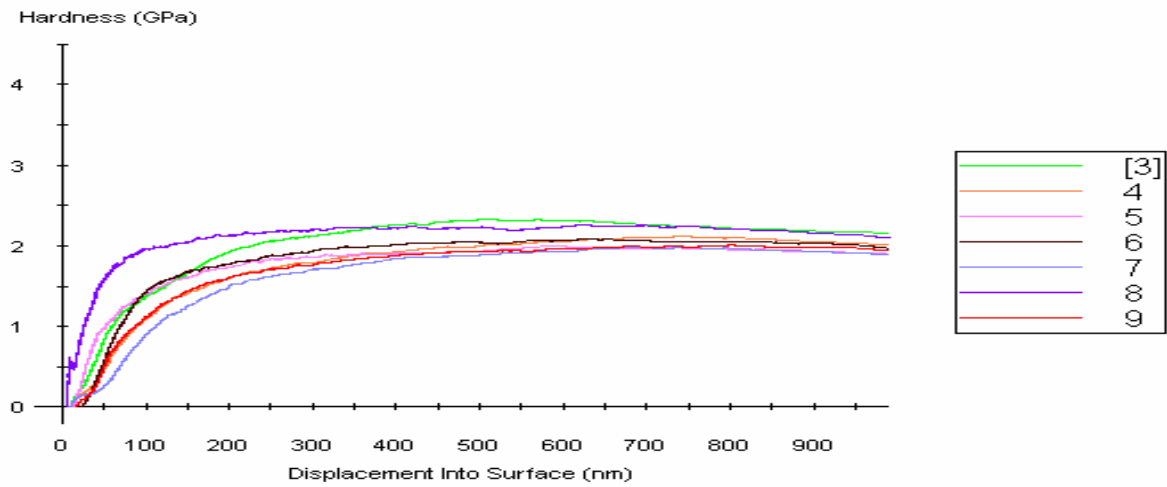
Figure 24 : Hardness vs displacement into surface for conical indentations on copper.
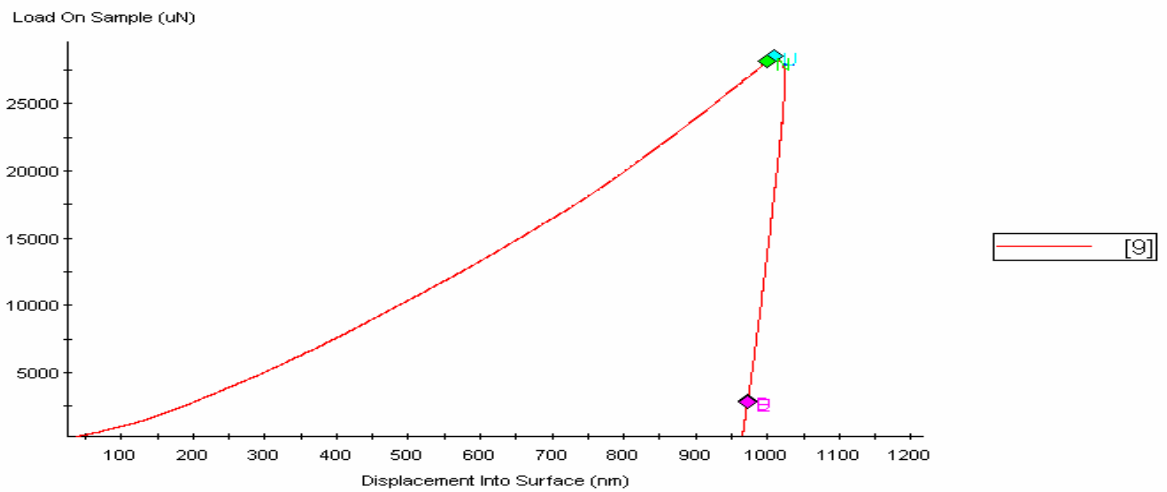
4.3.2 Conical Indentations on Copper

Figure 25a: Representative P vs h for conical iron.
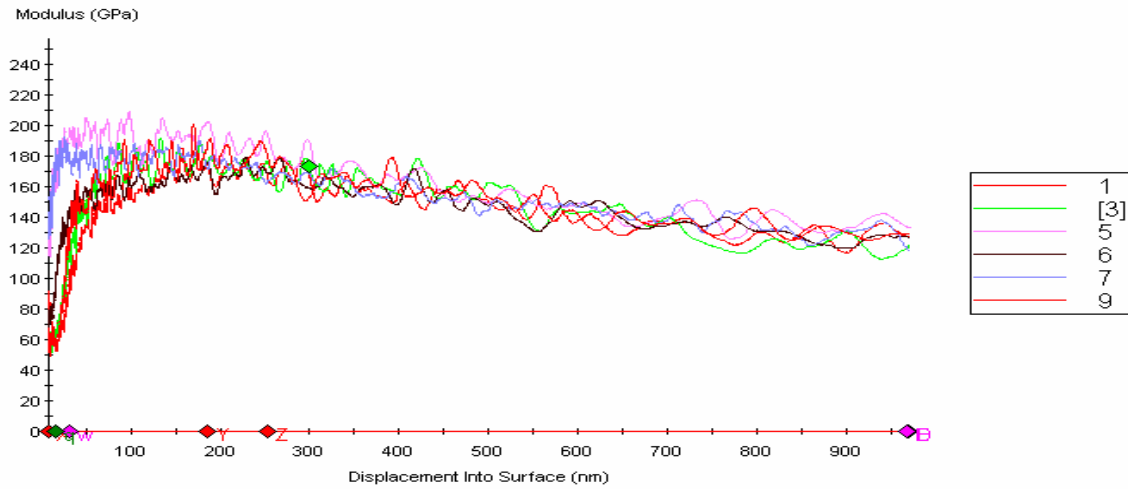
Figure 25b: Elastic modulus vs displacement into surface for conical indentations on iron.

Figure 26: Hardness vs displacement into surface for conical indentations on iron.

A typical data set obtained on nine conical indentations on iron is shown above. Elastic modulus and hardness gradually attain a constant value after the initial rise with increasing displacement into the surface.

4.3.3 Conical Indentations on Nickel

Figure 27a: Representative P vs h for conical nickel.

Figure 27b: Elastic modulus vs displacement into the surface for conical indentations on nickel.
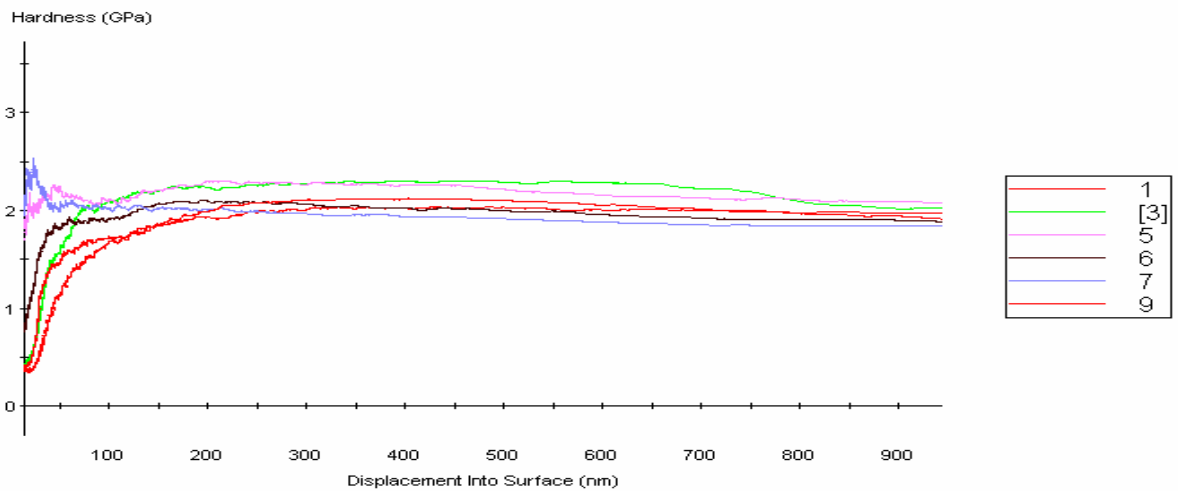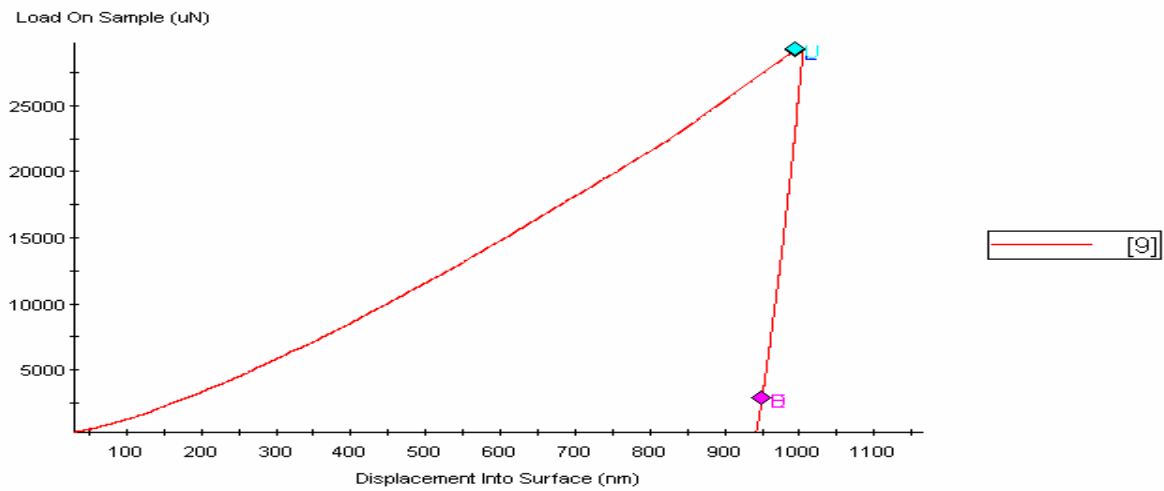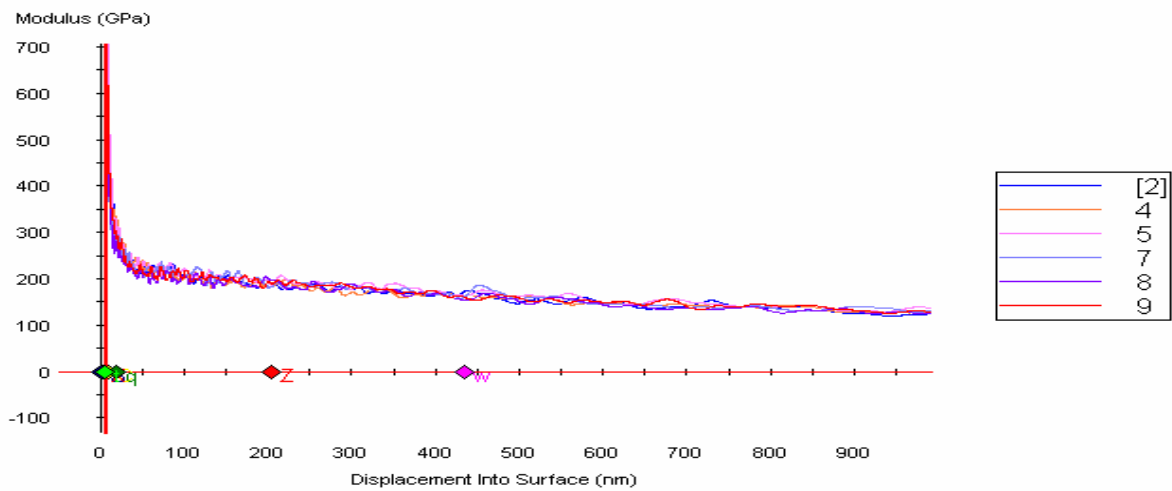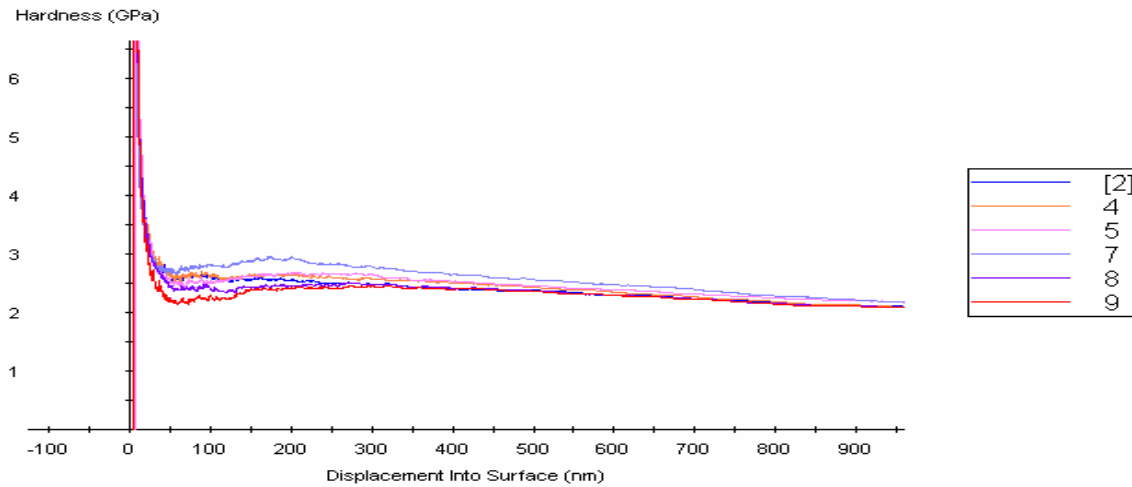
Figure 28: Hardness vs displacement into the surface for conical indentations on nickel.

A typical data set obtained on nine conical indentations on nickel is shown above. Elastic modulus and hardness gradually attain a constant value after the initial rise with increasing displacement into the surface.

4.4   Nanovision Profiles

These profiles were obtained by the Nanovision feature of the Nanoindenter, working of which has been described in detail. One can see the rotating three dimensional view of indentations which gives a better understanding of the phenomena.

4.4.1 Nanovision Profiles of Berkovich Indentations

Figure 29: From top to bottom, top, random and front three dimensional view of Berkovich indentations on copper.

Figure 30: From top to bottom, top, random and front three dimensional view of Berkovich indentations on iron.

Figure 31: From top to bottom, top, random and front three dimensional view of Berkovich indentations on nickel. Pile-ups and sink-ins are seen from the above three dimensional views of indentations. There are also some areas where no pile-ups are seen.
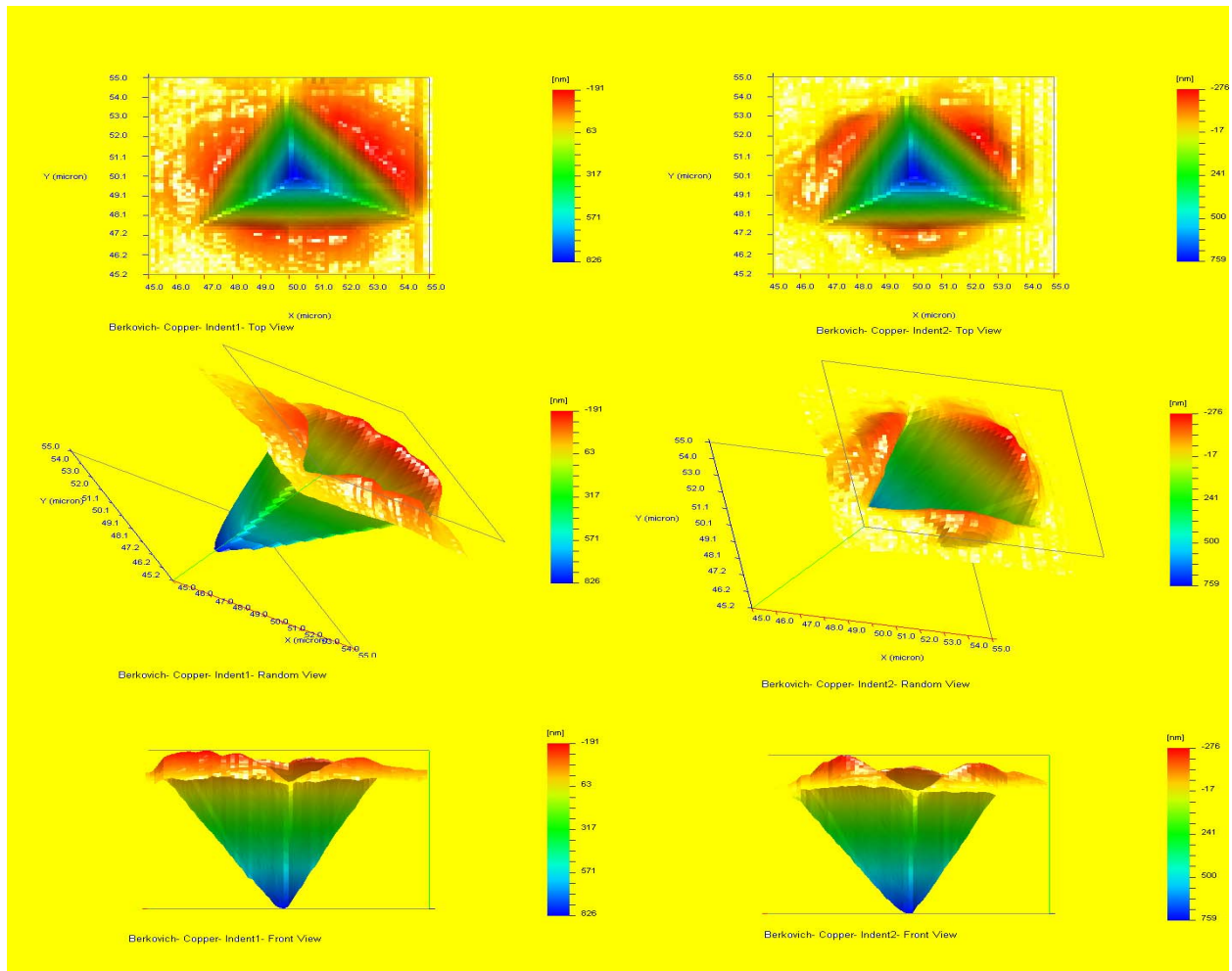
4.4.2 Nanovision Profiles of Cube Corner Indentations

Figure 32: From top to bottom, top, random and front three dimensional view of cube corner indentations on copper.

Figure 33: Top to bottom, top, random and front three dimensional view of cube corner indentations on iron.

Figure 34: Top to bottom, top, random and front three dimensional view of cube corner indentations on nickel.

Cube corner indenter is sharp and produces more plastic deformation. This could be seen by the smaller indents and more pronounced areas of pile-up on all the indentations.

4.4.3   Nanovision Profiles of Conical Indentations
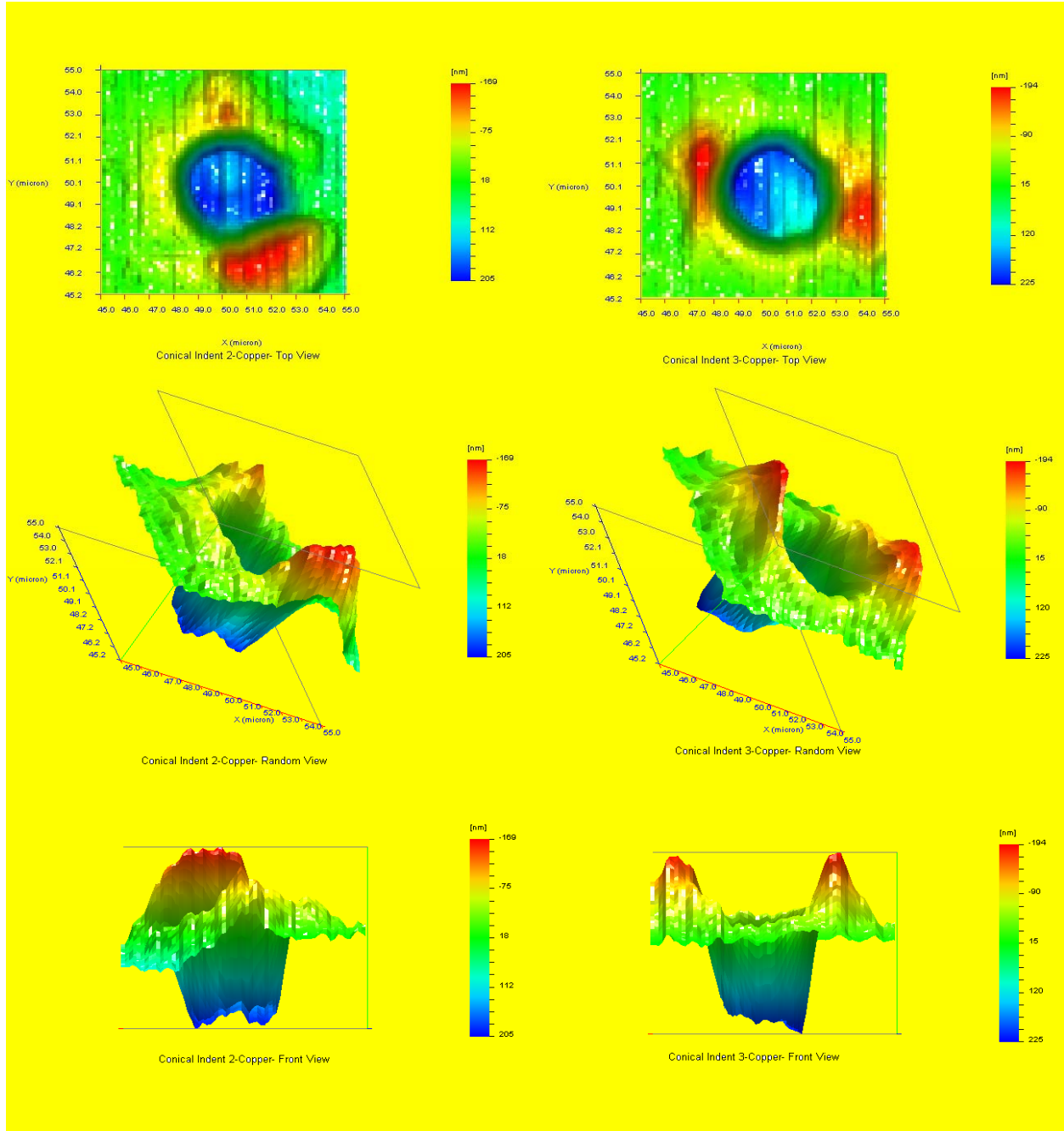
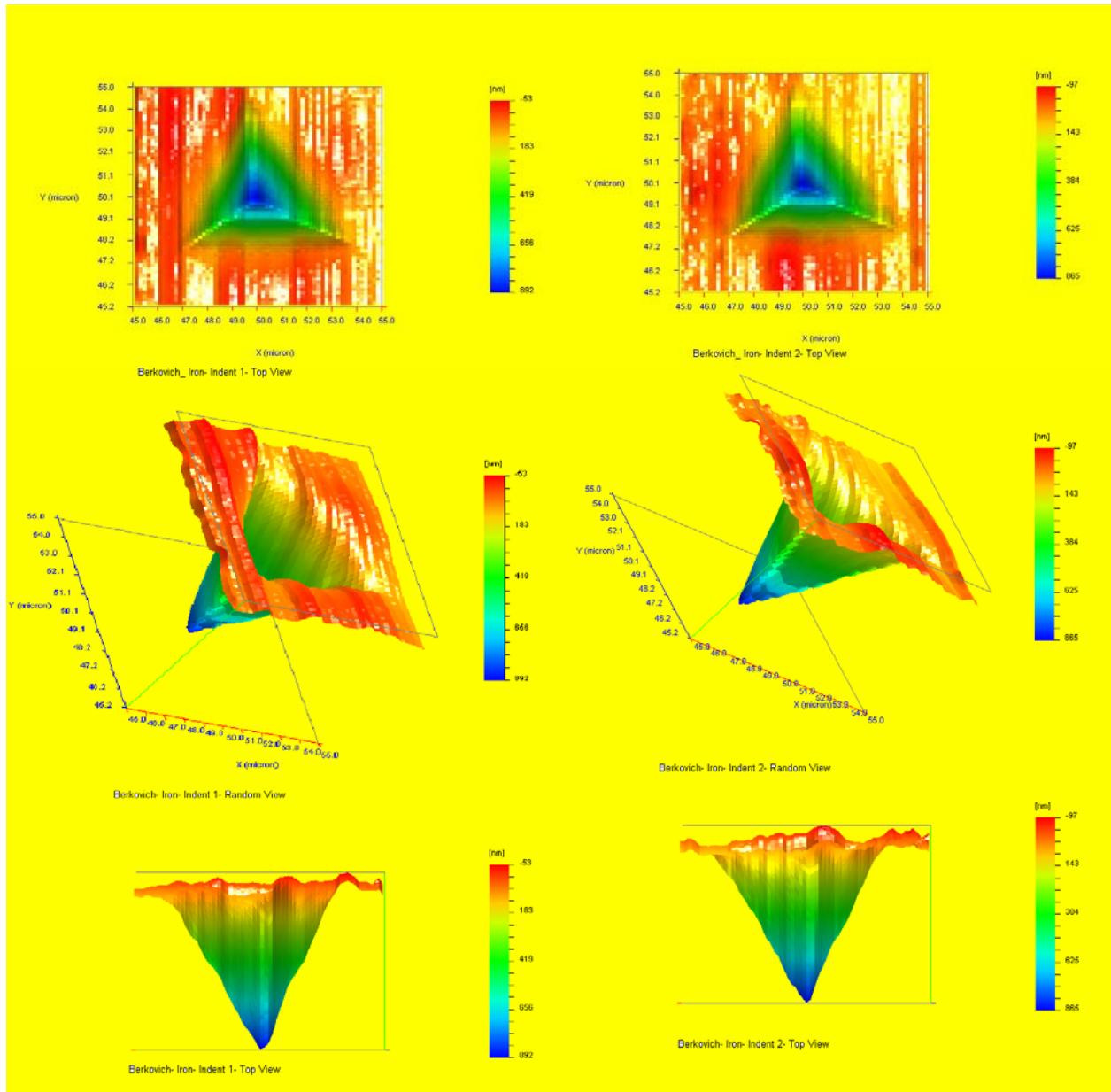Figure 35:   Top to bottom, top, random and front three dimensional view of conical indentations on copper.

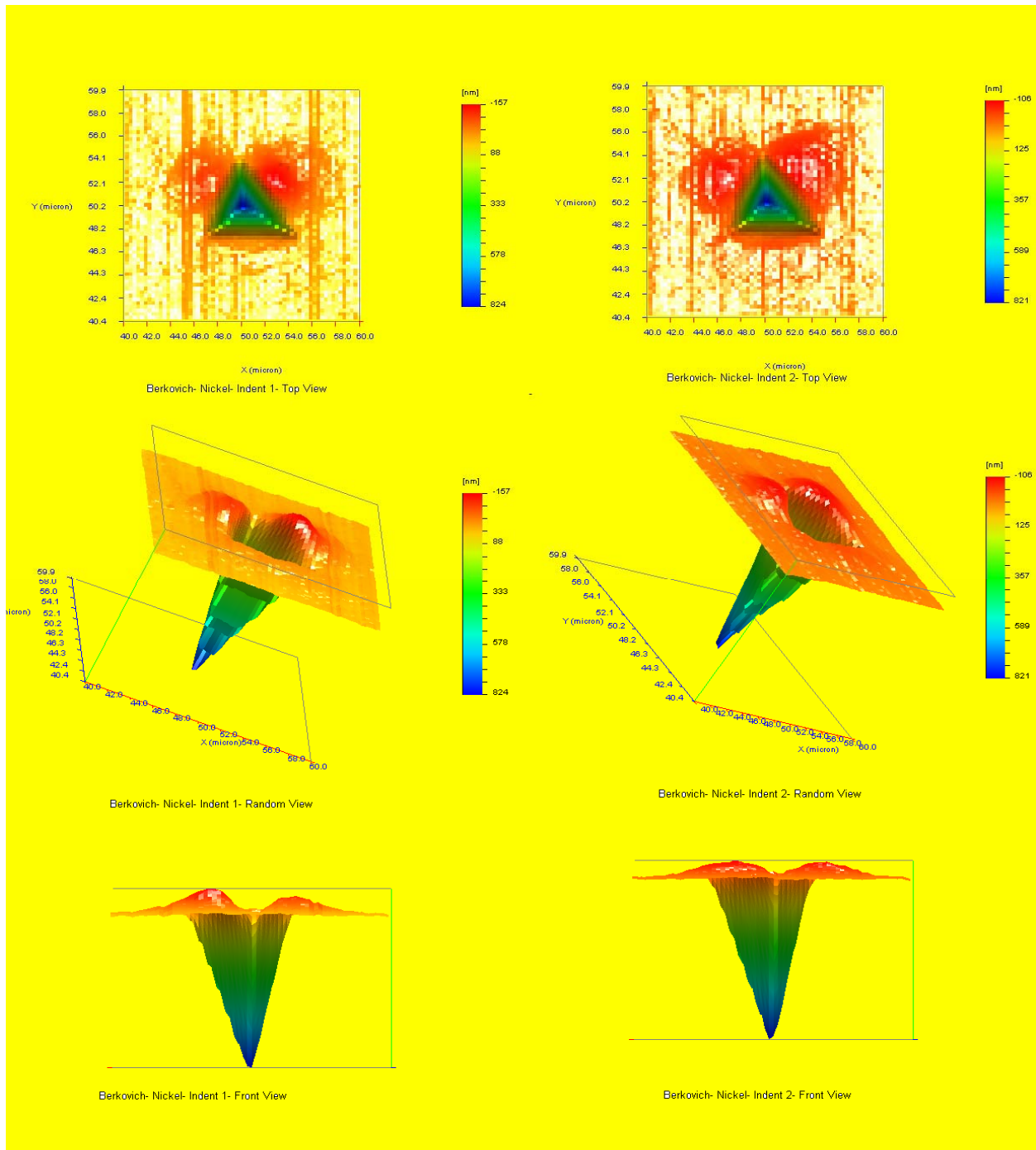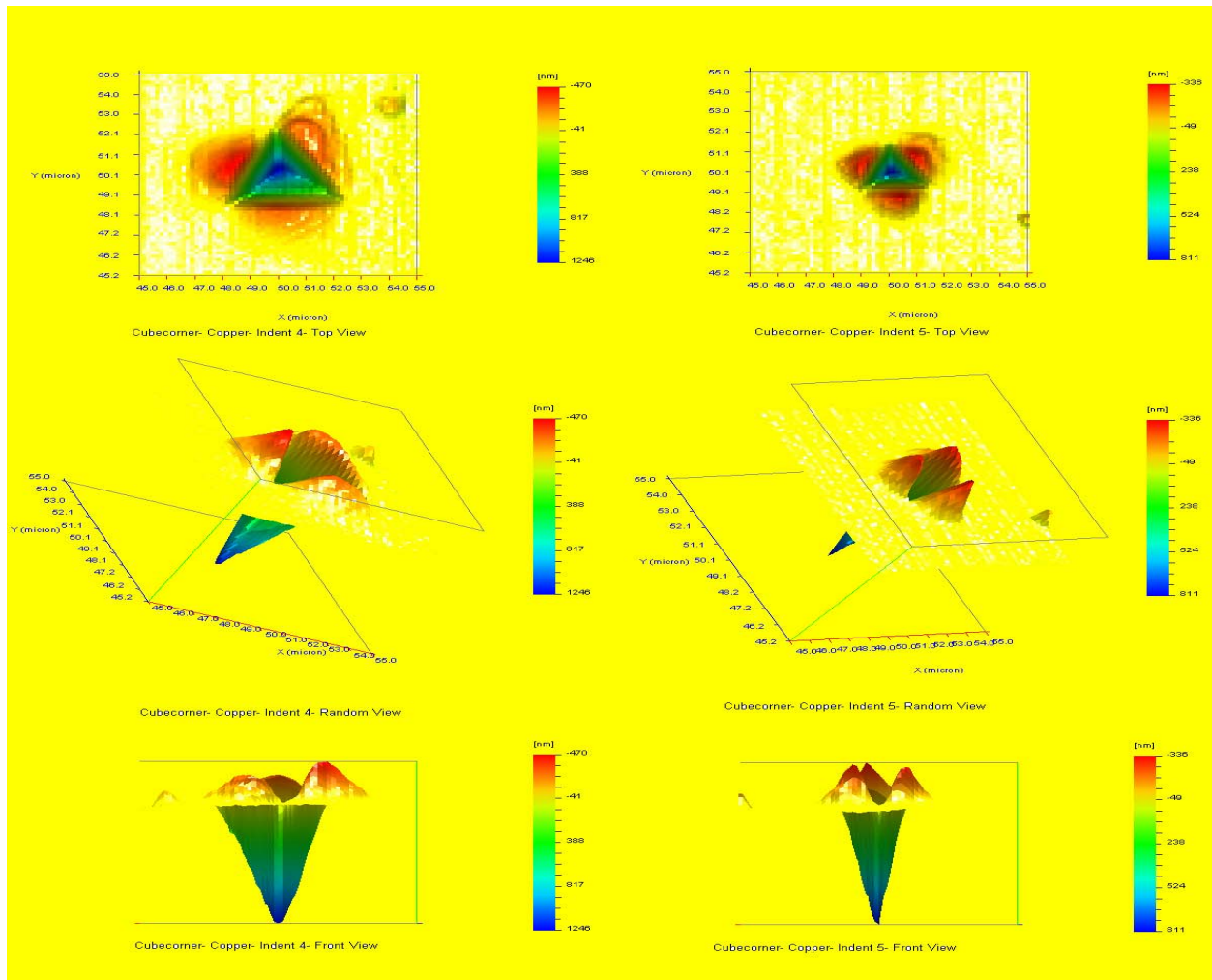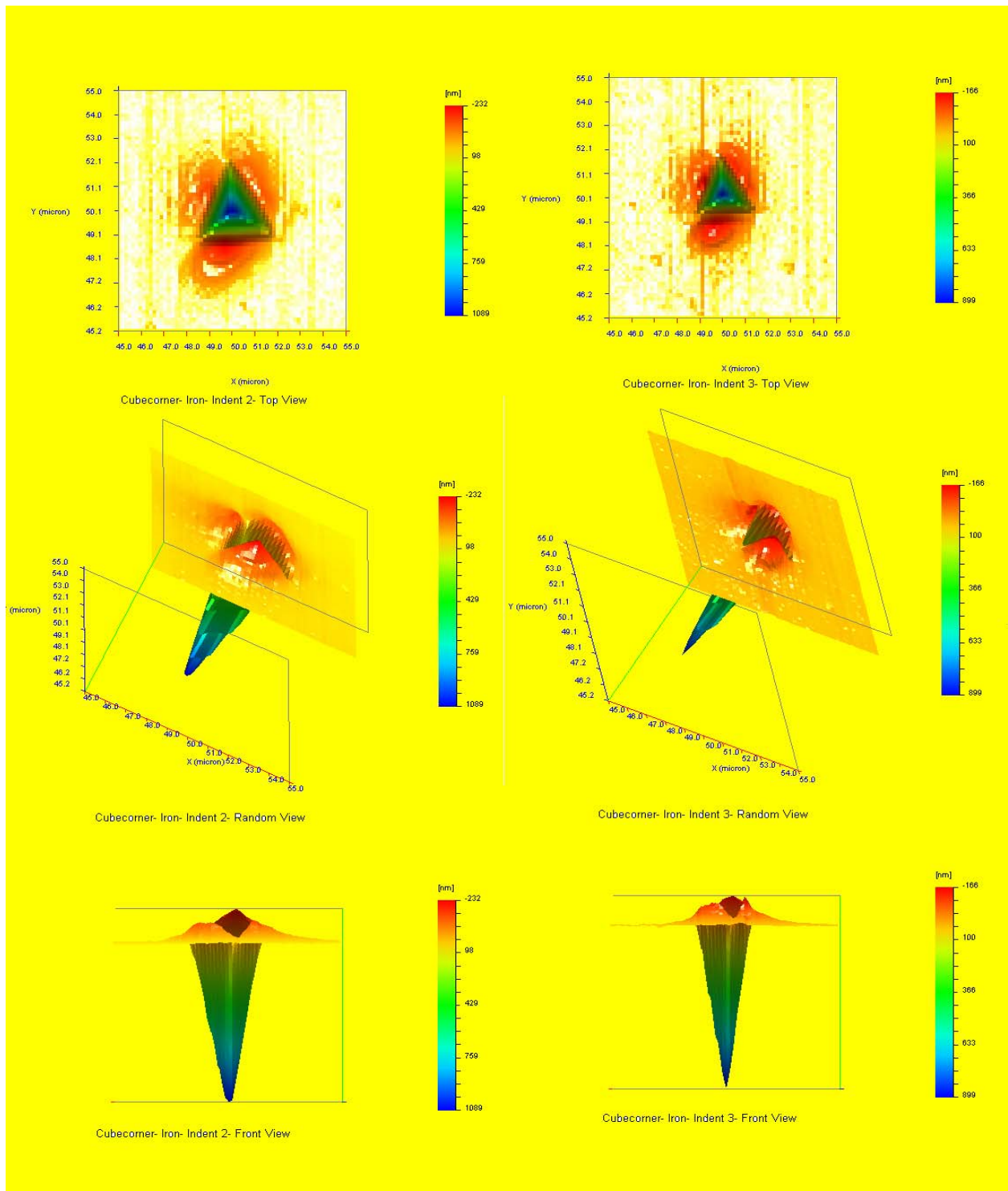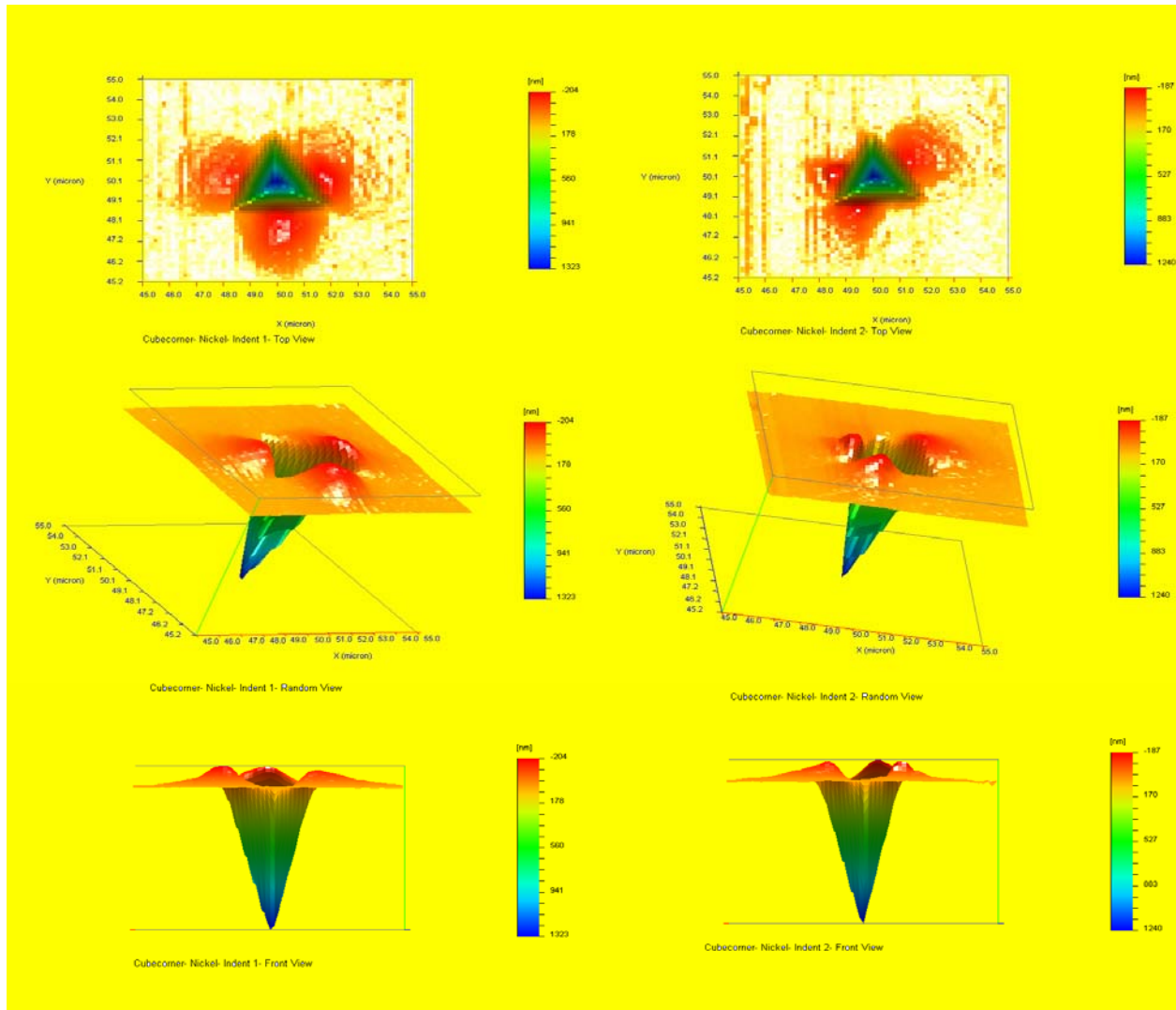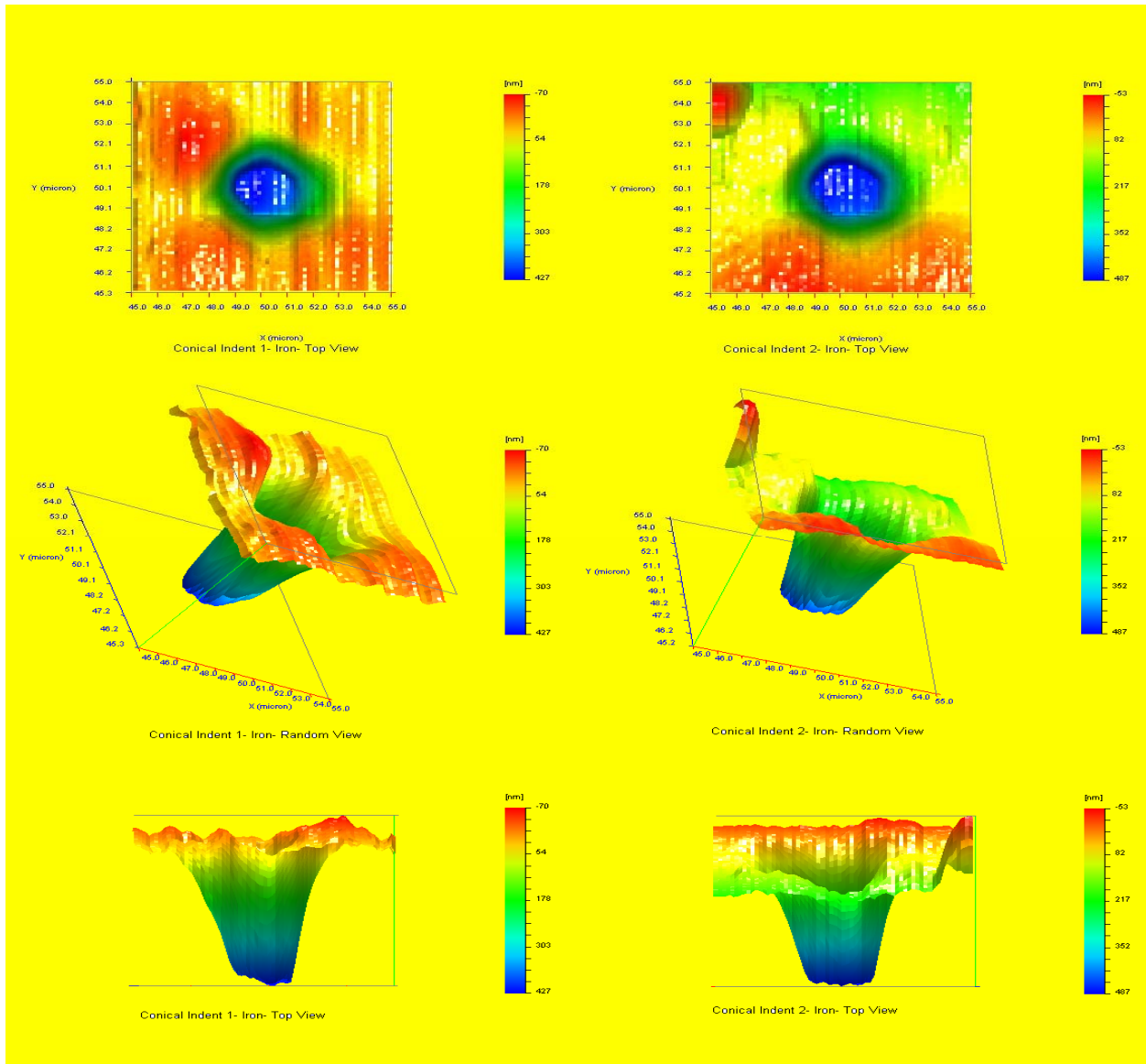Figure 36: Top to bottom, top, random and front three dimensional view of conical indentations on iron.
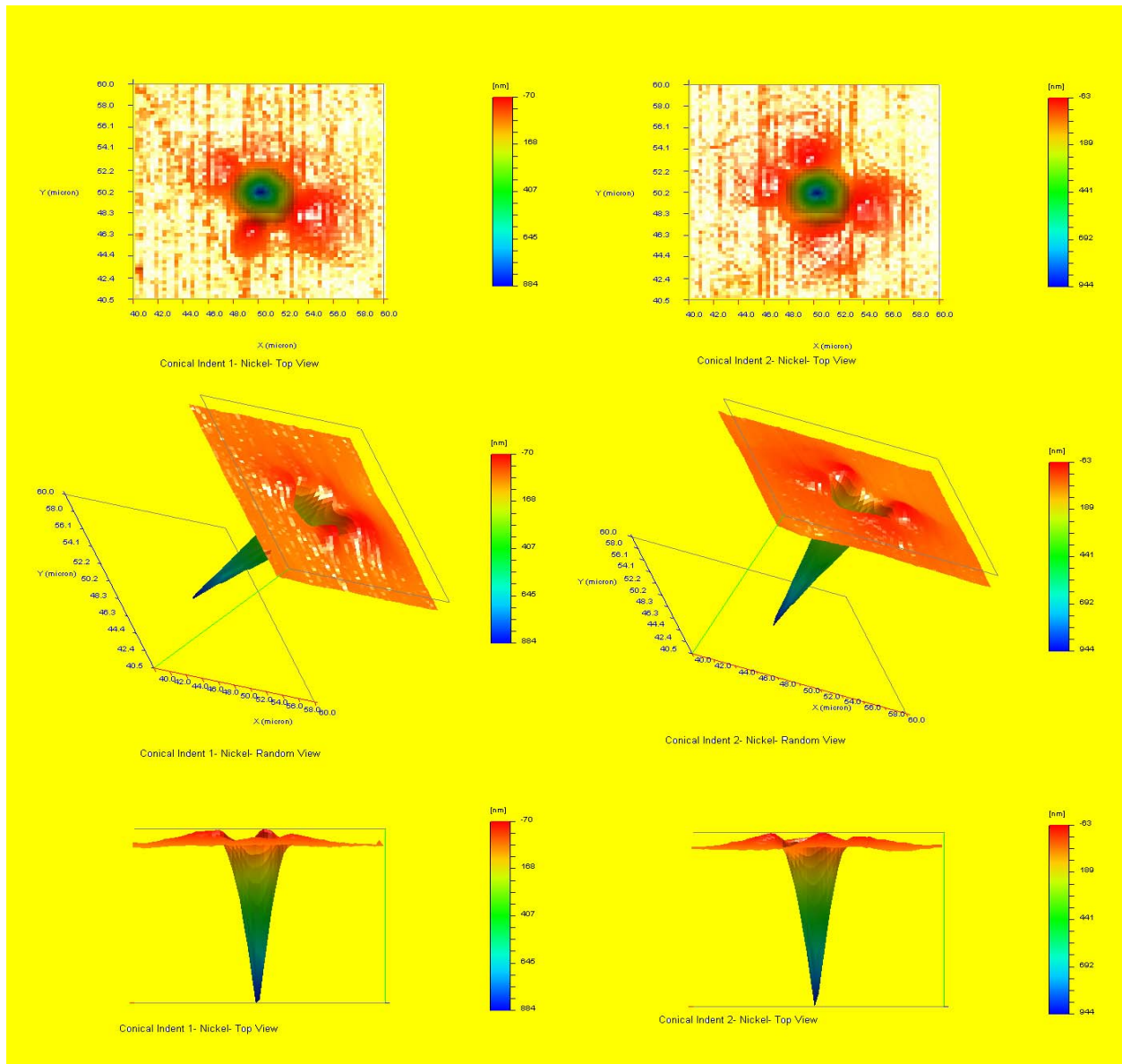
Figure 37: Top to bottom, top, random and front three dimensional view of conical indentations on nickel.

Conical indentations expose the crystal anisotropy [2,28], which could be seen in form of pile-up lobes. In some cases conical indentations form uniform rings around the indent because of their symmetry. These are sharp and produce high plasticity which could be seen through small indent diameter and pronounced pile-up behavior.

4.5 EBSD Pictures of Berkovich Indents on Iron
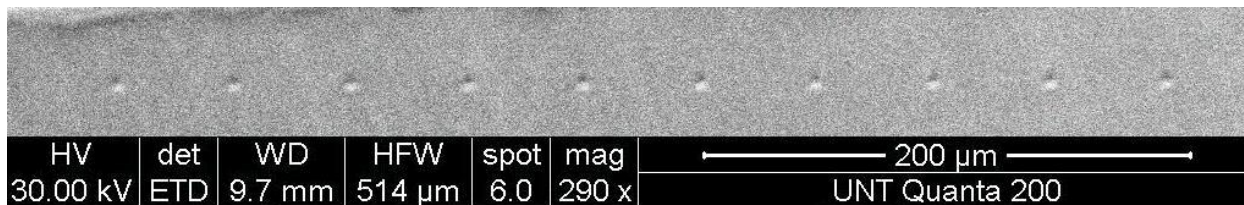
Figure 38: Scanning electron micrograph of Berkovich indentations on iron. Spacing between these indentations was kept at 50 microns to avoid interaction of respective plastic zones of indentations.
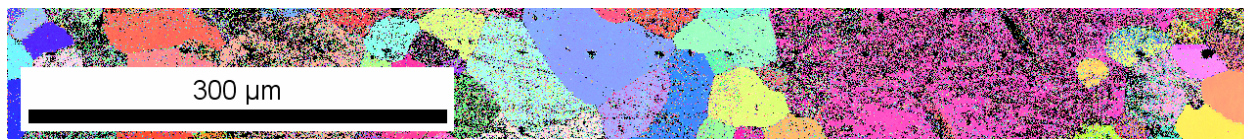
Figure 39: Electron back scattered diffraction image of Berkovich indentations on iron revealing different crystallographic orientations for different indentations. First indent from right is indent number 1 as per SEM image.
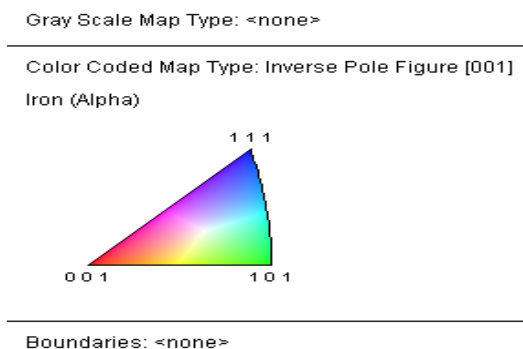

Figure 40: Orientation color code scheme for the EBSD image of Berkovich indents on iron.

4.6 Pile-Up Measurement through Nanovision Traceline Method

All the pile-ups were measured using the Nanovision traceline method specially devised for the Nanovision indent and scan displacement method and indent and scan load limit method. The traceline envelopes the scan area along a thin line of 0.2 micron width. This line could be moved along the surface by changing the

profile number which is the reading on the Nanovision sheet for the indenter displacement in the X direction. This when varied, touches the indent along the Y direction. The 2 dimensional cross sectional view can be seen by switching to the 2 D graph and pile-up heights can be measured by selecting the Y axis channel to be the scan profile or the z axis. A measurement of these different profiles pile-ups is depicted below in the graphs shown.

4.6.1 Pile-Up Measurement for Berkovich Indentations

Figure 41: Pile-up measurement for Berkovich indentations on nickel.

Figure 42: Pile-up measurement for Berkovich indentations on copper.

Figure 43: Pile-up measurement for Berkovich indentations on iron.

4.6.2   Pile-Up Measurement for Cube Corner Indentation

Figure 44: Pile-up measurement for cube corner indentations on nickel.

Figure 45: Pile-up measurement for cube corner indentations on copper.

Figure 46: Pile-up measurement for cube corner indentations on iron.

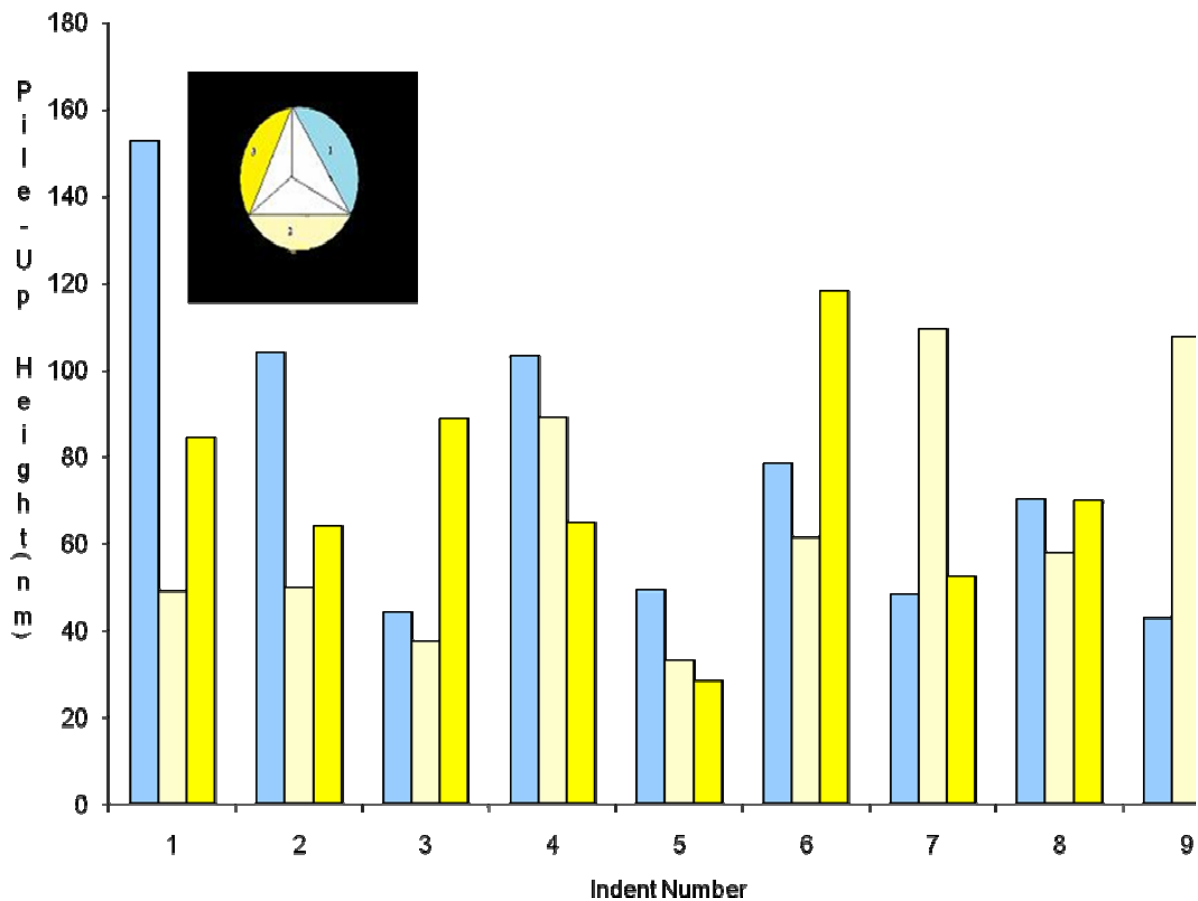4.6.3 Pile-Up Measurement for Conical Indentations

.

Figure 47: Pile-up measurement for conical indentations on nickel.

Figure 48: Pile-up measurement for conical indentations on copper.
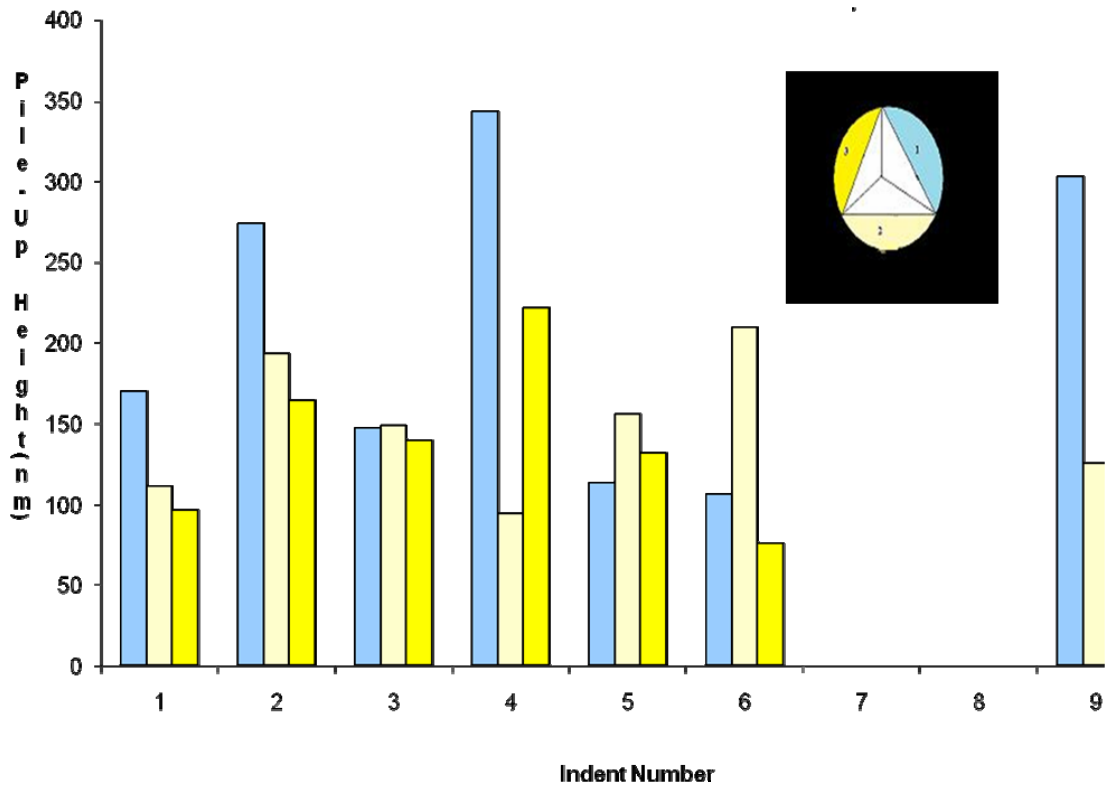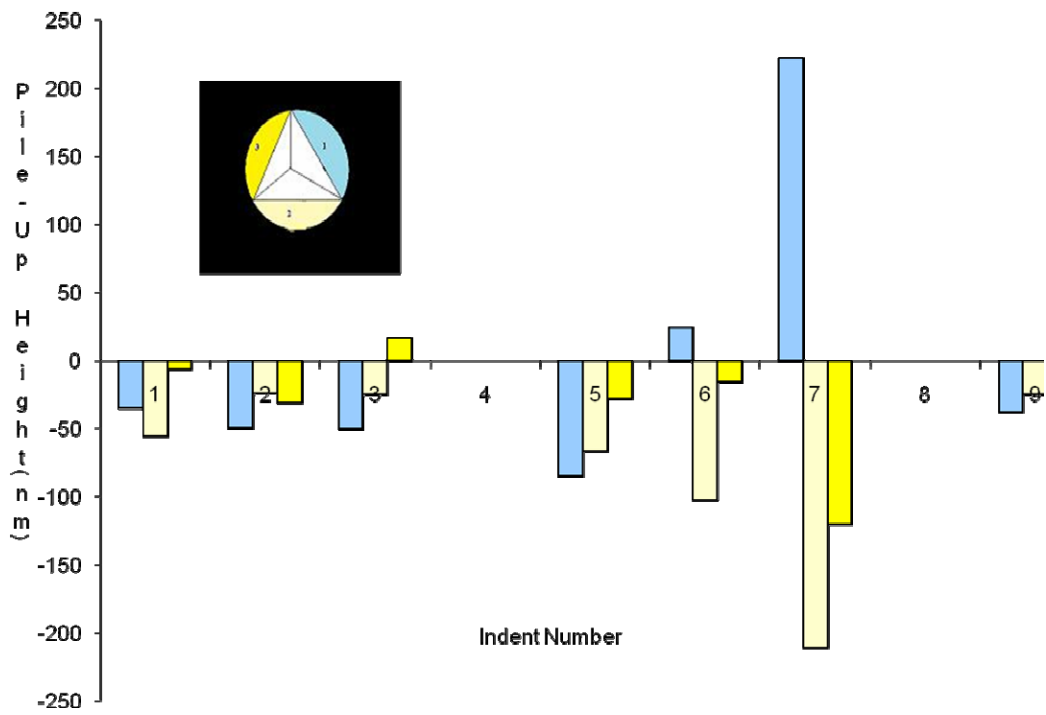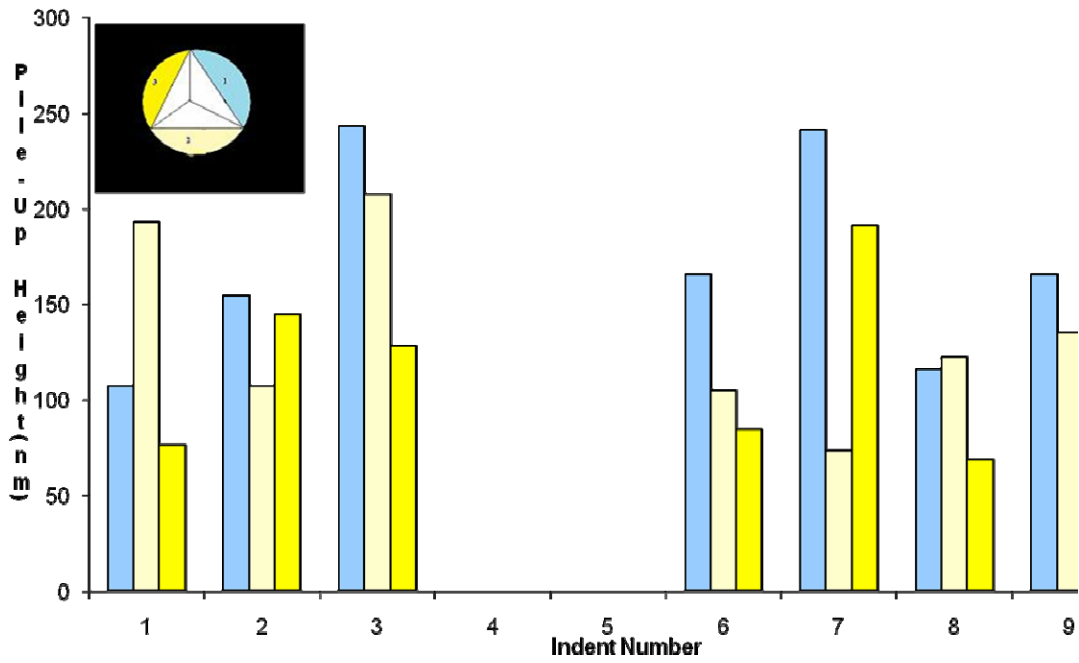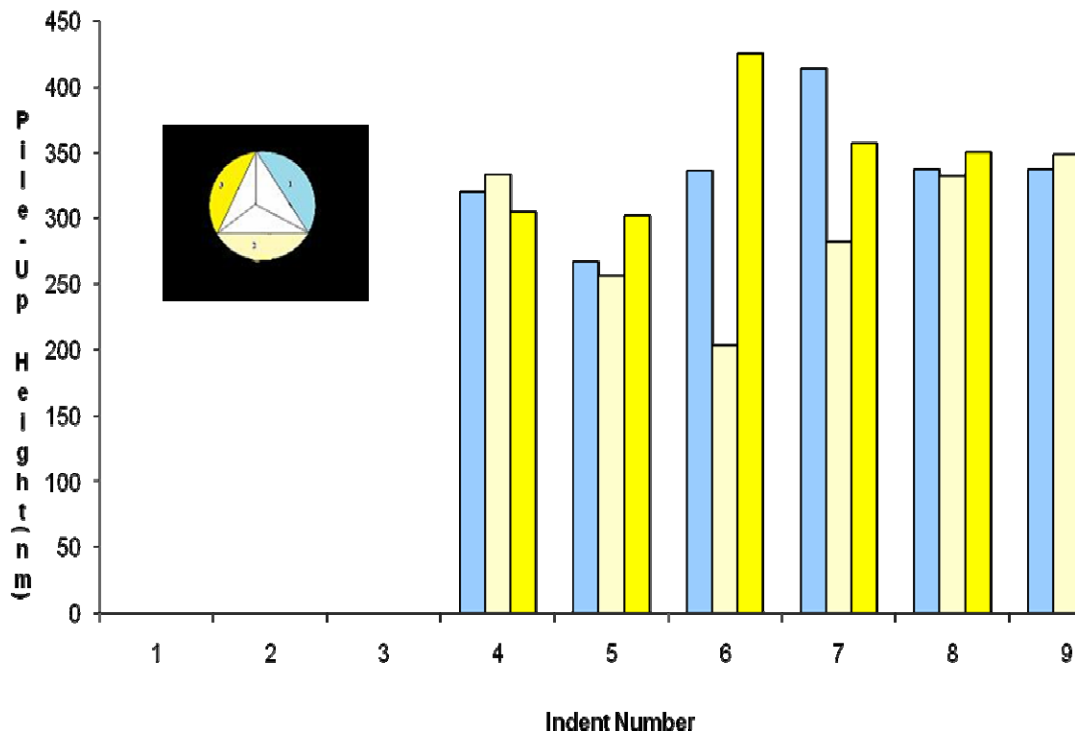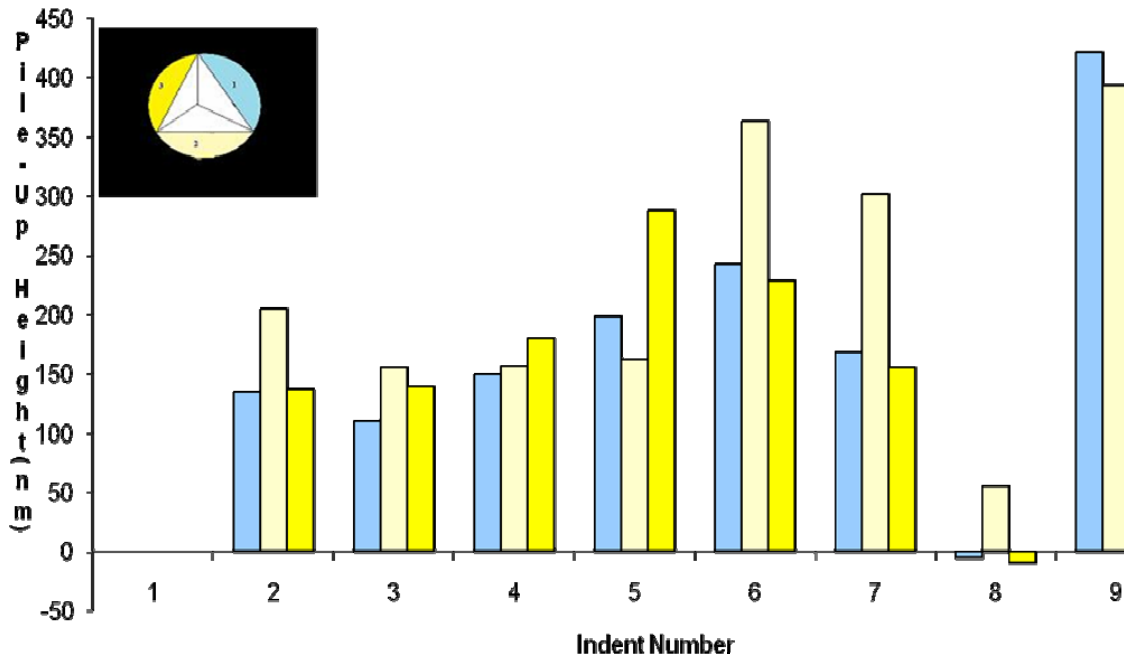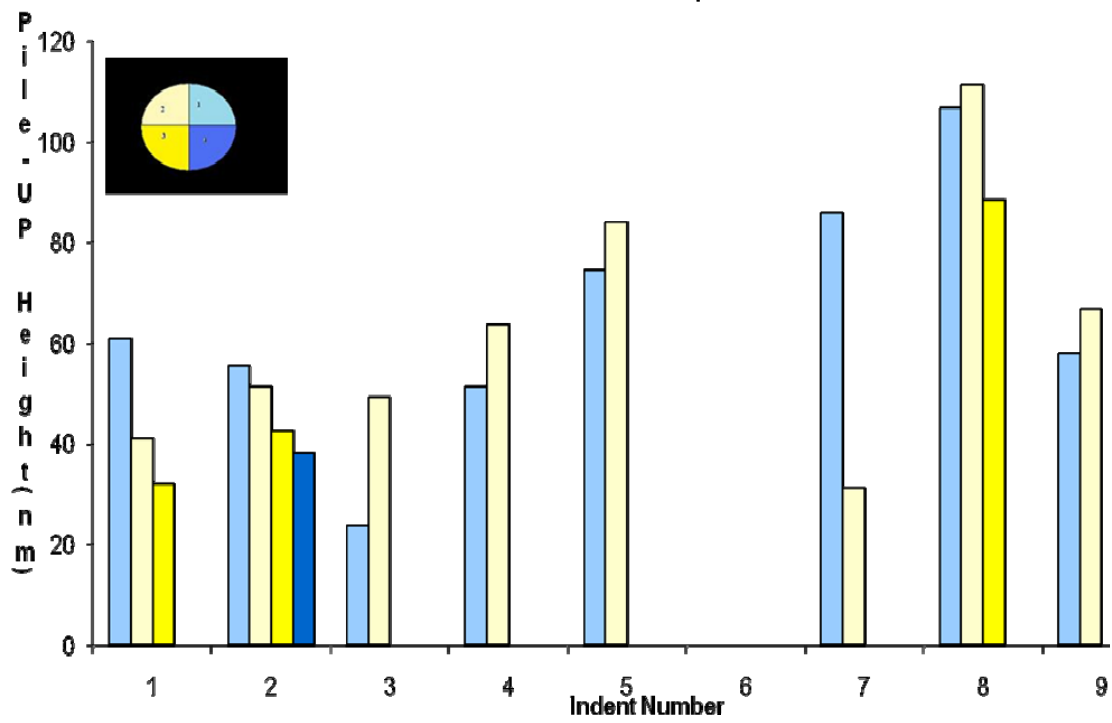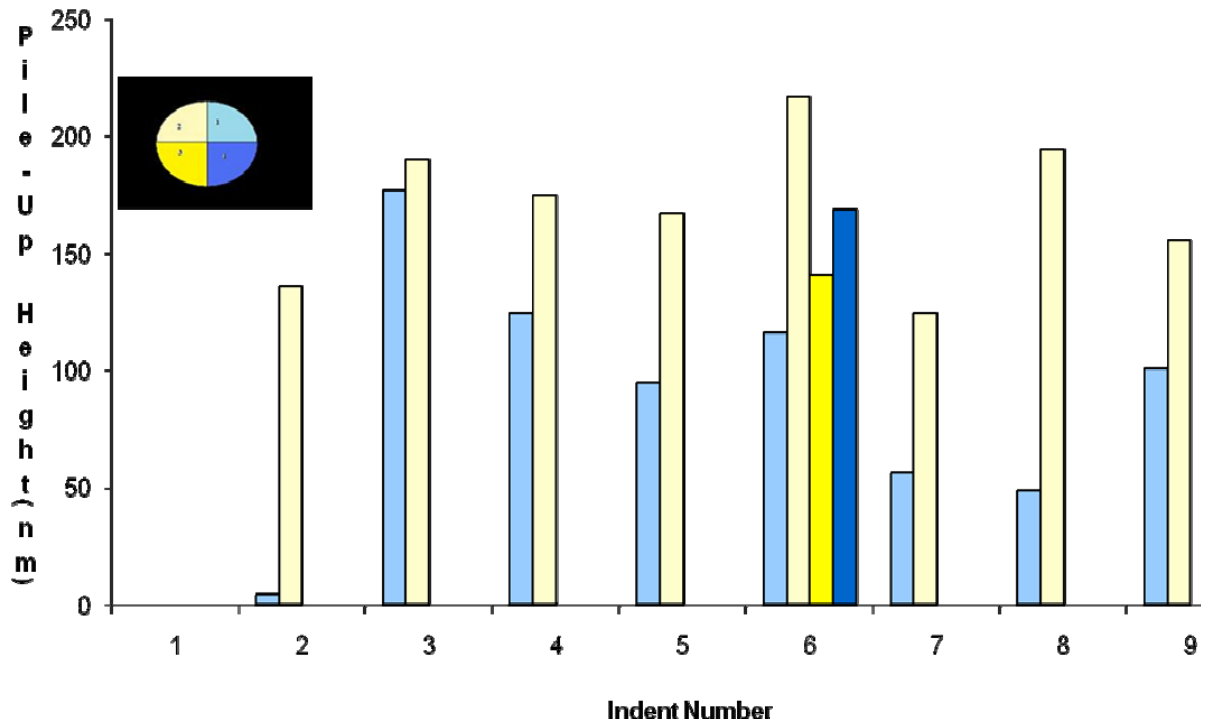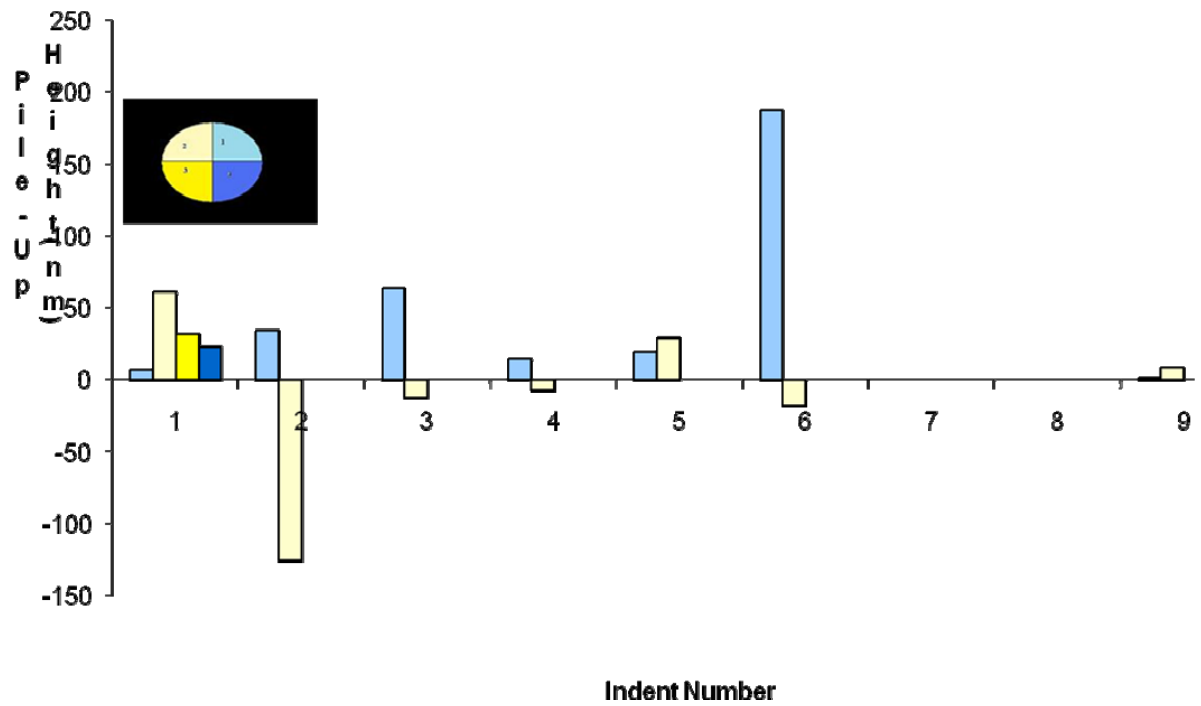

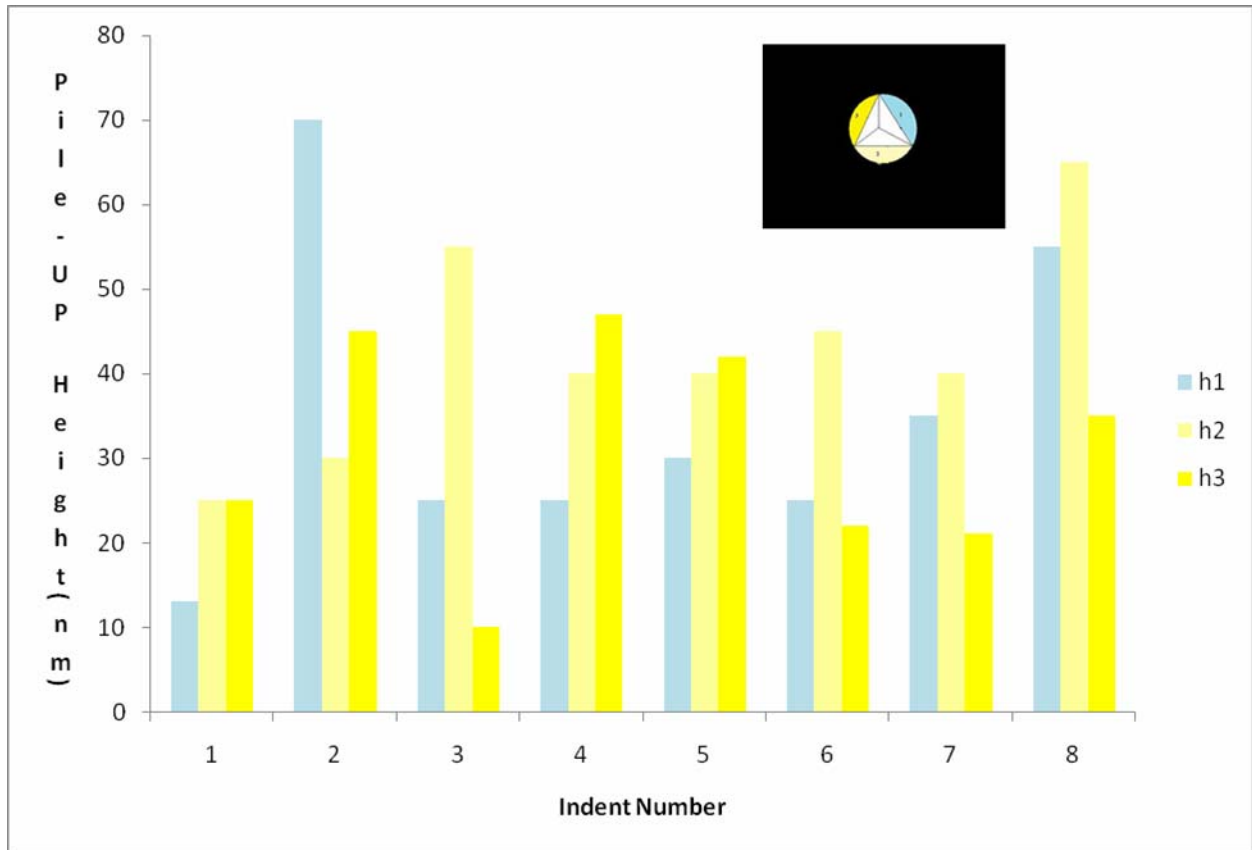Figure 49: Pile-up measurement for conical indentations on iron.

Figure 50: Pile-up measurement for Berkovich indentations on iron for the EBSD matrix.

CHAPTER 5

DISCUSSION

Different kinds on indenters impose different sets of stresses due to their inherent geometry. This is apparent in the different elastic modulus and hardness values for the same material with different indenters.

5.1   Tip Wise Comparison

As discussed in earlier section, three materials were chosen to span a variety of material behavior, with differing stacking fault energies, Poisson's ratio, elastic modulus, hardness ad different crystal structure categories. A clear trend in these values is seen, which is in accordance with literature [7]. For Berkovich indentations, nickel is the hardest material, followed by copper and iron. This is by far the accepted trend in values for these materials. However, for cube corner and conical indentations, this trend differs between iron and copper. Their hardness values are quite close for cube corner and conical indents. This could be attributed to the low stacking fault energy in copper providing easy shear, high plasticity and hence low hardness for copper. For iron, a lack of truly close packed plane could be a reason observed low hardness. The difficulty of propagation of dislocations in iron or in body centered cubic (BCC) metals in general could be another explanation for this behavior. The difference in the maximum and minimum values for these parameters is quite close, with the exception of some indents for which the hardness values are low or high from the average. This can be attributed to grain boundary indentations, which are discussed in greater detail later in this section for iron. This constancy in values of maximum and minimum hardness suggests that

irrespective of the nature of stress imposed, the material has a certain behavior which is the same. The individual values are different but on a larger scale, these values tend to be average out with a general trend closely resembling the macroscopic values for these materials, with nickel being the hardest material, followed by iron ad copper respectively. For elastic modulus though, the trend seems to be different, with nickel and iron tending to overlap to a greater extent in the values with copper lagging behind. This can be attributed to the high amount of elastic recovery for iron and nickel, followed by the high plasticity in copper, which essentially keeps its elastic modulus values to be low. The low elastic recovery in copper can again be attributed to the low stacking fault energy, low shear strength and hence high deformation potential for copper. This trend seems to be persistent for all three materials when tested with three different indenters of pyramidal and conical stress distributions.

A tip-wise comparison of elastic modulus and hardness is given below.

Figure 51: Hardness comparison for Berkovich indentations on copper, iron and nickel.
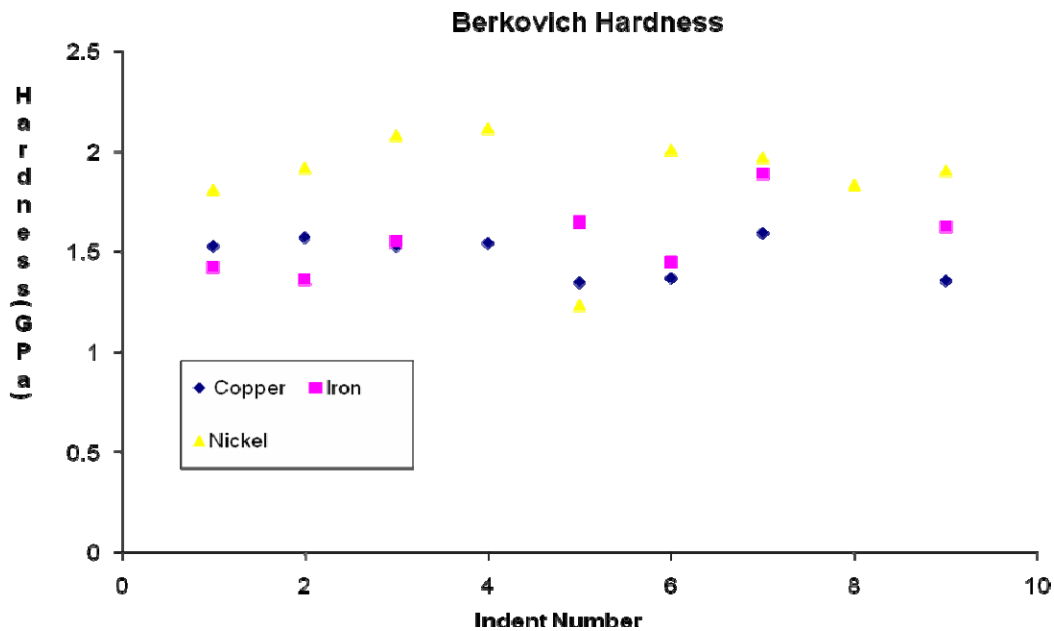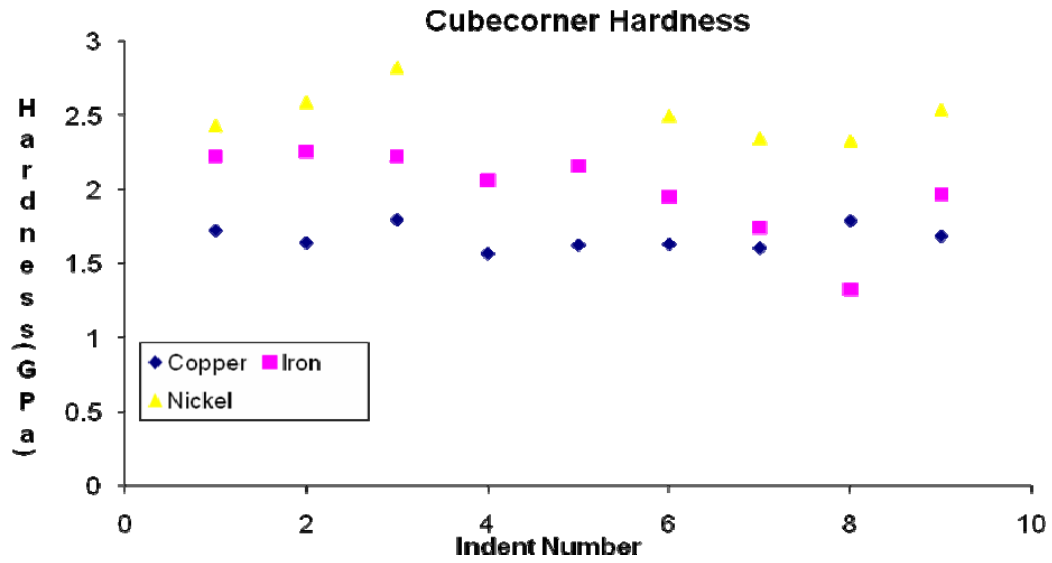
Figure 52: Hardness comparison for cube corner indentations on copper, iron and nickel.
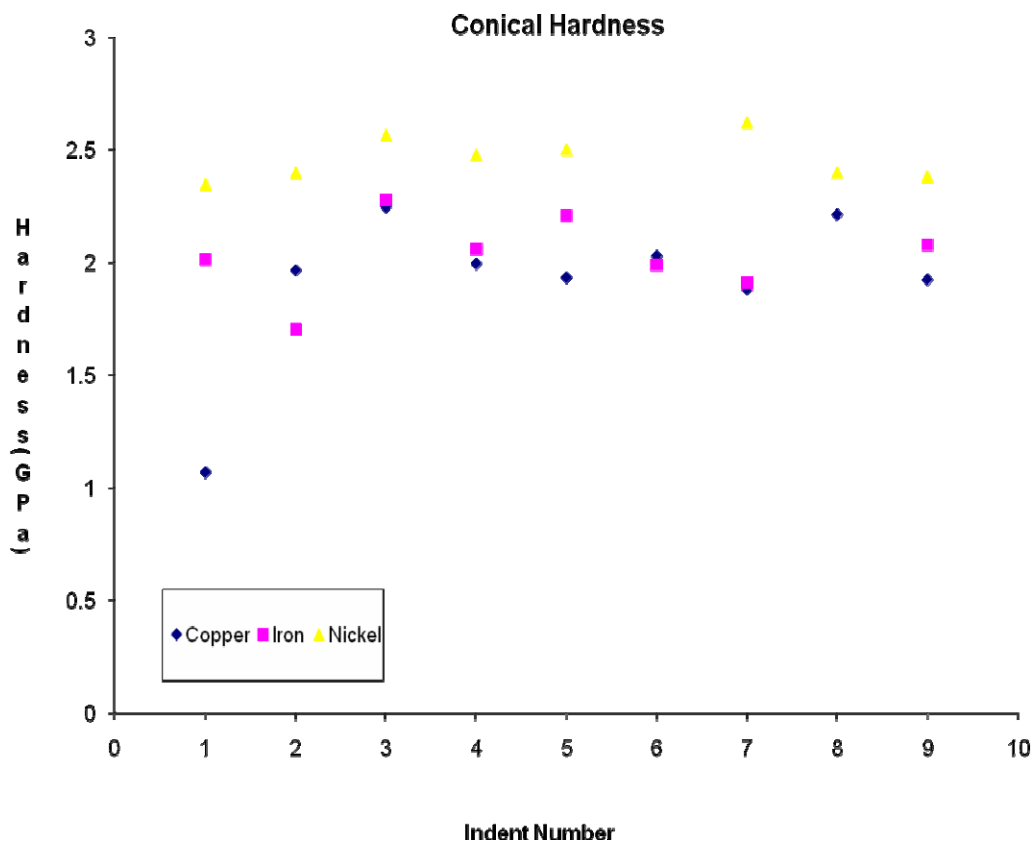

Figure 53: Hardness comparison for conical indentations on copper, iron and nickel.
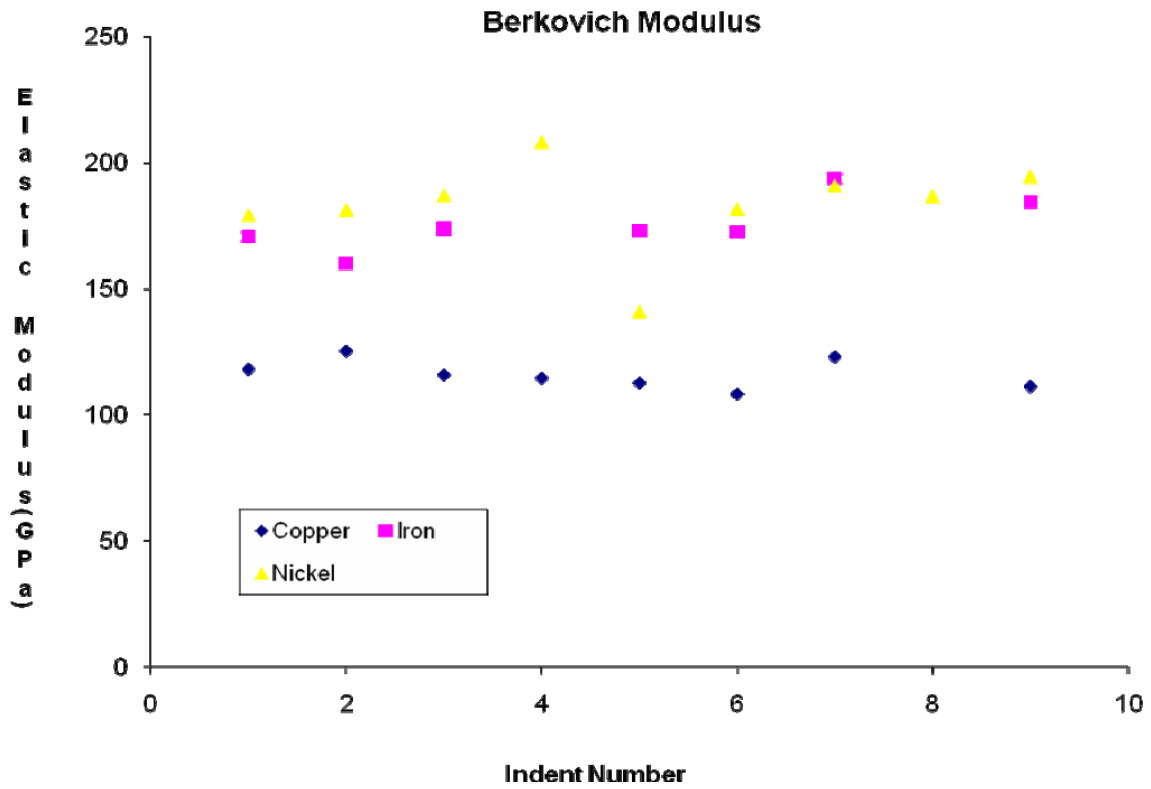
Figure 54: Elastic modulus comparison for Berkovich indentations on copper, iron and nickel.
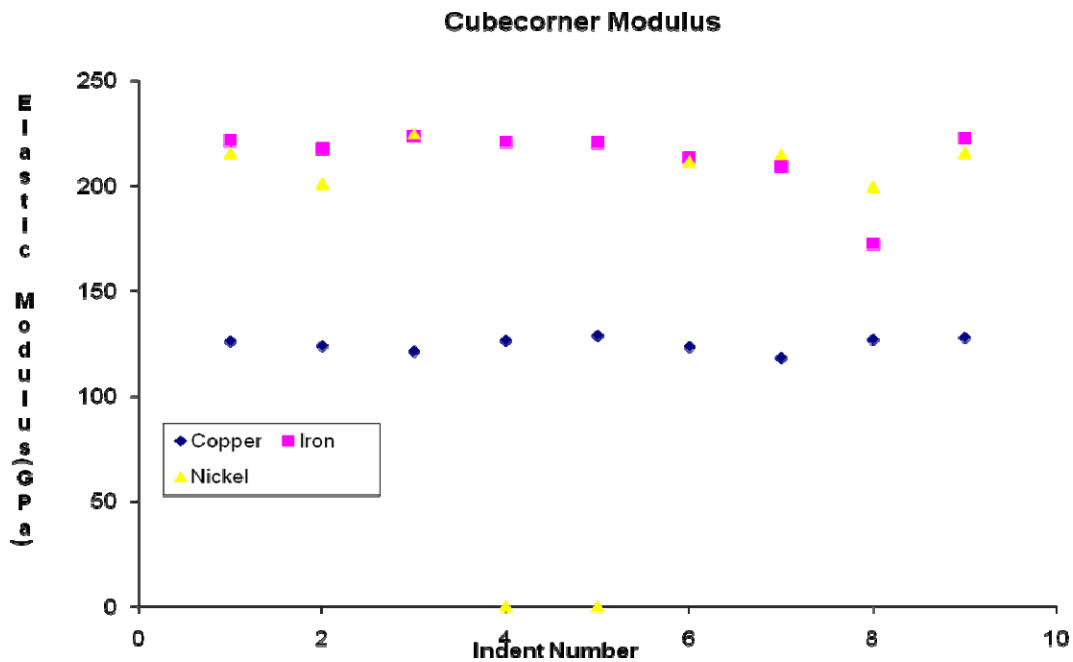
Figure 55: Elastic modulus comparison for cube corner indentations on copper, iron and nickel.
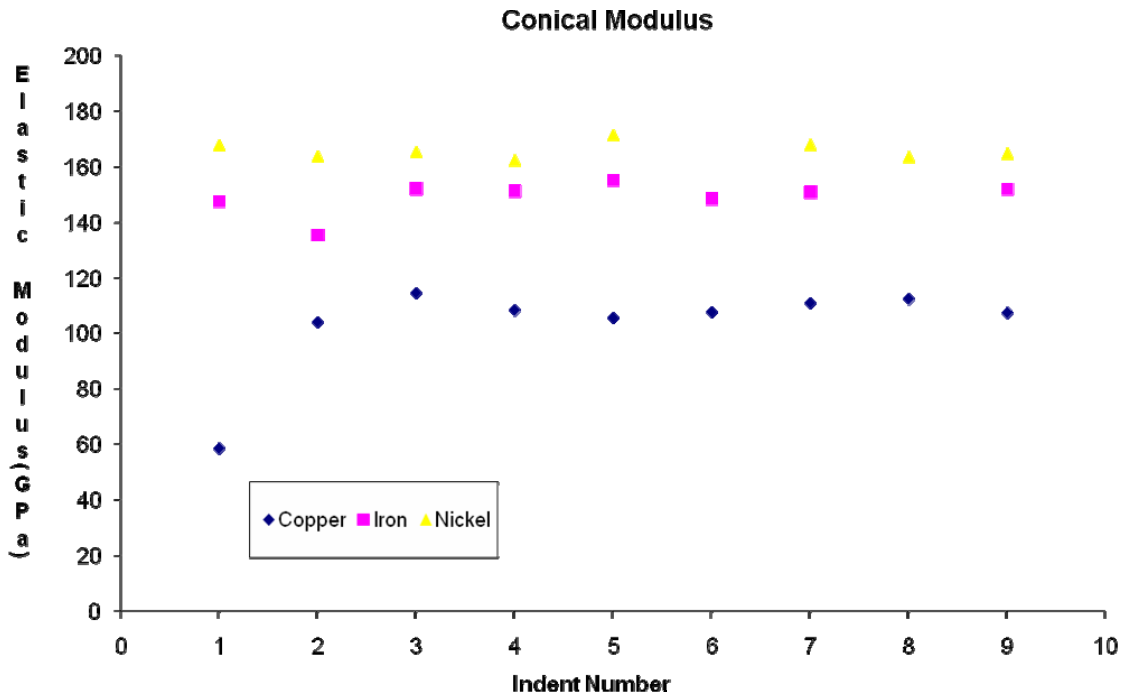
Figure 56: Elastic modulus comparison for conical indentations on copper, iron and nickel.

The above observation can be summarized with copper being the softest and nickel being the hardest material. However, they might exchange places depending on the local material conditions, like the grain boundary effects. However, the general trend seems to agree with the macroscopic values reported in literature [7,25].

5.2 Material-Wise Comparison

A different set of data is however obtained when we compare the behavior of material with respect to the Berkovich, cube corner and conical indenters respectively. The same material, with different sets of stress imposed, tends to behave differently. This could be attributed to the orientation of the indentation plane of the material with respect to the indenter stress imposed. Different orientations have different atomic arrangements and coupled with the shear stress component available

for deformation and the stacking fault energy of the material, they show different behavior. For a given material, the values of hardness and elastic modulus are seen to vary with different indenter geometries. This suggests that the relative orientation of the material and the stress conditions must be taken into account before reaching a value for these mechanical property parameters. Hardness values, depend on the plastic deformation produced, this again relates to the stress intensity at the tip of the indenter. Conical is the sharpest tip, followed by cube corner and the Berkovich. The plastic deformation potential again, follows the same trend for these materials. A similar trend is expected and seen for these materials, with conical and cube corner hardness values exceeding the Berkovich hardness values for all the materials. The relatively blunt tip of Berkovich indenter, produces low plastic deformation as compared to the other tips, conical and cube corner. This results in low contact area for conical and cube corner, while the contact area of the indenter with the material is high for Berkovich. The hardness values are, therefore, lowest for Berkovich and there is an overlap between conical and cube corner for the higher values. This could be because of the tip rounding effects of the conical, which makes it blunt and of comparable contact area relative to a cube corner. In an ideal world, with no tip rounding effect, however, conical hardness would be expected to be the highest, followed by cube corner and Berkovich indentation values. This trend is seen in the values obtained here. For elastic modulus values, however, there is again a reversal in trend. Elastic modulus depends on the elastic properties of the material. The capability of an indenter to produce plasticity beneath it, is inversely proportional to the elastic modulus number that it can generate. Berkovich indenter, being the bluntest of three used in the study, produces lowest deformation,

hence the highest elastic recovery occurs for the Berkovich indents. This is followed by the second bluntest of three indenters, the cube corner followed by the conical. There is, however, an overlap between the top two. This could be attributed to the tip rounding effects for Berkovich and cube corner indenters as well as the local prevailing material conditions at the point of indentation. The cube corner indenter shows the highest amount of elastic recovery here. In a ideal world, however, Berkovich modulus would be the highest, followed by the cube corner and conical thereon. Another interesting feature in this data set is the range of indentations. The entire spread of indent matrix is around 450 microns in X and Y directions. The grain size as determined by EBSD analysis is around 20 microns for iron and nickel. This essentially means that we are sampling a wide variety of grain orientation for a give stress condition. This could be a possible explanation for the difference in values for the same indenter hardness and elastic modulus numbers. This point is further illustrated in a later section on iron, where elastic modulus is calculated based on Hooke's law of elasticity for different orientations. This value shows to be quite different for different crystallographic directions. These values are calculated for three different directions <100>, <111>, <110>, depending on different crystal structures their stiffness values differ quite a bit [Table 15a]. This variation is depicted in the data set below too. This analysis is presented in form of scatter point chart below.
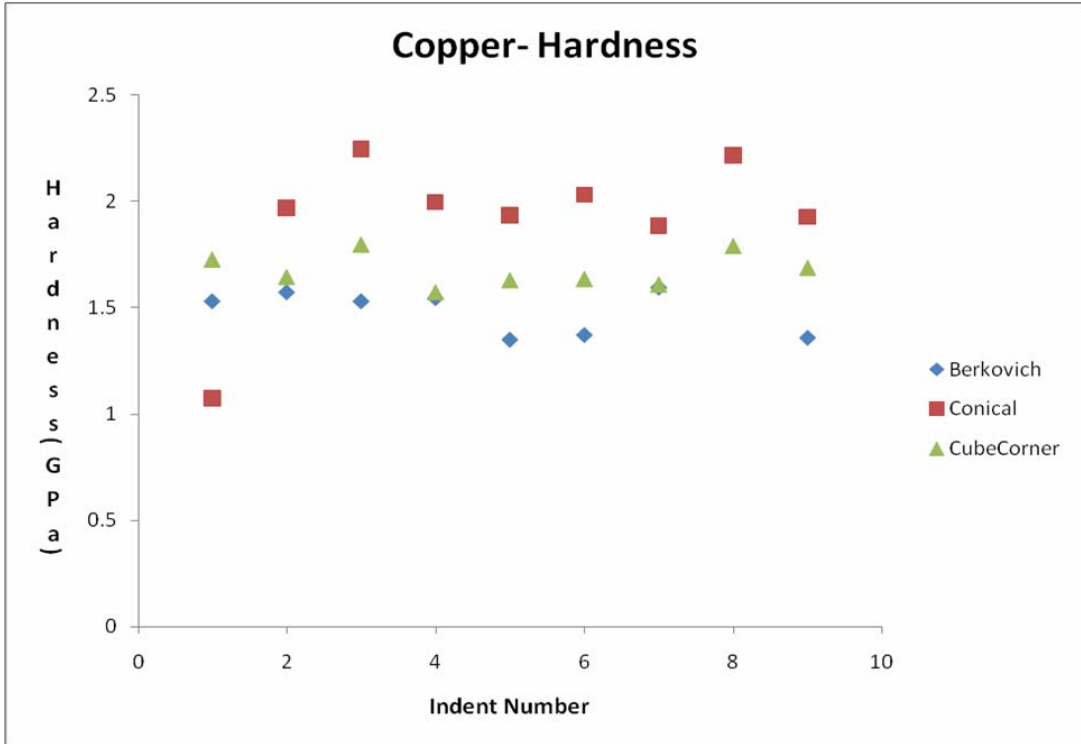
Figure 57: Comparison of   hardness of copper when indented with all three indenters.
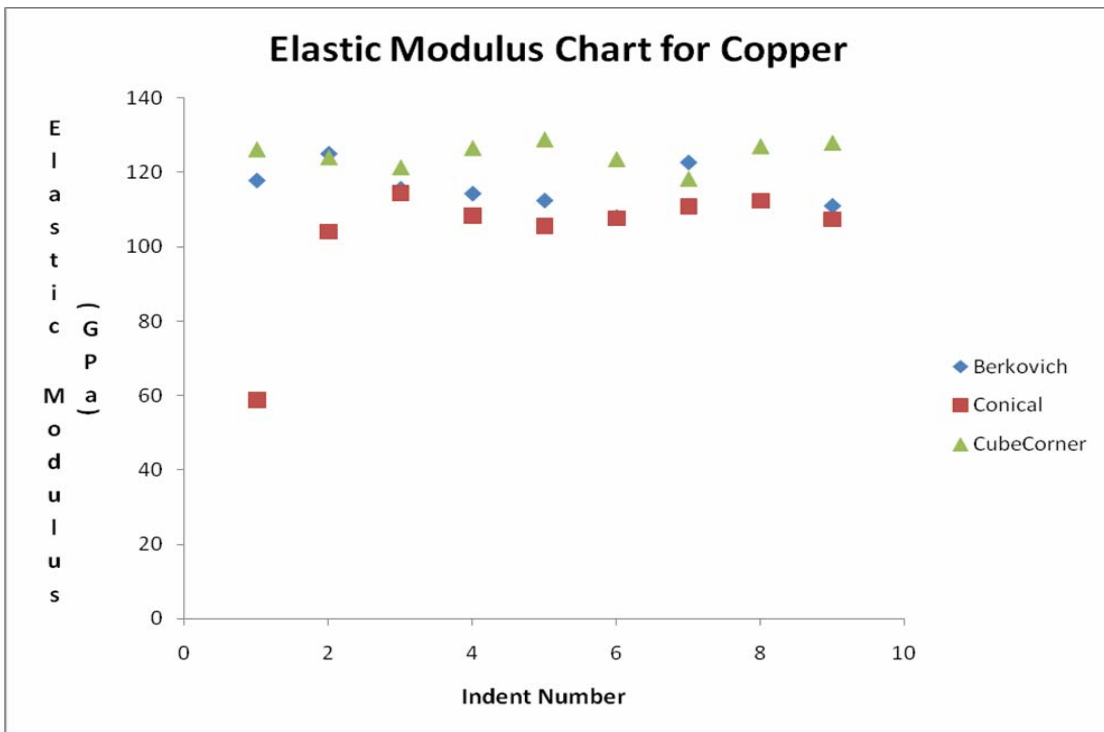

Figure 58: Comparison of elastic modulus of copper when indented with all three indenters.
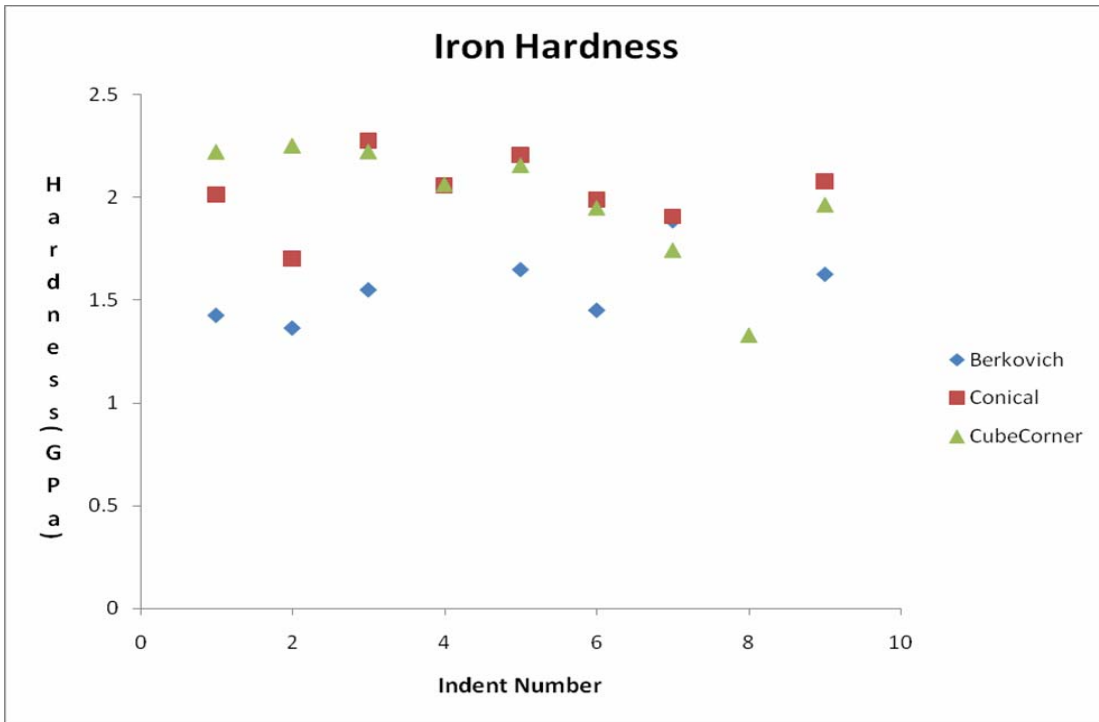
Figure 59: Comparison of hardness of iron when indented with all three indenters.
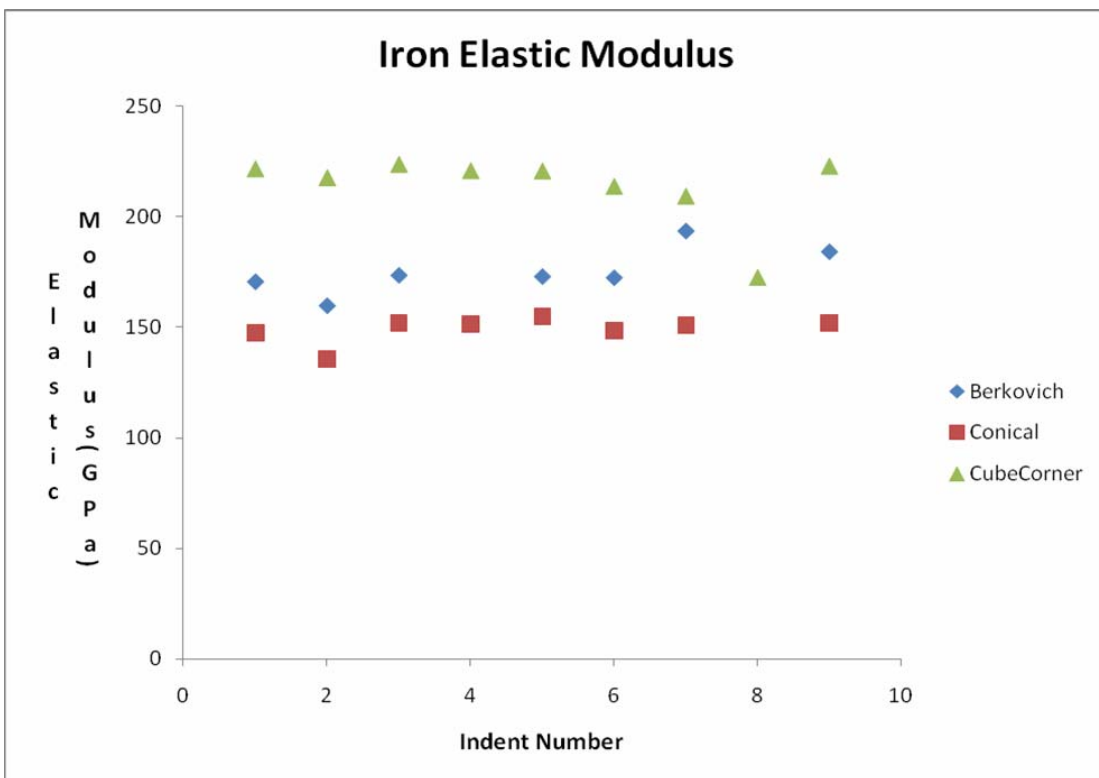

Figure 60: Comparison of elastic modulus of iron when indented with all three indenters.
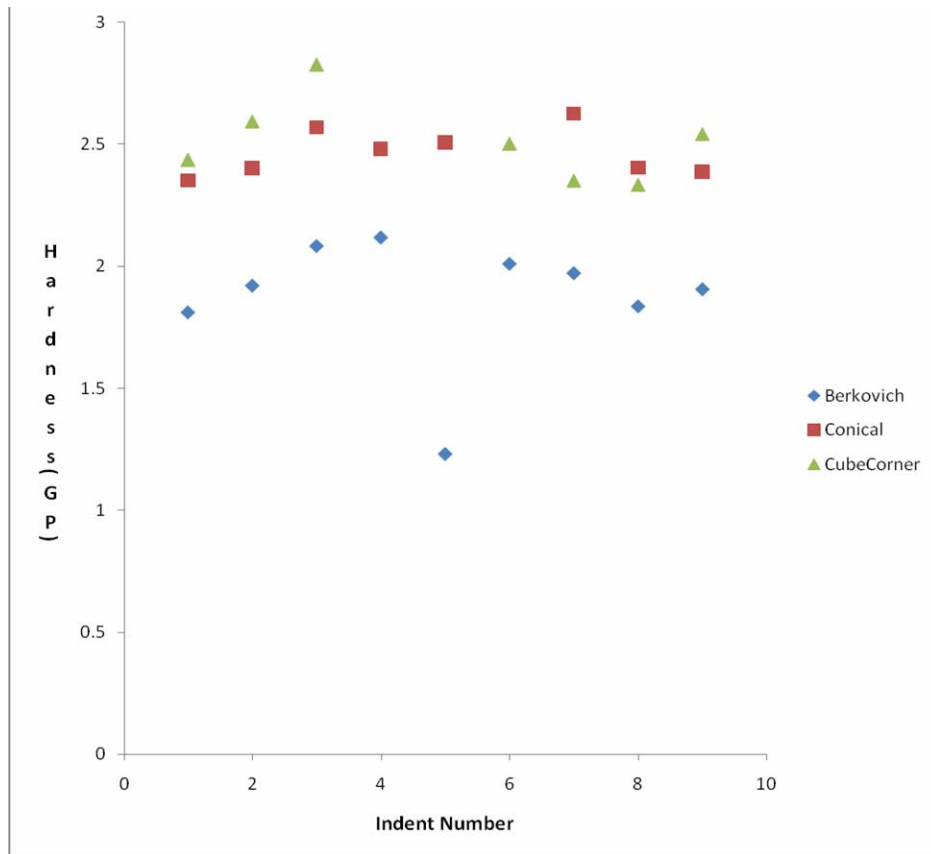
Figure 61: Comparison of hardness of nickel when indented with all three indenters.
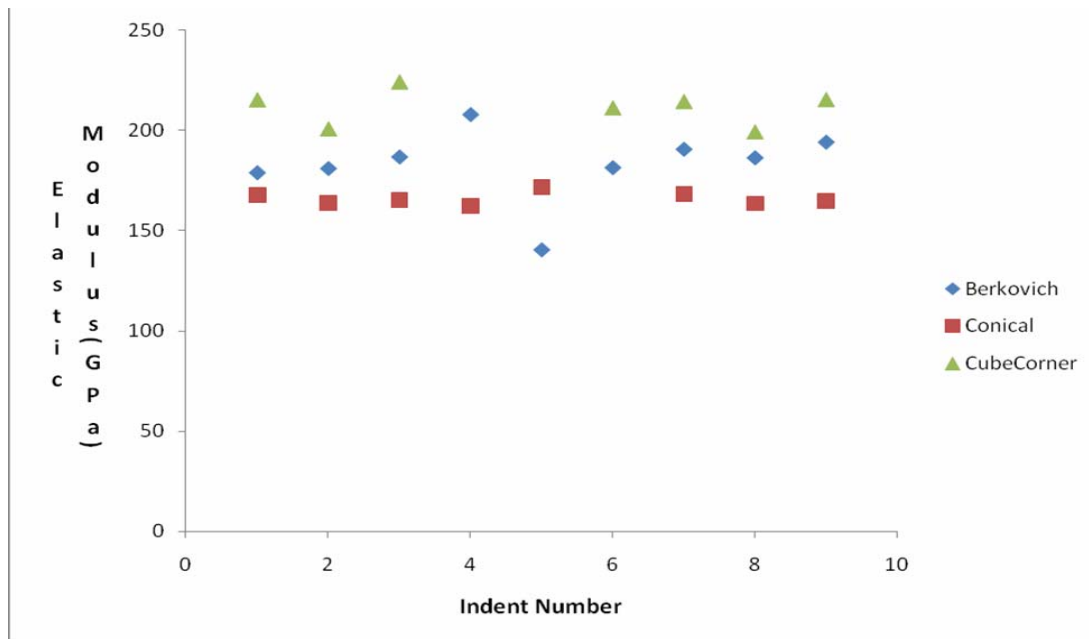

Figure 62: Comparison of elastic modulus of nickel when indented with all three indenters.

Overall, the elastic modulus and hardness values show reversing trends. This is due to the difference in indenter geometry. For hardness values, the indenters capable of producing highest deformation have the lowest contact area, hence the highest hardness value. For elastic modulus though, the indenters which are the bluntest and capable of producing the lowest deformation, lead to high amount of elastic recovery of material, hence a high value of the elastic modulus. Data presented above is derived from the basic Oliver and Pharr approach. However, due to various pile-ups coming into contact with the indenter, the contact area deviates from the ideal contact area employed in the Oliver Pharr relations.

5.2.1 Pile-Up Area Calculation

The pile-ups and sink-ins change the ideal area of contact with the indenter, which is derived from the geometry. This results in the contact area over and underestimation, leading to inaccuracies. Several methods are devised to calculate this overestimation. One of the most popular methods is the semi-ellipse method for Berkovich indenter. Calculation and relations for the cases of cube corner and conical indentation contact area overestimation are still not in the literature. We have extrapolated here the relations for Berkovich indenter for the case of cube corner indenter and have devised a new method for conical indentations as discussed below.

5.2.1.1   The Semi-Ellipse Approximation for Pyramidal Indenters
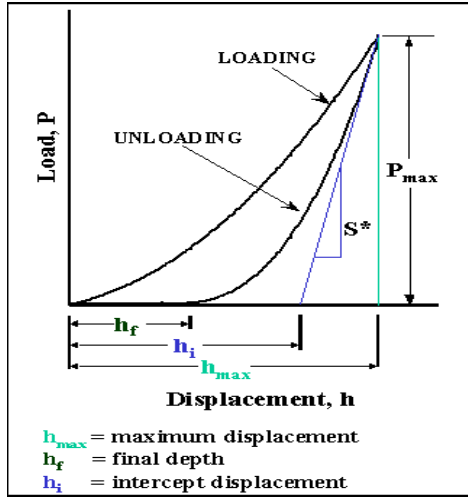
$$h_c = h_{max} - \varepsilon \left(\frac{P_{max}}{S} \right)$$

$$\varepsilon_{berkovich} = 0.75$$

$$\varepsilon_{cubecorner} = 0.75$$

$$\varepsilon_{cone} = 0.727$$

Figure 63: Typical load displacement curve for nanoindentation [3].

The Oliver-Pharr contact area is given by the following relations for Berkovich, cube corner and conical indenters respectively.

$$\text{Berkovich: A=24.56 } h_c^2 \quad (1)$$

$$\text{Cube corner: A=2.60} h_c^2 \quad (2)$$

$$\text{Conical: A=1.047} h_c^2 \quad (3)$$

The cylindrical punch as discussed earlier [1], could be summarized in the mathematical relation stated below [5].

$$E_{eff} = \frac{\sqrt{\pi}}{2\beta} \frac{S}{\sqrt{A}}$$

Above relation can be used to calculate the hardness and elastic modulus as follows [5],

$$\frac{1}{E_{eff}} = \frac{1 - v^2}{E} + \frac{1 - v_i^2}{E_i}$$

$$and$$

$$H = \frac{P_{max}}{A}$$

where H and E_{eff} are the hardness and the elastic modulus respectively.

The front cross section and the radial view of one pyramidal indent is shown below.
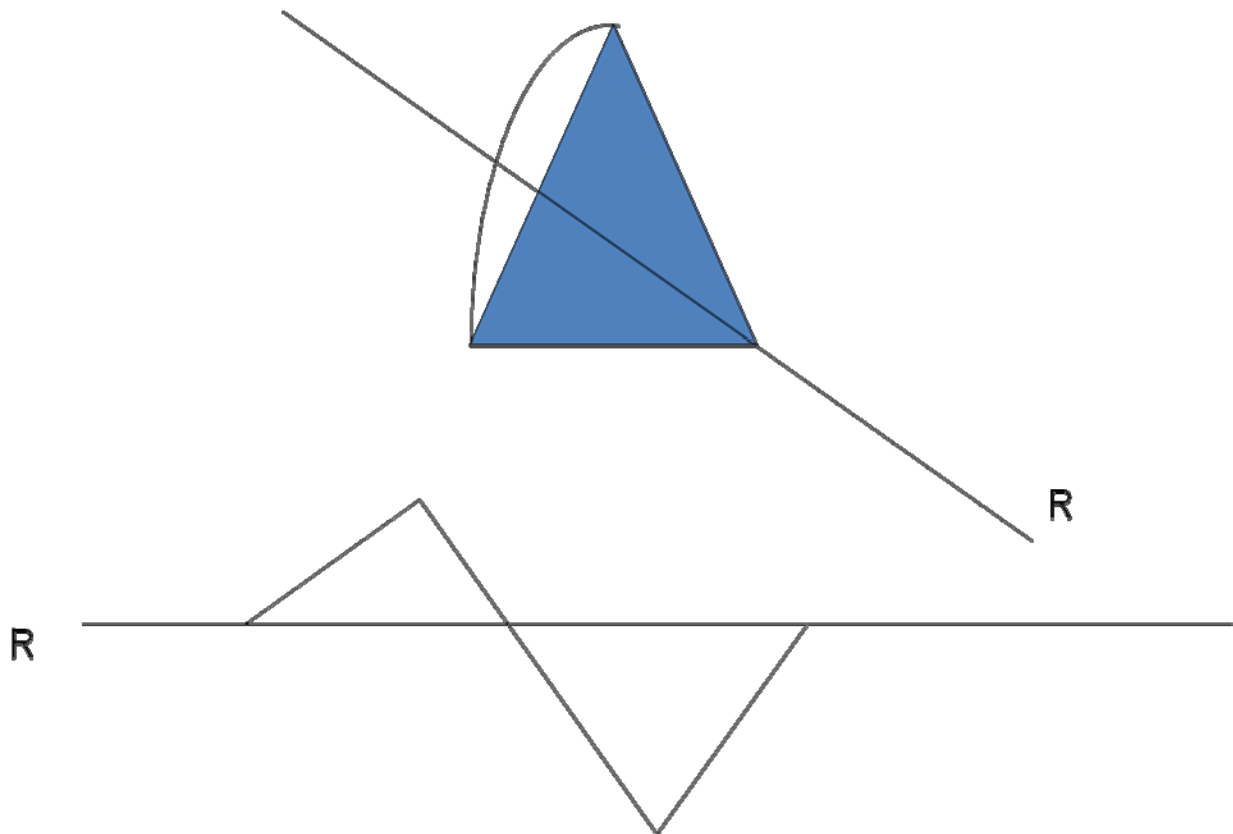

Figure 64: R-R radial cutting through the indent and the projection showing the pile-up contact area and pile-up height of the indent [22].

The true contact area is given by the sum of the Oliver Pharr area and the pile-up area as follows,

$$A_{true} = A_{O-P} + A_{PU}$$

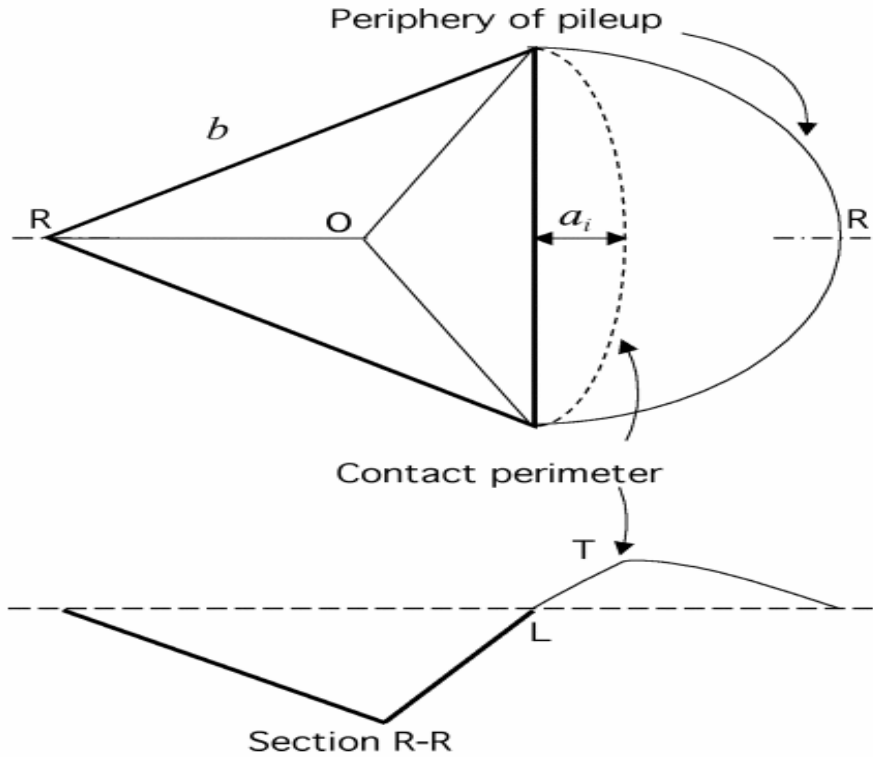The pile-ups are approximated as semi-ellipses for the pyramidal indenters [22].

Figure 65: The semi- ellipse approximation schematic, a is the contact perimeter, used for contact area calculations, while the vertical projection of section LT is the pile-up height. b is the side of the indent, which depends on the indenter geometry and the depth of indentation [22].

Berkovich and cube corner are both pyramidal indenters. The side of the indent as shown in the figure above could be defined as follows,

Major axis (b) for Berkovich indenter, $b=7.531h_c$

Major axis (b) for cube corner indenter, $b=2.45h_c$

Similarly, area difference for Berkovich could be given as,

$$\Delta A = A_T - A_{O-P} = 1.923 h_c \sum a_i$$

And for cube corner, we could summarize the pile-up area mathematically in a similar fashion as follows,

$$\Delta A = A_T - A_{O-P} = 1.923 h_c \sum a_i$$

5.2.1.2   The Semi-Ellipse Approximation for Conical Indenters

Indentations with conical indenter are different with pyramidal indenters. The two kinds of behavior that were observed while indenting where formation of 1) uniform pile-up and 2) discrete pile-ups. In case of uniform pile-ups, a homogeneous ring of contact was assumed around the indenter. In case of discrete pile-ups, different pile-ups were assumed as ellipses due to the nature of the contact of discreet pile-ups around the indenters.
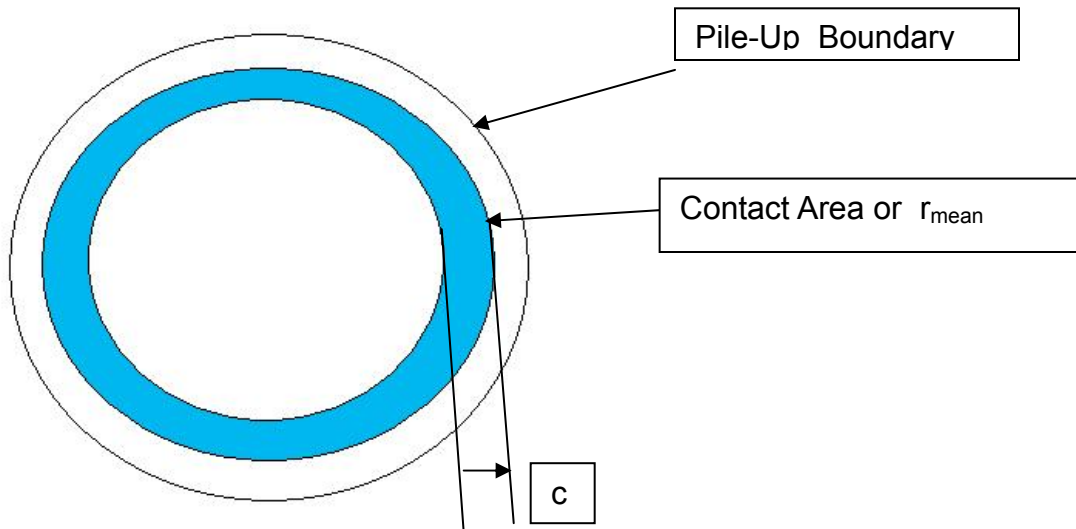
Figure 66: Schematic of homogeneous pile-up area around a conical indent, c is the contact radius between the indenter and the material in case of homogeneous pile-up formation of conical indentations. It defines the contact area. Pile-up boundary is the overall pile-up spread around the indent. This assumption is based on the fact that there is a continuum of bulk material.
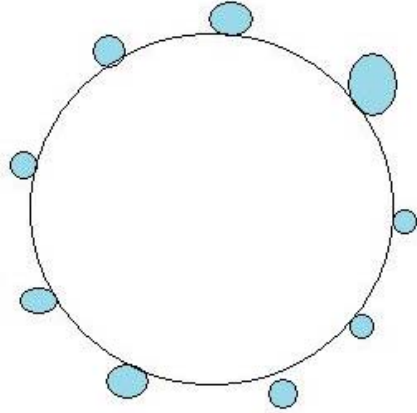
Figure 67: Schematic representation for pile-up in case of discrete pile-ups. Discrete pile-ups are shown as individual lobes around the general big circle, representing the conical indent. This assumption is based on the fundamentally discrete structure of the polycrystalline bulk material.

For the case of uniform pile-up, area difference could be mathematically represented as,

$$\Delta A = A_T - A_{O-P} = \pi (r_{mean} - 0.57 h_c)^2$$
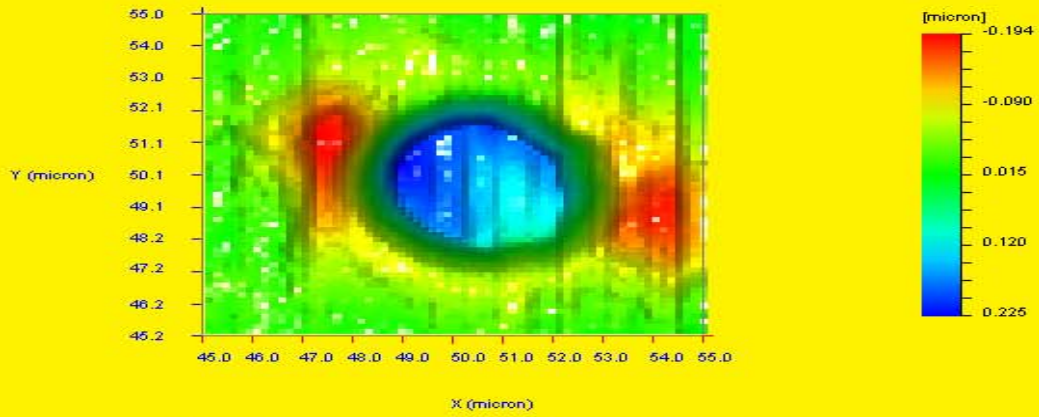
where, r_{mean} is the radius of pile-up ring around the indent.

For the case of non-uniform pile-up , area difference could be mathematically represented as,

$$\Delta A = \pi b \sum_i a_i$$

where a_i is the radius of the ith discreet pile-up and b is the major diameter.

5.3   Nanovision Profiles of Symmetrical Pile-Up Behavior

The symmetry behavior in pile-ups was observed and is portrayed in form of Nanovision™ profiles shown below.
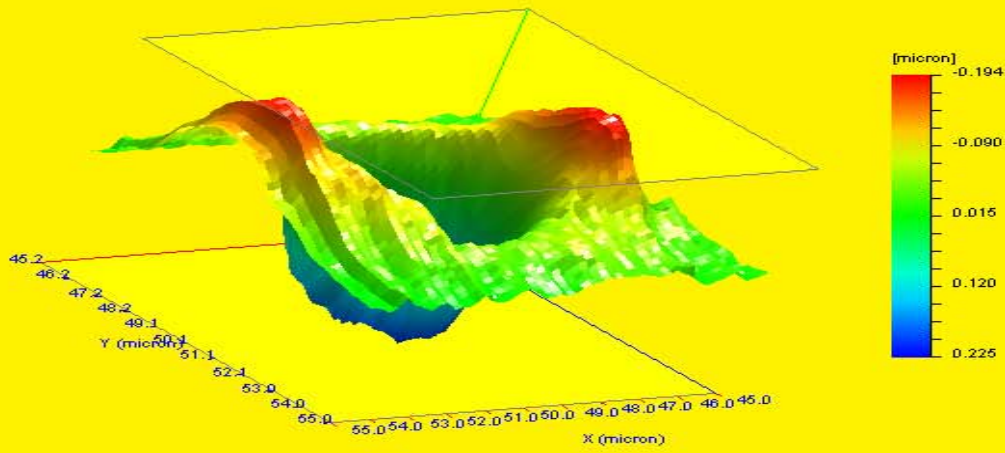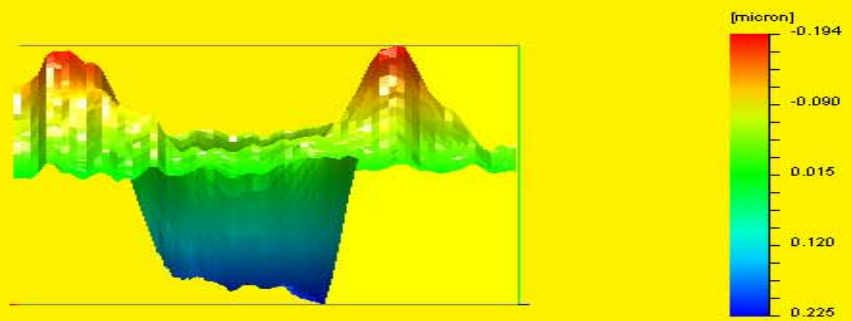
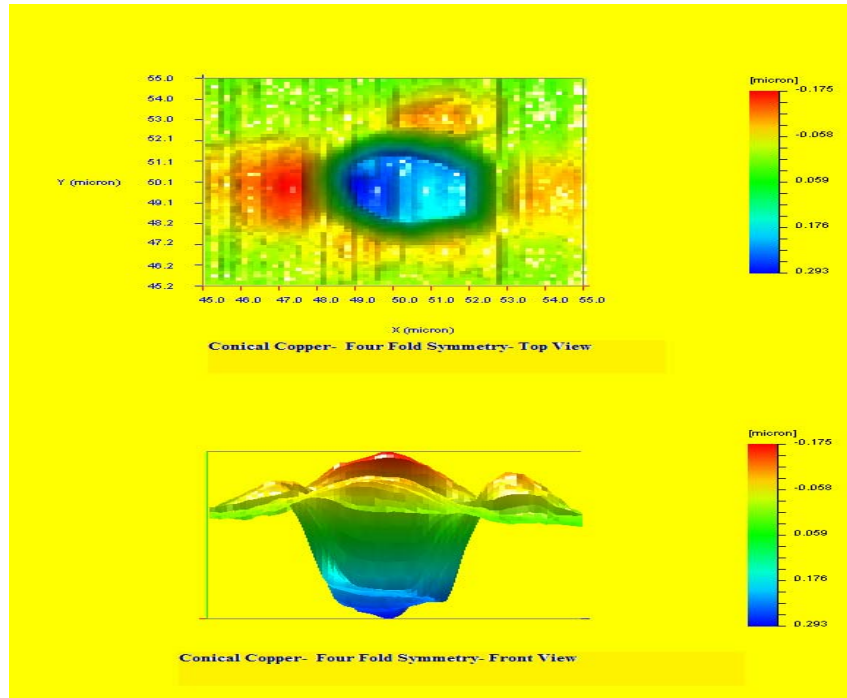Figure 68: Nanovision profile of two fold symmetry behavior in copper.

Figure 69: Nanovision profile of four fold symmetry behavior in copper.
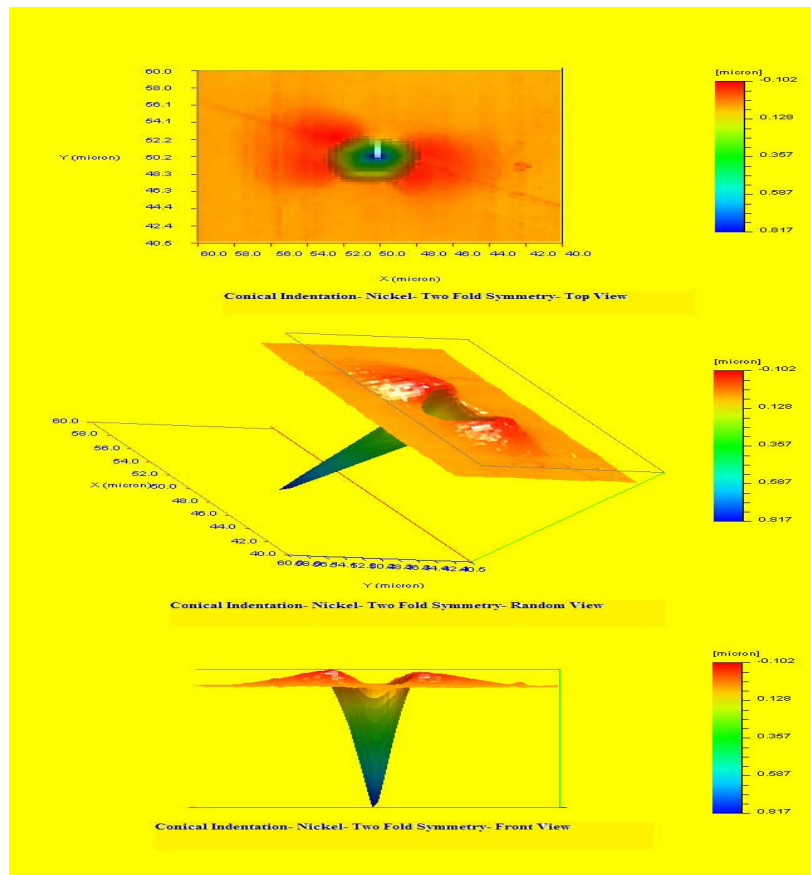

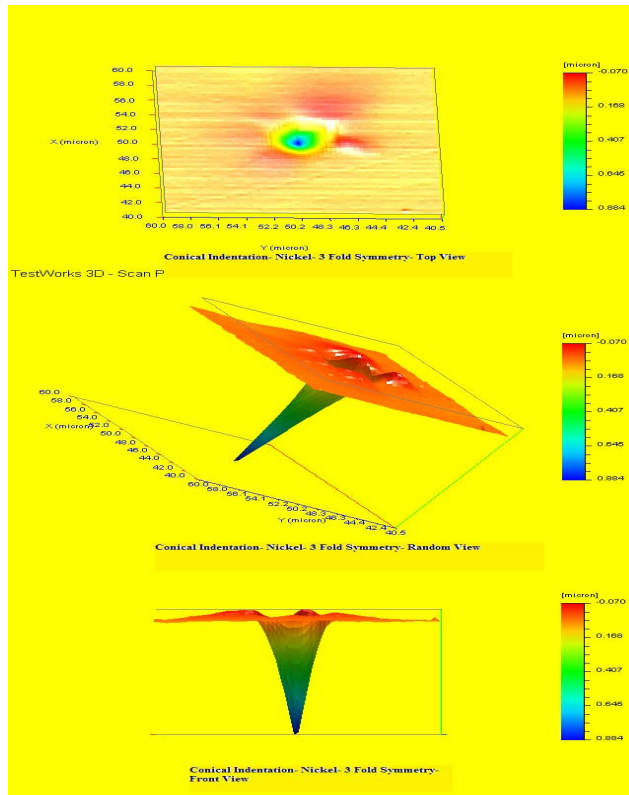Figure 70: Nanovision profile of two fold symmetry behavior in nickel.

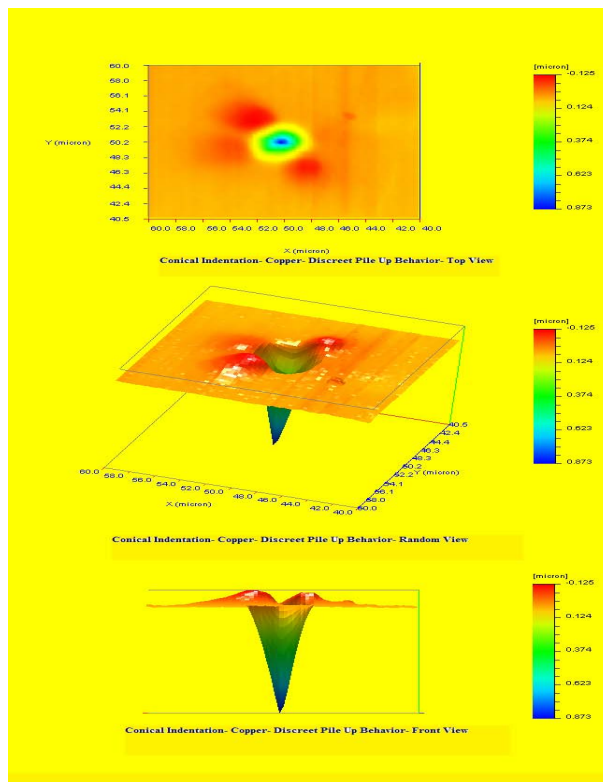Figure 71: Nanovision profile of three fold symmetry in nickel.

Figure 72: Nanovision profile of discreet pile-up behavior in copper.

5.3.1 Contact Area Overestimation for Berkovich Indentations

The Berkovich indentations leave the residual impression as an equilateral triangle whose sides have been calculated above. Together with the contact depth, this information was used to calculate the pile-up area and hence the overall overestimation.

Table 3: Calculation of Pile-Up Area for Berkovich Indentations on Nickel

Indent Number	Contact Depth (nm^2)	Oliver Pharr Area (nm^2)	Pile-Up Area (nm^2)	Total Contact Area (nm^2)
1	960.315	23162615	22721052	45883667
2	958.739	23088747	28354705	51443453
3	960.547	23176498	22726542	45903040
4	963.648	23319223	23939907	47259130
5	1067.648	28471434	25260551	53731985
6	958.443	23074886	25511356	48586243
7	963.655	23319552	27360092	50679645
8	963.922	23332121	31358792	54690914

Table 4: Pile-Up Area Calculation for Berkovich Indentations on Copper

Indent Number	Contact Depth (nm^2)	Oliver Pharr Area (nm^2)	Pile-Up Area (nm^2)	Total Contact Area (nm^2)
1	974.8	23847448	19604363	43451812
2	966.03	23430197	19427286	42857483
3	955.6	22942019	16957139	39899159
4	958.8	23092821	20984386	44077208
5	967.8	23518504	13739925	37258429
6	966.3	23445060	11431541	34876602
9	975.3	23873220	16730654	40603874

Table 5: Pile-Up Area Calculation for Berkovich Indentations on Iron

Indent Number	Contact Depth (nm^2)	Oliver Pharr Area (nm^2)	Pile-Up Area (nm^2)	Total Contact Area (nm^2)
1	988	24479494	22207276	46686770
2	971	23666542	25845593	49512134
3	985	24335033	18061453	42396485
4	976	23904219	21360248	45264467
5	988	24479494	19869668	44349162

5.3.2 Contact Area Overestimation for Cube Corner Indentations

Cube corner indenters are sharp. As a result, the indentations are small in size. Nevertheless, the pile-up heights are the highest of the three indentation types because of the extremely high plasticity induced by the sharp cube corner tip.

Table 6: Pile-Up Area Calculation for Cube Corner Indentations on Nickel

Indent Number	Contact Depth (nm^2)	Oliver Pharr Area (nm^2)	Pile-Up Area (nm^2)	Total Contact Area (nm^2)
1	986.99	3046456	3795963	6842420
2	987.99	3049390	3608105	6657496
3	987.21	3047694	3796825	6844520
6	991.05	3068946	2477535	5546482
7	989.767	3061815	2664650	5726466
8	1019.58	3229158	3333108	6562276
9	987.023	3046639	3416481	6463120

Table 7: Pile-Up Area Calculation for Cube Corner Indentations on Copper

Indent Number	Contact Depth(nm^2)	Oliver Pharr Area(nm^2)	Pile-Up Area(nm^2)	Total Contact Area (nm^2)
1	1003.297	3137203	3665746	6802949
2	1000.533	3121727	3270842	6392569
3	1000.025	3118887	3846096	6964983
4	994.781	3089645	3825927	6915572
5	999.988	3118680	4615144	7733825
6	989.0709	3057961	3613768	6671730
9	995.267	3092349	3062237	6154586

Table 8: Pile-Up Area Calculation for Cube Corner Indentations on Iron

Indent Number	Contact Depth (nm^2)	Oliver Pharr Area (nm^2)	Pile-Up Area (nm^2)	Total Contact Area (nm^2)
1	982	3021860	3589862	6611723
2	981	3015138	2641870	5657009
3	1003	3140534	2915028	6055562
4	1001	3129029	3275108	6404138
5	1002	3134199	3278125	6412325
6	1003	3141022	3764766	6905789
7	1023	3250948	-1771205	1479743
8	995	3094058	3637528	6731586

5.3.3 Contact Area Overestimation for Conical Indentations

Conical indenters have been used in past to expose the crystal anisotropy. This becomes possible because of the uniform stress applied by the indenter due to its inherent conical symmetry. Discreet pile-ups as well as uniform rings were observed around the indents. Discreet pile-ups are explained by the crystal anisotropy. Uniform pile-up rings are uneven and vary in height around the indent; however, they manage to maintain contact with the indenter most of the time, which is different from the discreet pile-up behavior where the pile-ups have clearly defined boundaries and are in contact with the indenter only at specific areas as restrained by the crystal anisotropy, the crystal structure and the symmetry of the surface being indented.

Table 9: Pile-Up Area calculation for Conical Indentations on nickel.

Indent Number	Contact Depth (nm^2)	Oliver Pharr Area (nm^2)	Pile-Up Area (nm^2)	Total Contact Area (nm^2)
1	966	14508757	12568000	27076757
2	959	14348071	22308200	36656271
3	959	14348334	73510	14421844
4	954	14219428	6072	14225500
5	953	14204954	26078600	40283554
7	953	14202236	26078600	40280836
8	955	14250080	10525700	24775780
9	954	14212965	9111800	23324765

Table 10: Pile-Up Area Calculation for Conical Indentations on Copper

Indent Number	Contact Depth (nm^2)	Oliver Pharr Area (nm^2)	Pile-Up Area (nm^2)	Total Contact Area (nm^2)
1	1027	16004085	22980	16027065
2	971	14642290	10839900	25482190
3	969	14593057	191916	14784974
4	968	14546838	631287	15178125
5	973	14690529	3236260	17926789
6	966	14504066	634150	15138216
7	955	14259314	650712	14910027
8	970	14598341	627858	15226200

Table 11: Pile-Up Area Calculation for Conical Indentations on Iron

Indent Number	Contact Depth (nm^2)	Oliver Pharr Area (nm^2)	Pile-Up Area (nm^2)	Total Contact Area (nm^2)
1	959	14335155	12348060	26683215
2	1036	16231167	181965	16413133
3	962	14409135	194010	14603145
4	977	14788179	77897	14866077
5	961	14402434	7339	14409773
6	961	14379021	192892	14571914
9	969	14582720	8696	14591416

As can be seen, the spread in pile-up area is largest in case of conical indentations. This can be rationalized on the basis of the fact that conical indenters are the sharpest of three indenters used in the study. They are capable of producing the maximum amount of plastic deformation. The pile-up heights are in general the sharpest and highest for conical. However, in certain cases when we are near grain boundaries the observed peak is not that significant. This explains the spread of pile-up areas in case of conical indentations.

5.3.4 Contact Area Overestimation for EBSD Berkovich Indentations

Table 12: Pile-Up Area Calculation for EBSD Berkovich Indentations on Iron

Indent Number	Contact Depth (nm^2)	Oliver Pharr Area (nm^2)	Pile-Up Area (nm^2)	Total Contact Area (nm^2)
9	438	5168349	3374921	8543270
11	450	5424409	4261970	9686380
12	473	5968580	6165169	12133749
13	480	6134929	4834272	10969201
14	527	7311502	5615014	12926517
15	562	8257794	5320973	13578767
16	525	7253968	3727798	10981767
17	558	8161744	6941009	15102754

As can be seen from the contact area calculations, the pile-up area is over and under estimated in all cases of indentations due to the fact that pile-ups are bound to happen in a crystalline material. They can be minimal but can never be absent, due to the plastic properties of material. Therefore, the Oliver-Pharr contact area can never be taken as a final word in calculation of the elastic modulus and hardness values. The method used above to find these extra pile-up sink in areas should be considered in addition to the general analysis for accurate results.

An area summary is given below in form of bar chart for all the indentations including the EBSD

Berkovich Indentations
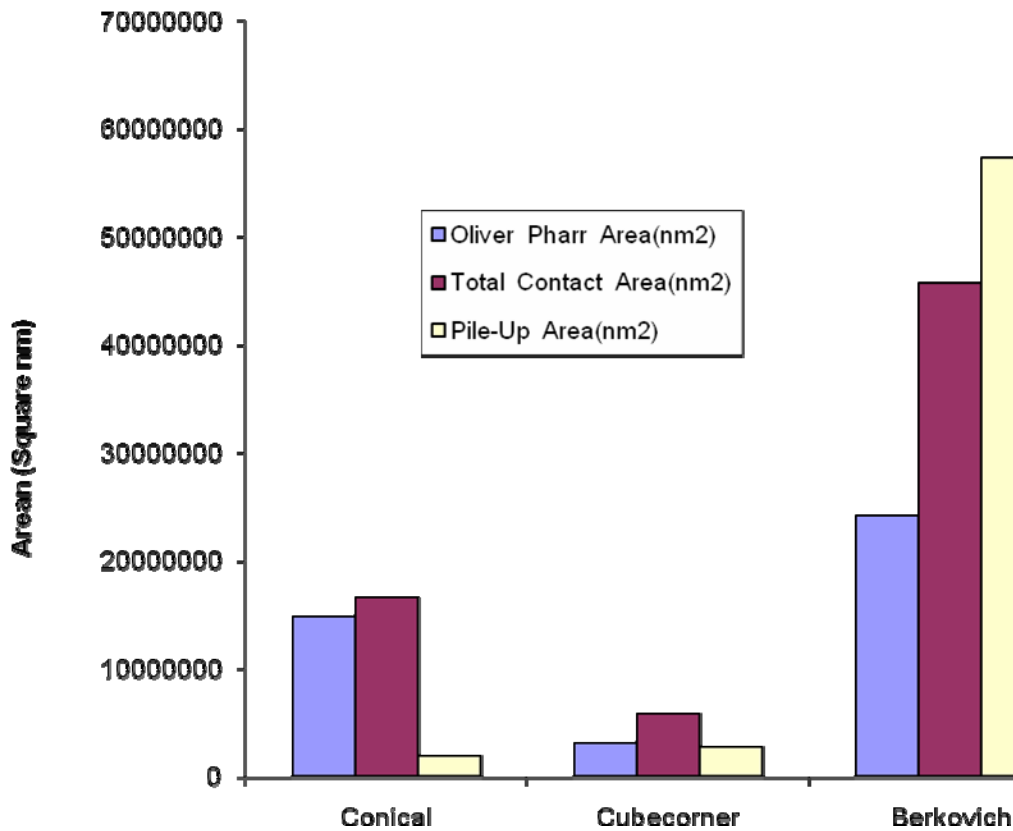
Figure 73a Contact area summary for iron.
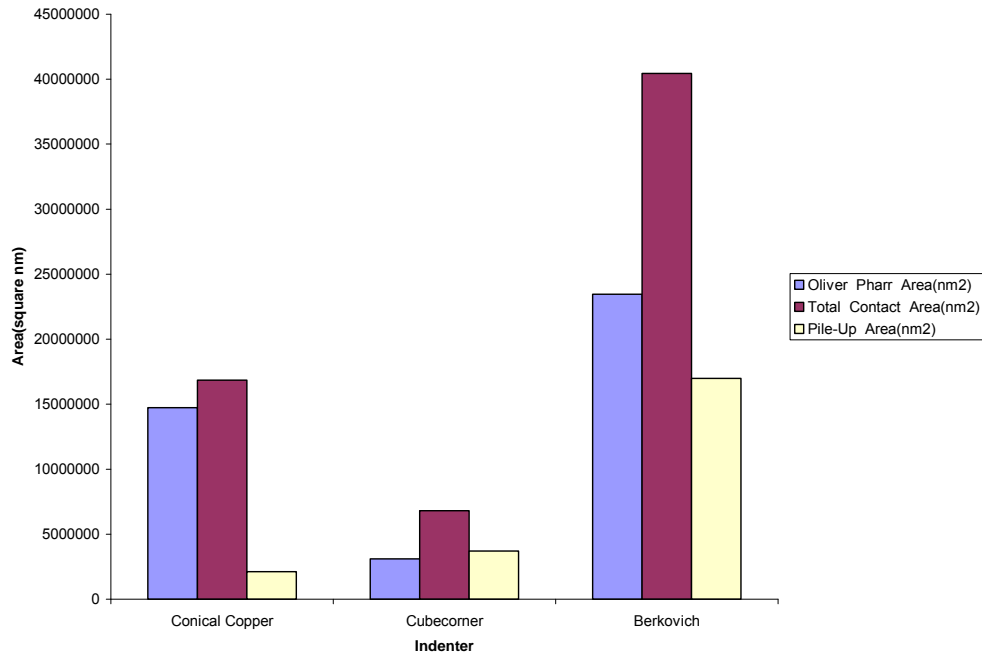
Figure 73b: Contact area summary for copper.
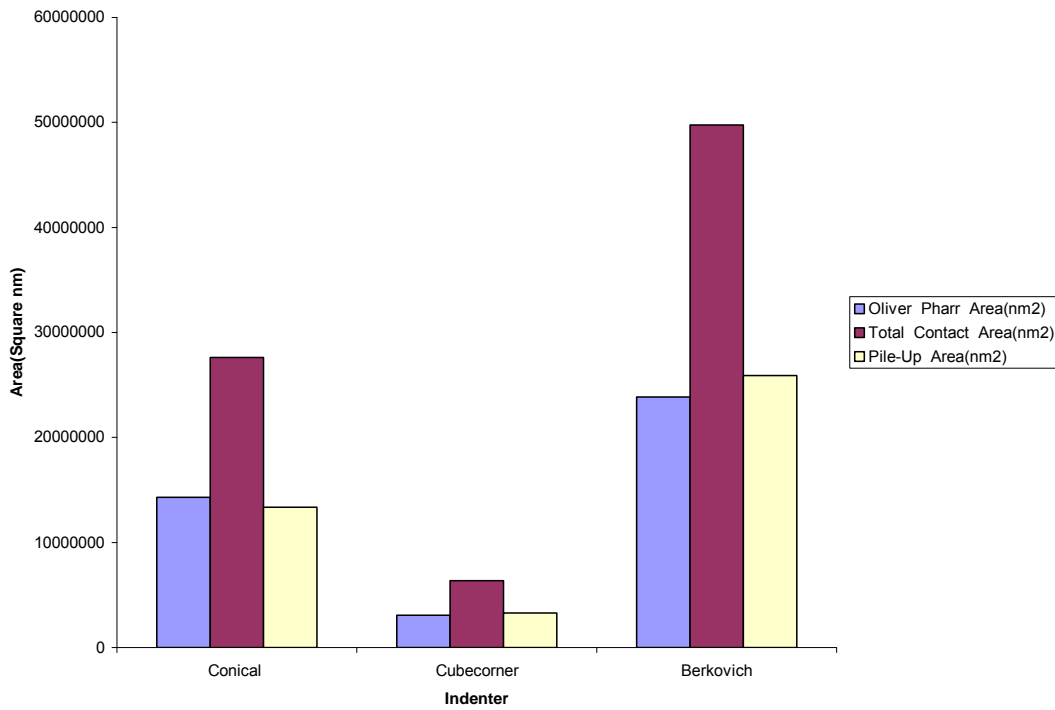
Figure 73c: Contact area summary for nickel.
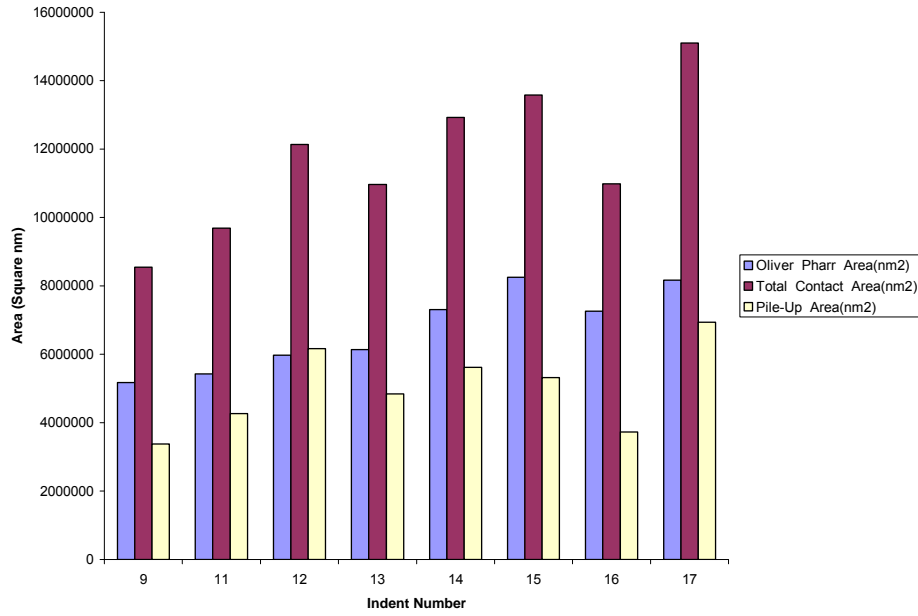
Figure 73d: Contact area summary for Berkovich indentations on EBSD iron matrix.

These pile-up corrections show up in hardness calculations where the new value

curves are smoother than the Oliver-Pharr hardness curves. These are shown below.
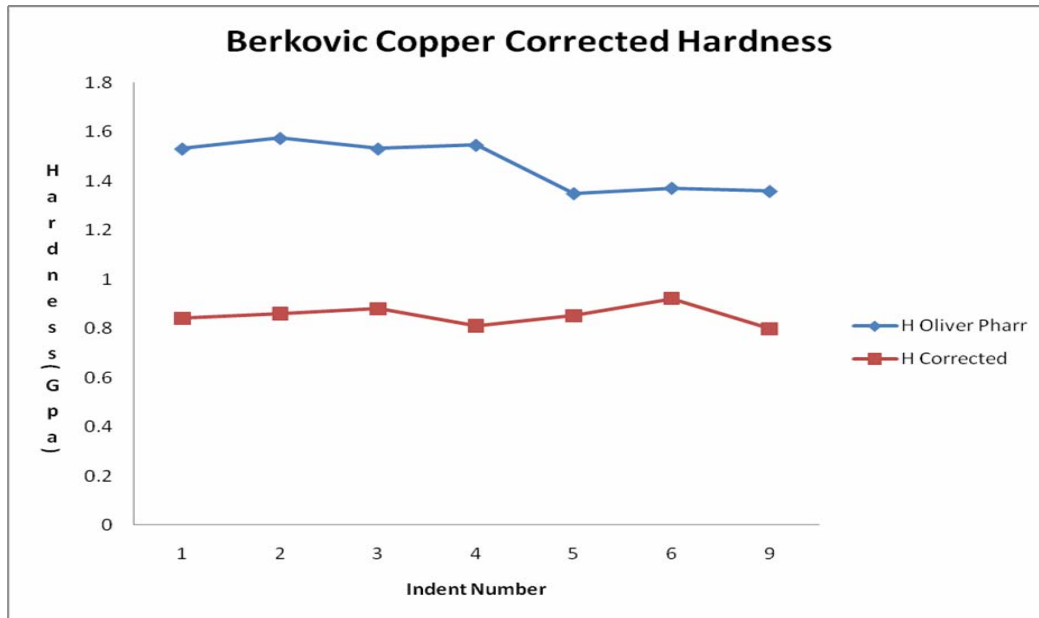
Figure 74a: Berkovich copper corrected hardness.
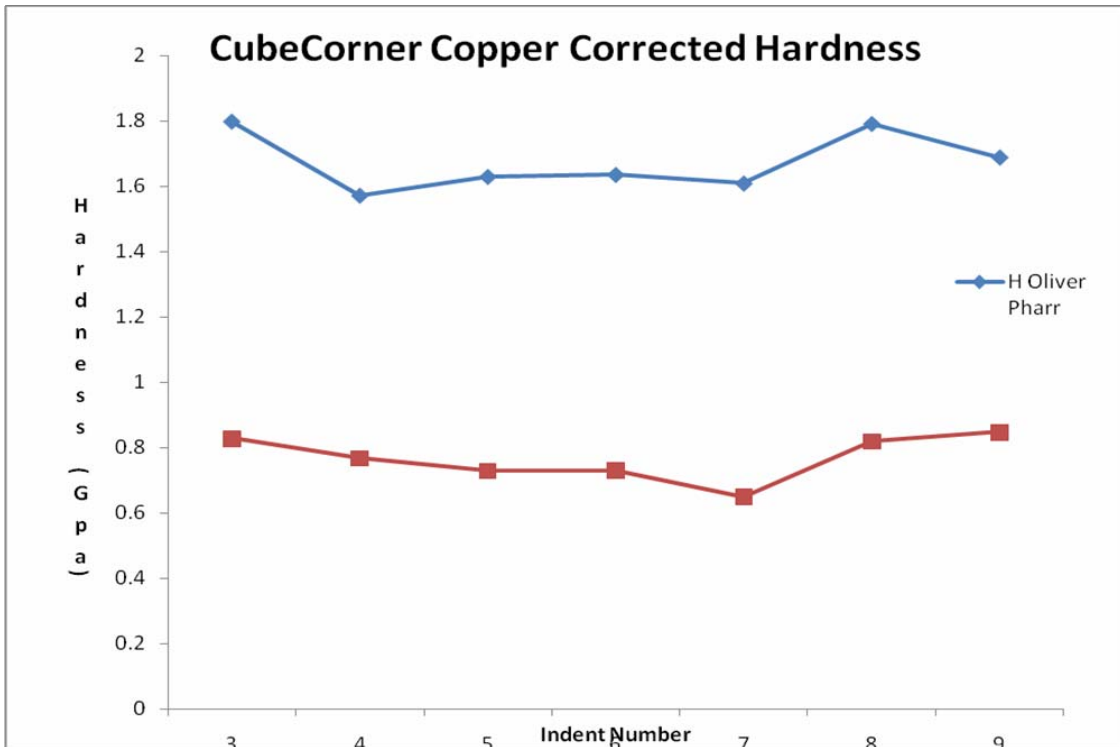
Figure 74b: Cube corner copper corrected hardness.
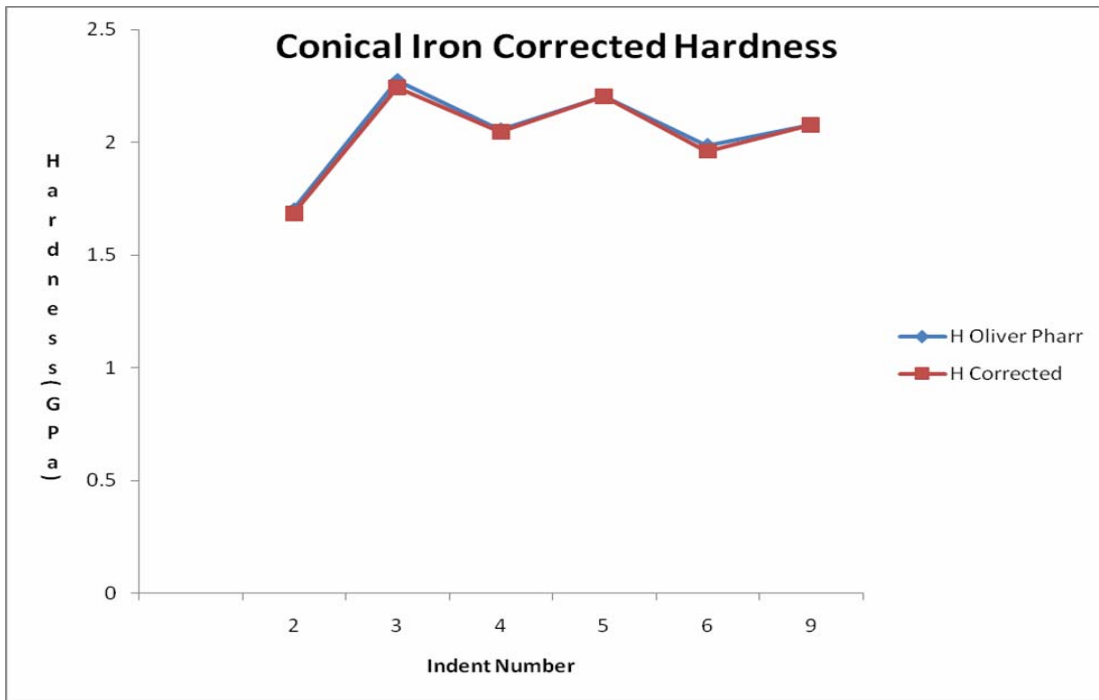
Figure 74c: Conical iron corrected hardness.
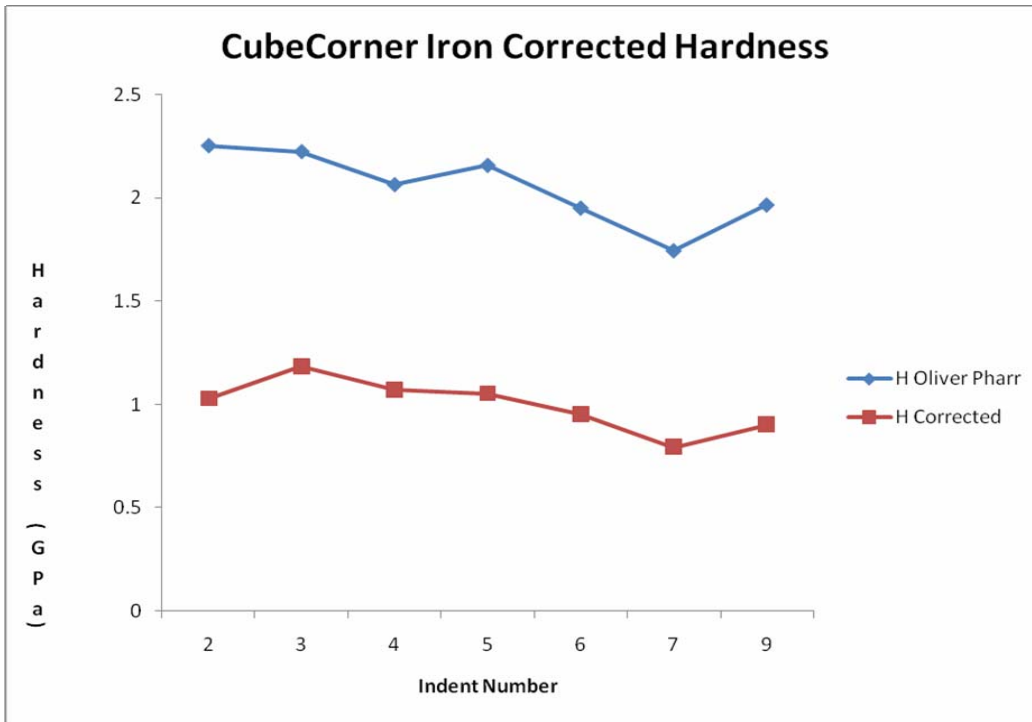
Figure 74d: Cube corner iron corrected hardness.
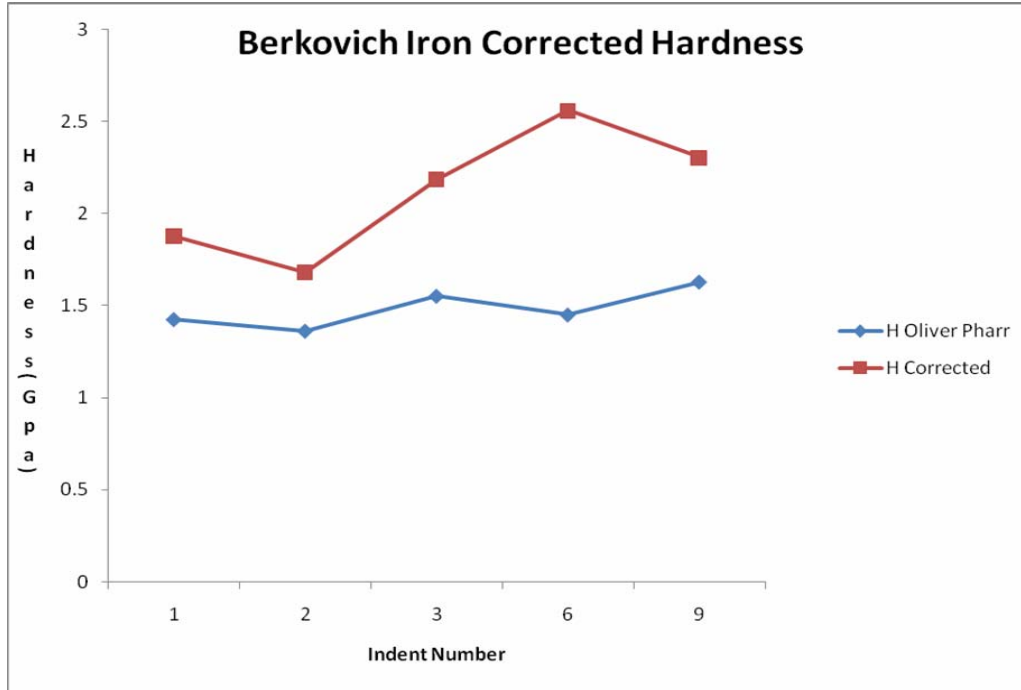
Figure 74e: Berkovich iron corrected hardness.
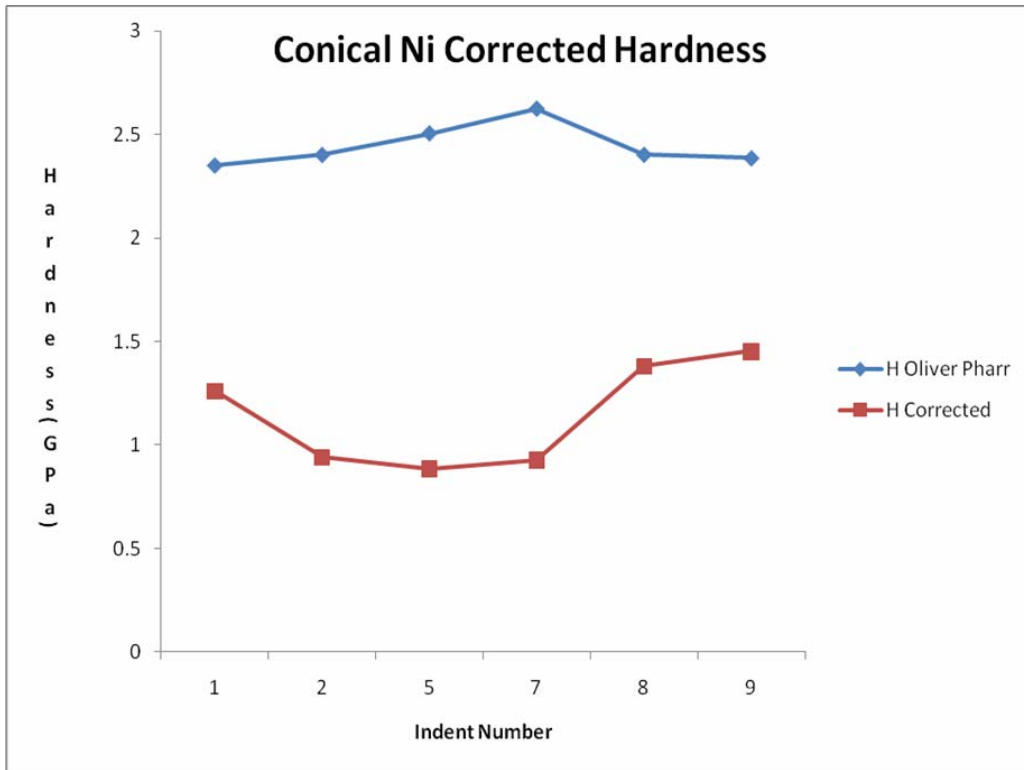
Figure 74f: Conical nickel corrected hardness.
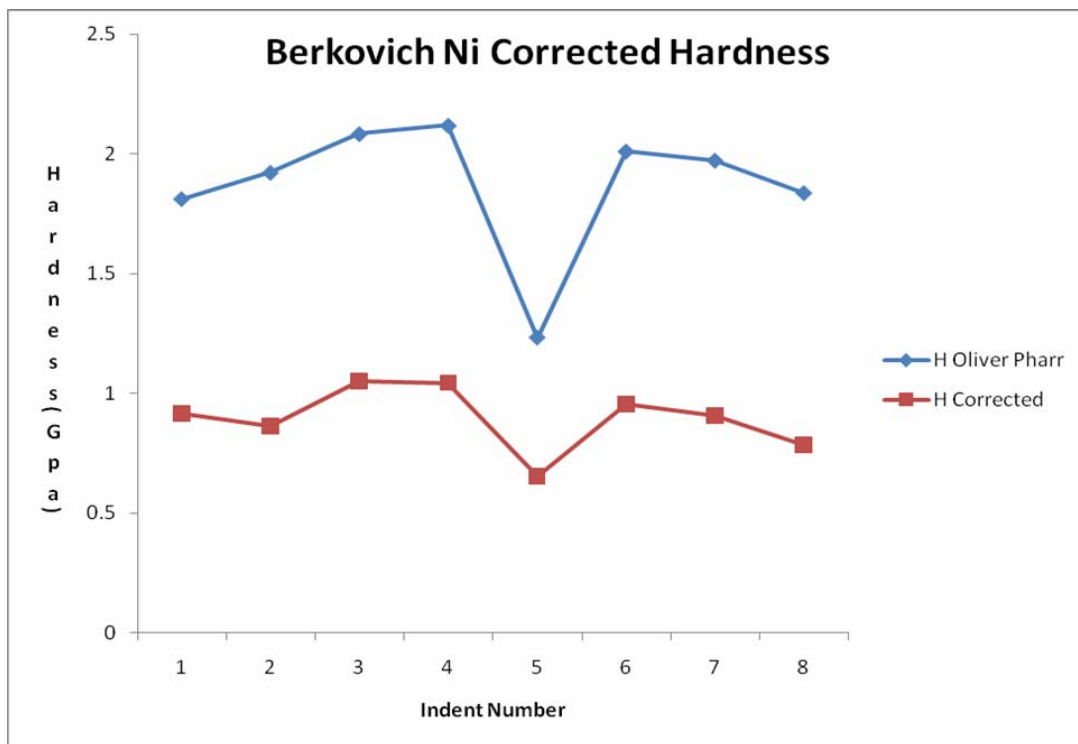
Figure 74g: Berkovich nickel corrected hardness.

5.3.5 Elastic Modulus Calculation for Specific Directions

Elastic modulus for a specific direction <hkl> is based on Hooke's law and is given by the following relation for cubic crystal structures [23],

$$\frac{1}{E_{hkl}} = S_{11} - 2[S_{11} - S_{12} - 0.5\,S_{44}][l^2 m^2 + m^2 n^2 + l^2 n^2]$$

where l, m and n are direction cosines for the specific directions and are given by the following relations [23],

$$l = \frac{h}{\sqrt{h^2 + k^2 + l^2}}$$

$$m = \frac{k}{\sqrt{h^2 + k^2 + l^2}}$$

$$n = \frac{l}{\sqrt{h^2 + k^2 + l^2}}$$

A table listing the values for direction cosines for specific directions is given below.

Table 13: Direction Cosines for <111>, <110> and <100> Directions

hkl	l	m	n
<111>	0.577	0.577	0.577
<110>	0.709	0.709	0
<100>	1	0	0

The values for stiffness constants [23] is given in table below.

Table 14: Stiffness Coefficients for Copper, Nickel and Iron [23]

Material	$S_{11}(10^{-3}\,GPa^{-1})$	$S_{12}(10^{-3}\,GPa^{-1})$	$S_{44}(10^{-3}\,GPa^{-1})$
Iron	8	-2.8	8.6
Copper	15	-6.3	13.3
Nickel	7.3	-2.7	8

The elastic modulus values for copper, nickel and iron are thus calculated and presented in the table below.

Table 15a: Elastic Modulus Values along Major Poles

Material	E<111>(GPa)	E<110>(GPa)	E<100>(GPa)
Copper	190.204	131.75	66.67
Nickel	302.1	234.74	136.98
Iron	271.9	212.09	125

Table 15b: Elastic Modulus Values in Different Indent Directions for Copper, Nickel and Iron

Indent No.	Actual Orientation (hkl)	Elastic Modulus (GPa) (Theoretical)	Elastic Modulus (GPa) Experimental	Hardness (GPa)
9	(240,56,245)	217.9	201.9	2.19
11	(75,142,337)	167.68	178.24	2.05
12	(115,100,333)	165.48	173.85	1.87
13	(155,103,307)	190.62	171.5	1.81

5.4   Inverse Pole Figure and Pole Figure Analysis for Berkovich Indentations

These indents were done on a polycrystalline surface. An EBSD profile picture of the inverse pole figure, image quality and the cleaned inverse pole figure is shown below.

| 18 | 17 | 16 | 15 | 14 | 13 | 12 | 11 | 10 | 9 | 8 | 7 | 6 | 5 | 4 | 3 |
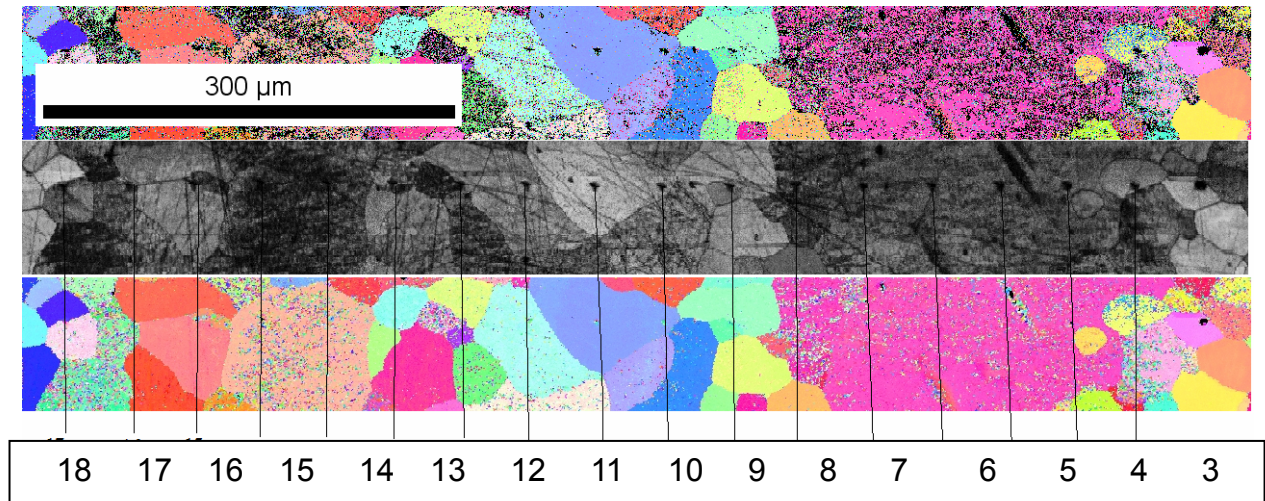
Figure 75: The inverse pole figure map, the image quality map and the cleaned IPF map from top to bottom respectively. Indents are marked on the map.

Figure 76: Color coded map for the inverse pole figure map shown above.

An indent-wise inverse pole figure map is necessary to find the exact location of the indents on the stereographic triangle and is shown below.

5.4.1 Pole Figure for Individual Indents
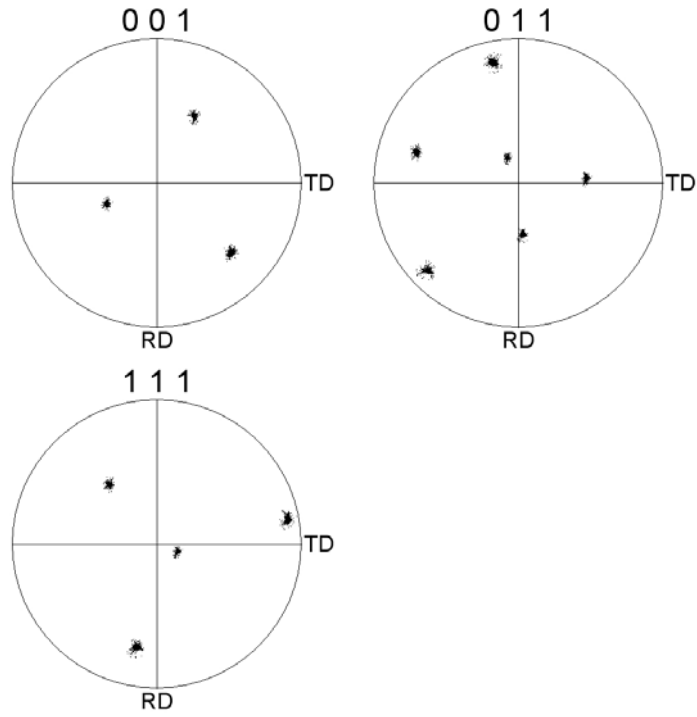
Figure 77: Pole figure map for Indent 9 on iron with Berkovich indenter.
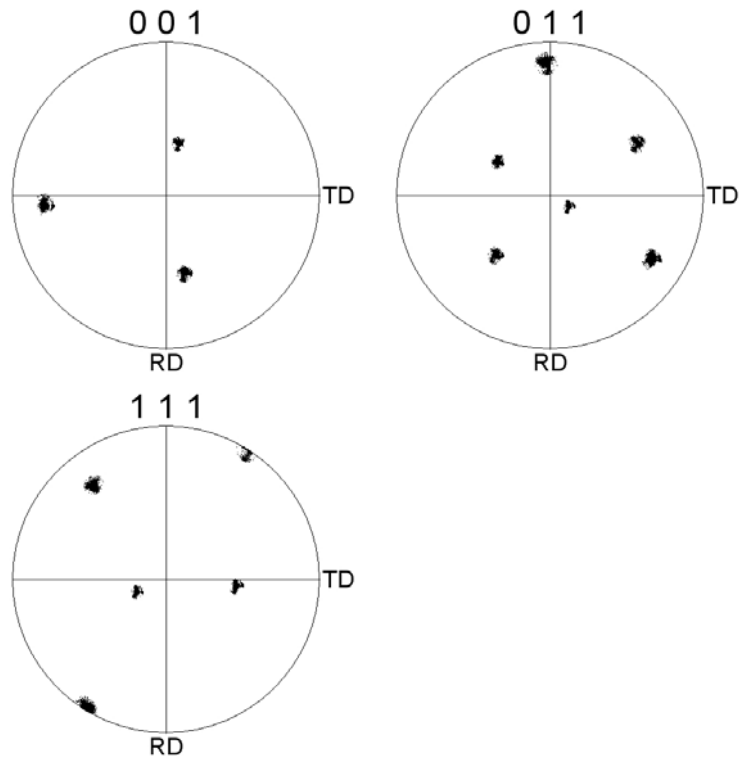
Figure 78: Pole figure map for Indent 11 on iron with Berkovich indenter.
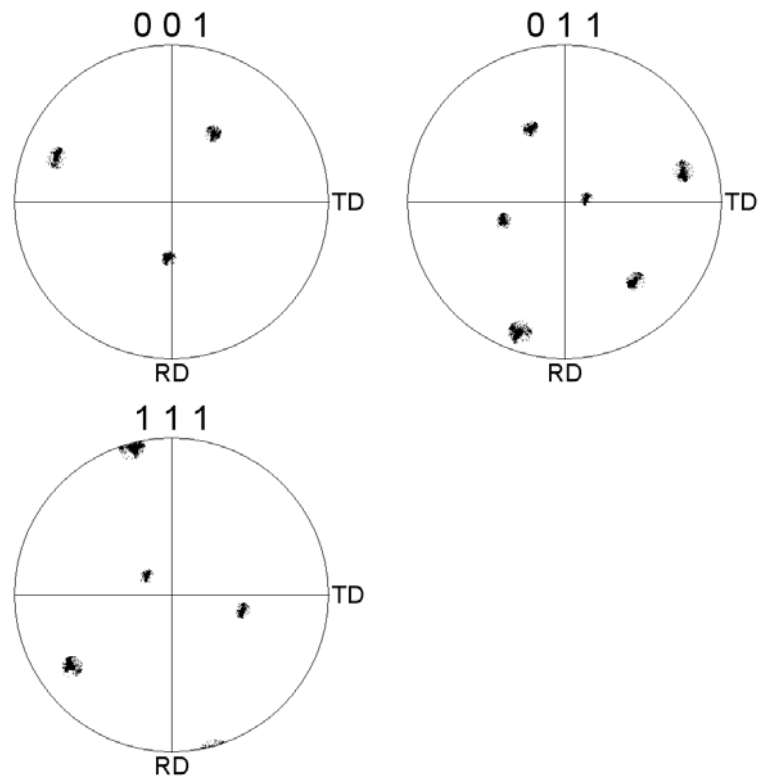
Figure 79: Pole figure map for Indent 12 on iron for Berkovich indenter.
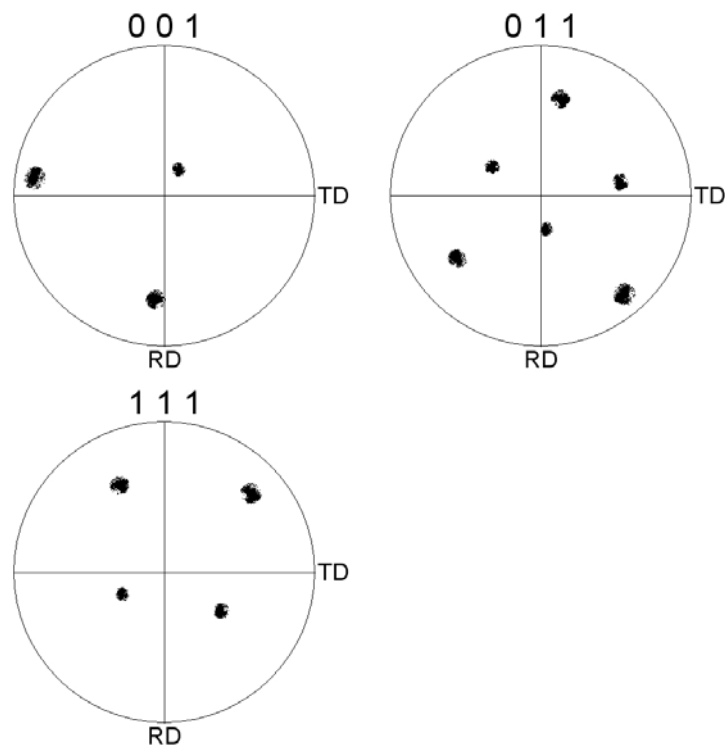
Figure 80: Pole figure map for Indent 13.

5.4.2 Composite Inverse Pole Figure Analysis for All Indentations

A combined inverse pole figure for all these indents is shown below. A tentative estimate of their hardness and elastic modulus behavior with respect to their grain orientations can also be seen from these figures. Different behaviors with respect to elastic modulus and hardness values are to be seen. These are however, dependant on their respective location with respect to the grain. For example, indents near the grain boundaries show a dip in elastic modulus and hardness values (Indents 14,15,16,17), while indents that are centered on the grain (Indents 9,11,12,13) don't show this dip in the values. The first set of indents, Indents 14-17, show a deviation from the theoretical values, while the indents that are centered (Indents 9-13) show a decent agreement with the theoretical values as calculated from the three dimensional Hooke's law of elasticity.

Since grain boundaries are a host of dislocations, slip transmission is easier and hence there are yield excursions. Also, There is no long term grain boundary hardening is observed for BCC metals [8,26-27]. This rationalization can explain the low hardness and elastic modulus values for indents near grain boundaries. The deformation zone expands from one grain, hitting a cavity, which leads to a soft spot initially. This soft spot corresponds to the observed dip in elastic modulus and hardness curves observed initially. This deformation zone expansion is also facilitated by the presence of additional dislocations near the grain boundary. These dislocations provide the extra cushion for the observed dip in the elastic modulus and hardness curve by providing various slip systems available for deformation. However, as the deformation continues, these tend

to show a hardening pattern. As and when this deformation zone starts to interact with other grain, it leads to a gradual rise in the hardness value which attains a constant value thereof depending on the depth of indentation. It can be seen that all the indents are in agreement with the values predicted by the Hooke's law of elasticity except Indents 14-17. A closer look at their loading vs displacement into surface graph reveals the reason. It appears from the chart that the sample strain hardens and there is a distinct slope for these two indentations. Apart from these abnormalities, other indents tend to follow the values as predicted by the Hooke's law.

[001]
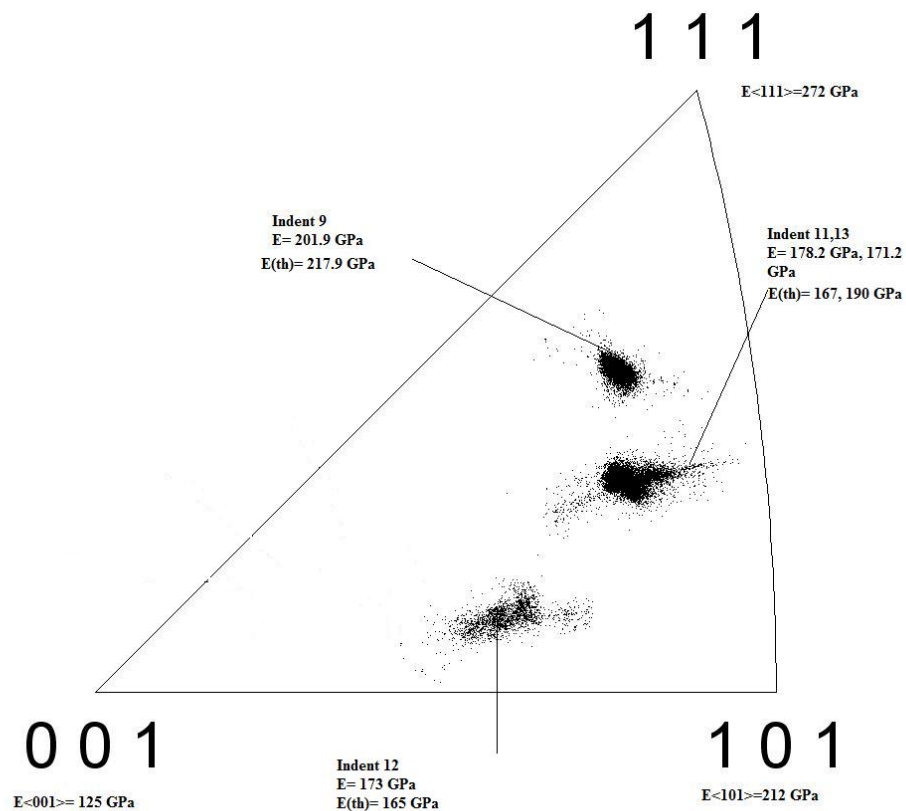
Figure 81: Inverse pole figure for all Set I Berkovich indentations. Black spots on the stereographic triangle represent various indentations.

5.5 Elastic Modulus, Hardness and Load vs Displacement into Surface

The elastic modulus and hardness variations of these indents with respect to the displacement into surface is shown below.
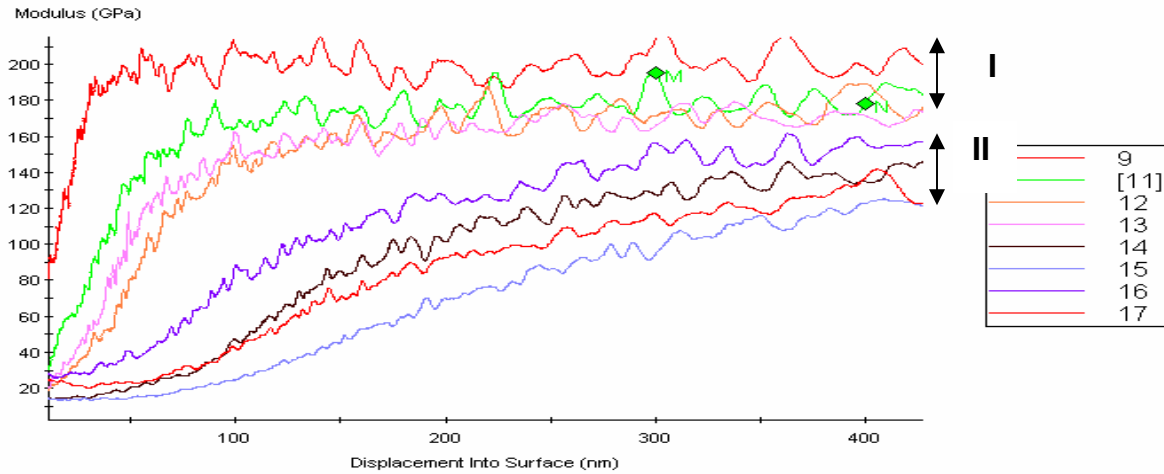
Figure 82: Elastic modulus vs displacement into surface for Berkovich indentations on iron.
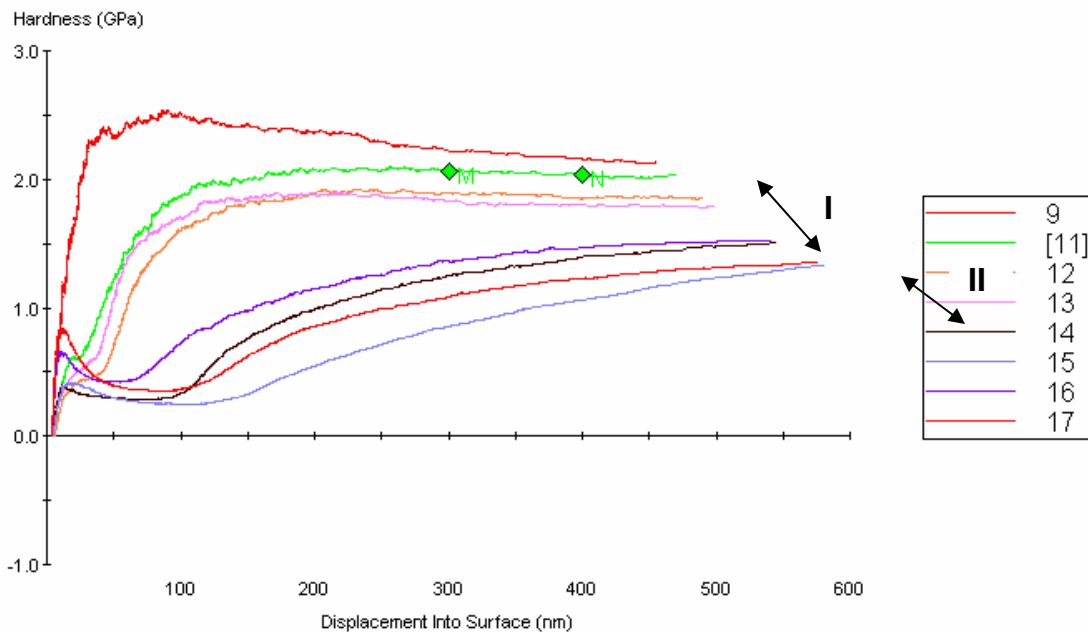
Figure 83a: Hardness vs displacement into surface for Berkovich indentations on iron.

It can be seen that the elastic modulus and the hardness depend on the orientation of the grain and these amounts vary significantly with respect to the grain orientation. The elastic modulus and hardness values seem to cluster for nearby orientations while there is a spread for these   for indentations which lie far apart on the stereographic triangle. The elastic modulus and hardness, however, flatten with displacement after the initial spike which is to be expected. The difference in the elastic modulus and hardness further aggravates with the pile-up formation and different pile-up behavior for different orientations as is shown above for copper and   nickel and could be assumed for iron. The orientation effect as well as the pile-up caused overestimation makes the elastic modulus and hardness data quite volatile and should be considered carefully while using the information.
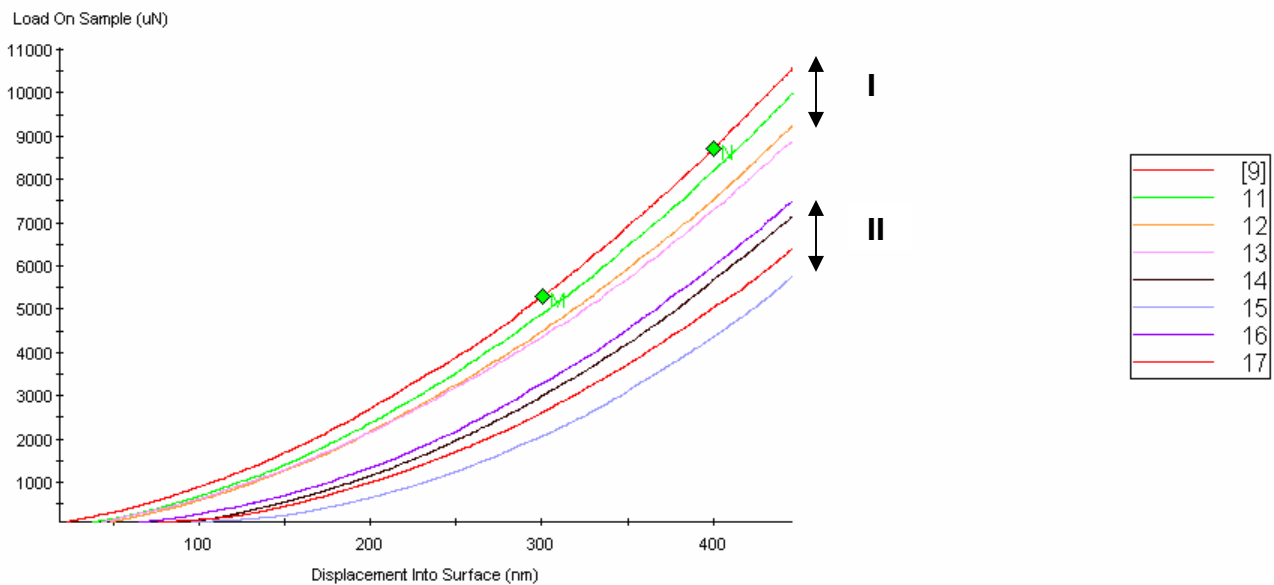
Figure 83b: Load vs displacement into surface for Berkovich indentations on iron. Only loading portion is shown for the composite curve for all the indents.

The load vs the displacement curves reveals another aspect for this data set. It can be seen that for the indents showing a disagreement with the theoretical values

99

(Indents 14-17), they are located at the grain boundaries. The load displacement curves show a definite clustering and a similar strain hardening behavior for two sets of indents, the indents which show agreement are centered and follow a similar trend and are clustered together on the composite load displacement curve. The indents showing disagreement (Indents 14-17) show similar clustering behavior, they show significant strain hardening and are located on grain boundaries.

These indentations were done on iron which has a body centered cubic (BCC) structure. The planes of closest packing are not clearly defined in the case of BCC structures. However, the closest packing is along the {110} family of planes and the slip direction is the <111> family. However, shear has also been reported on other planes in literature for the BCC crystal structure.

The model proposed by Li et al. proposes the pile-up formation along the intersection of the slip direction and the top surface indented. This is proposed for the conical indentations as there is no stress variation. However, stress imposed by the pyramidal indenters vary in space and thus require 3D modeling for accurate prediction of pile-ups. I apply the same model for pyramidal indenters to get a broad overview of the pile-up behavior with crystal orientation. At the same time, the excess contact area has been calculated and discussed with different models for all three indenters in the discussion above. The models proposed are semi-ellipse for the pyramidal indenters while assuming an elliptical contact of the pile-up with the indenter in case of conical indentations.

CHAPTER 6

SUMMARY AND CONCLUSIONS

All nanoindentation tests were done using three indenters, Berkovich, cube corner and conical. Materials studied involve two face centered cubic metals, copper and nickel while one body centered cubic metal, iron is also analyzed with all the indenters. Following conclusions are drawn from the above study.

6.1   Summary

Tip calibration for all the tips is done on the standard fused silica sample. Tip area coefficients are calculated with the help of Analyst™ software. An even weightage is given to all the points.

Method of analysis for the area overestimation calculation was indent and scan displacement limit method. The method employed for the analysis of the Berkovich indentations on iron was indent and scan load limit method.

The depth of indentation or the maximum displacement into surface was limited to 1000 nm. For the Berkovich indentations on iron, the displacement into the surface was 500 nm.

Pile-ups were measured using the Nanovision™ traceline method. Pile-up analysis is based on the semi-ellipse approximation for the pyramidal indenters while for conical indenters, elliptical contact with the indenter has been assumed. The excess area is calculated in case for pile-ups and in case for sink-ins based on this approximation.

Materials are compared with respect to indenters; their mechanical property variation is studied and portrayed. Materials are also compared with indenters kept constant and materials changing, to reflect the change or variation of mechanical properties of different materials under the same imposed stress.

Pile-up variations revealing different formations and underlying different orientations are discussed and rationalized. Nanovision profiles of these indents show clearly that the pile-ups formed are not random, but are oriented in certain specific directions on the indented plane depending on the orientation of the plane and the stress that is imposed on those while indenting them.

The three dimensional view of Nanovision™ profiles and the accuracy of the Traceline method gives a basic physical understanding of the phenomena. This accuracy rises from the low compliance of the scanning indenter tip. The sharp tip facilitates a better and accurate topographical map for the indentations. This observation is further strengthened by the electron back scattered study of the Berkovich indentations on iron.

6.2   Conclusions

Pure elemental copper, nickel and iron have been indented with Berkovich, cube corner and conical indenters respectively. The hardness values are different for all three materials and also change as a function of indenter geometry for the same material. In case of the Berkovich indenter, nickel exhibits the highest hardness material, followed by lower values for copper and iron. In case of cube corner and conical indenters too, nickel exhibits the highest hardness while values for copper and iron are relatively

close. The low stacking fault energy for copper permits easy shear and hence high plasticity resulting in low hardness values. In contrast, for iron higher stresses are required for dislocation motion, attributable to the higher Peirels-Nabarro stress in the body centered cubic (BCC) crystal structure . This leads to a relatively high hardness value. Based on the measurements of the pile-up associated with indentations of different geometry, the Oliver-Pharr hardness values have been corrected. These corrected hardness values for all three materials, show with a lesser spread as compared with the Oliver-Pharr hardness values.

Indenting the same material with the three different indenters, Berkovich, cube corner and conical, lead to differences in the plastic deformation behavior beneath the indenter tip. These differences are likely to be a direct consequence of the differences in indenter geometry. Thus, the Berkovich indenter has an enclosed half angle of 65.3 degrees followed by cube corner and conical which have enclosed half angles of 35.4 and 30 degrees respectively. The tip rounding effect is not prominent in this case as the depth of indents analyzed in the present study are all of the order of a micron, which is quite large compared to the normal tip rounding which is of the order of 200 nm. Since the conical indenter has the minimum half angle, it produces the maximum plastic deformation followed by cube corner and Berkovich, thus resulting in different Oliver-Pharr hardness values, which do not account for the effect of pile-ups. On correcting the contact area based on the experimental measurements of the pile-up, the corrected hardness values for different indenters for the same material exhibit a substantially lower variation. Another important point to note in the context of comparing different

indenters is that use of the conical indenter leads to indentations with pile-ups reflecting the crystallographic symmetry of the grain on which the indent is placed.

The influence of grain orientation on the measured elastic modulus has been investigated by correlating nanoindentation data with orientation imaging microscopy (OIM) data from the same region of the sample in case of polycrystalline iron. The elastic moduli for grains of different orientation have been computed using the generalized Hooke's law of elasticity and compared with the measured Oliver-Pharr moduli values for a Berkovich indenter. In case of indents placed near the center of grains, reasonably good agreement was found between these two values of elastic modulus. However, in case of indents placed near grain boundaries or triple junctions, the agreement was rather poor. The reason being that for such indents, while the deformation zone presumably initiates within a grain of a specific orientation, with increasing indentation depth this zone hits a grain boundary and is forced to expand into an adjacent grain with a different orientation. In addition, the grain boundary also acts as a source for dislocations. These complications in the deformation behavior lead to an erroneous measurement of the elastic modulus for such indents.

CHAPTER 7

FUTURE WORK

In this study, experiments are done with face centered cubic (FCC) and body centered cubic (BCC) metals, to see a basic trend and rationalize the observations on a basic level. Further work may include a broader material perspective by including HCP metals, ceramics and thin films. Also, the Berkovich indentations are rationalized on the assumptions and model based on conical indentation observations. Further work should include three dimensional modeling of the exact stress distribution. The pile-ups thus obtained should be related to the experimental values and lines of agreement should be drawn.

Electron backscattered diffraction (EBSD) studies of other FCC and HCP metals should be done in order to further the reasoning already being presented in this study. This should include EBSD maps of indentations with cube corner and conical indenters on these metal types. This should be coupled with a more basic transmission electron microscope study of the sectioned indent on a particular grain orientation to reveal the dislocation, crystal structure, orientation of the plane and a higher integration to the mechanical properties and the influence of pile-ups and sink-ins.

APPENDIX A

INDENTERS

Berkovich Indenter
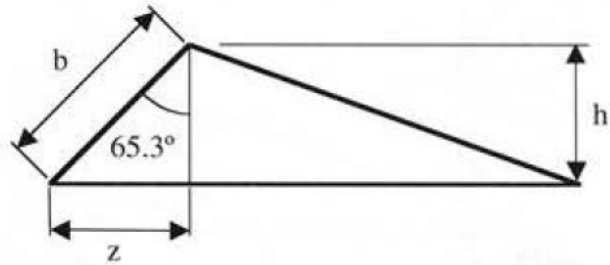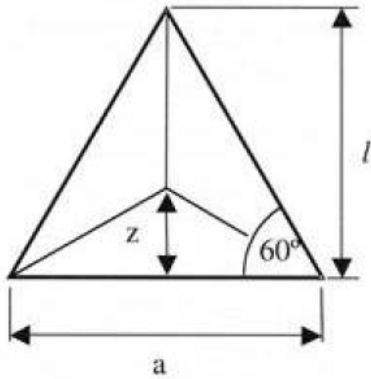
Projected area

$$\tan 60 = \frac{l}{a/2}$$

$$l = \frac{\sqrt{3}}{2}a$$

$$A_{proj} = \frac{al}{2}$$

$$= \frac{\sqrt{3}}{4}a^2 \quad 0.433a^2$$

$$\cos 65.27 = \frac{h}{b}$$

$$h = \frac{a\cos 65.3}{2\sqrt{3}\sin 65.3}$$

$$= \frac{a}{2\sqrt{3}\tan 65.3}$$

$$a = 2\sqrt{3}h\tan 65.3$$

$$A_{proj} = 3\sqrt{3}h^2\tan^2 65.3$$

$$24.56h^2$$

Surface area

$$A_{surf} = 3\frac{ab}{2}$$

$$\sin 65.3 = \frac{z}{b}$$

$$z = \frac{a}{2}\tan 30$$

$$= \frac{a}{2\sqrt{3}}$$

$$b = \frac{a}{2\sqrt{3}\sin 65.3}$$

$$A_{surf} = 3\frac{a^2}{4\sqrt{3}\sin 65.3}$$

$$0.477a^2$$

$$a = 2\sqrt{3}h\tan 65.3$$

$$A_{surf} \quad 27.05h^2$$

Equivalent cone angle:

70.32°

Vickers and Cube Corner
Indenter
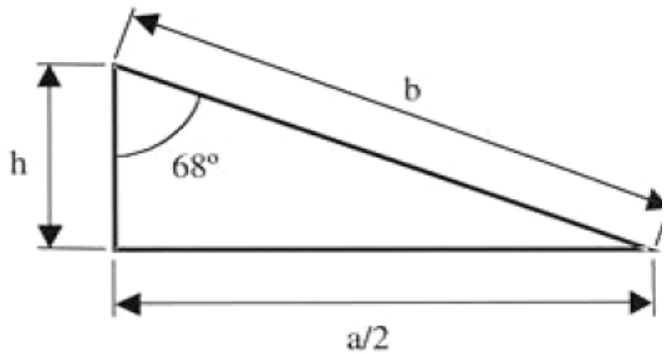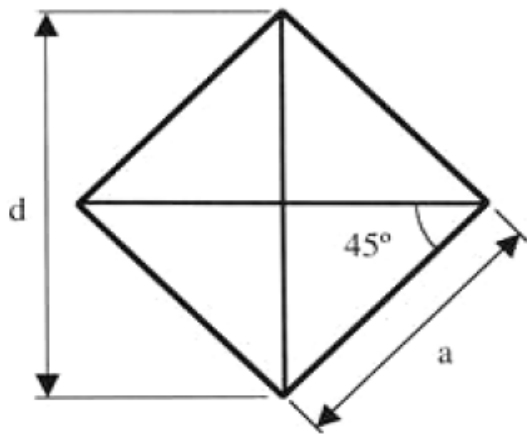
Projected area

$$\sin 45 = \frac{d}{2a}$$

$$a = \frac{d}{\sqrt{2}}$$

$$A_{proj} = a^2$$

$$= \frac{d^2}{2}$$

$$\tan 68 = \frac{a}{2h}$$

$$a = 2h \tan 68$$

$$A_{proj} = a^2$$

$$= 4h^2 \tan^2 68$$

$$24.504h^2$$

Surface area

$$A_{surf} = 4\frac{ab}{2}$$

$$\sin 68 = \frac{a}{2b}$$

$$b = \frac{a}{2\sin 68}$$

$$A_{surf} = \frac{a^2}{\sin 68}$$

$$= \frac{4h^2 \tan^2 68}{\sin 68}$$

$$26.429h^2$$

For cube corner, replace 68Ƴ with 35.264°

Equivalent cone angle: 42.28°

Equivalent cone angle:
70.3°

Conical Indenter
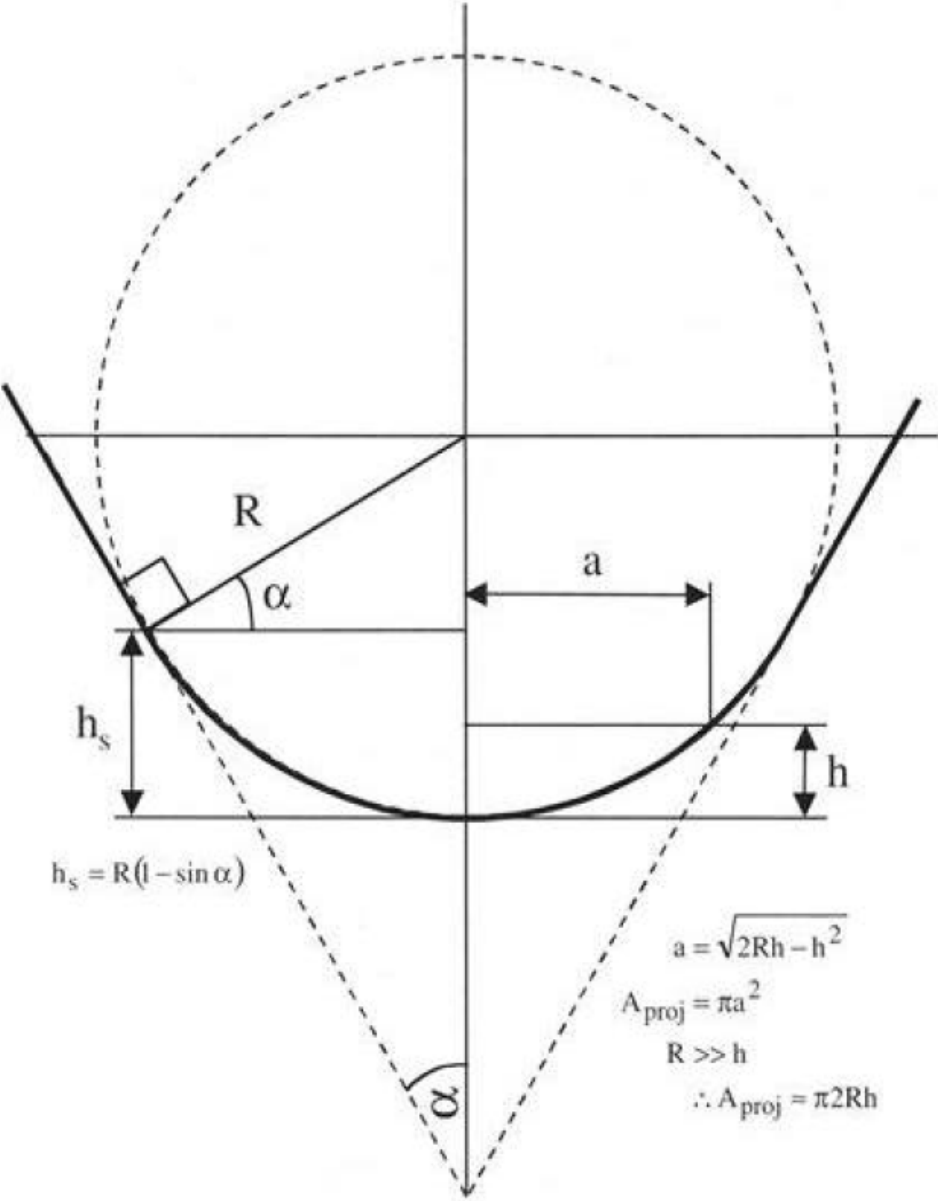
Source: C. Fisher-Cripps, Nanoindentation, New York, Springer (2002) [1]

APPENDIX B

PILE-UP NOMENCLATURE

Pyramidal Indenter
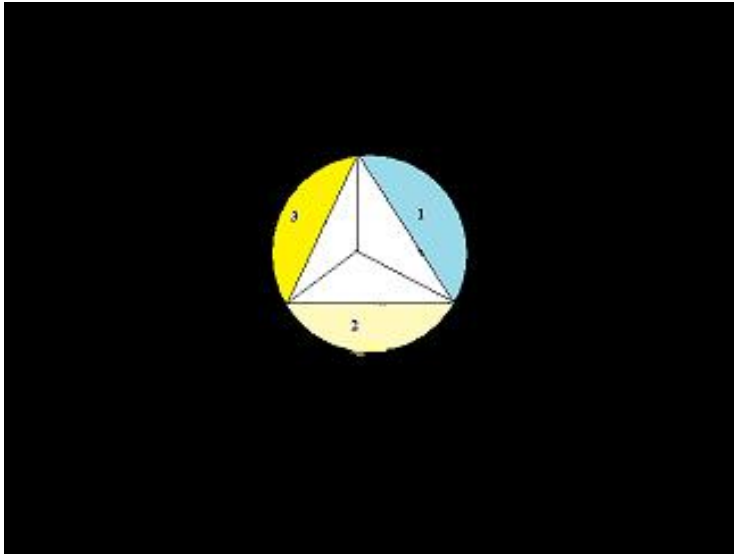
1, 2 and 3 are the different segments of pile-up in contact with the indenter. Same terminology is used for Berkovich and pyramidal indenters.

Conical Indenter
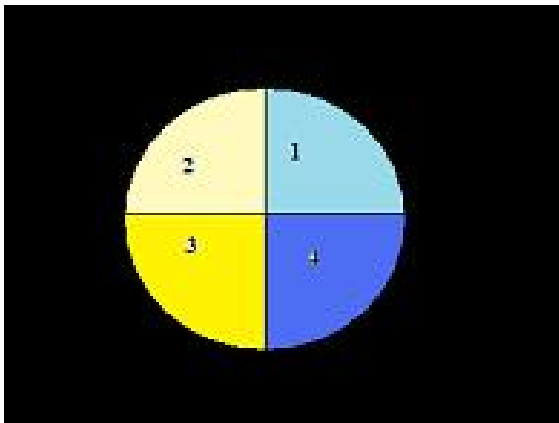
1, 2, 3 and 4 are the different segments around the conical indent in anticlockwise direction. This nomenclature is used for all the conical indentations.

REFERENCES

[1] C Fisher-Cripps, Nanoindentation, New York, Springer (2002) P. 1-9

[2] Y Wang, D Raabe, C Kluber, F Roters, Orientation dependence of Nanoindentation pile-up patterns and of Nanoindentation micro textures in copper single crystals, Acta Materialia 52 (2004) 2229-2238

[3] MF Doerner, WD Nix, A method for interpreting data from depth sensing indentation instruments, 1, (1986) 601

[4] JG Swadener, EP George, GM Pharr, The correlation of the indentation size effect measured with indenters of various shapes, Journal of the Mechanics and Physics of Solids 50 (2002) 681-694

[5] GM Pharr, WC Oliver, An improved technique for determining hardness and elastic modulus values using load and depth sensing indentation experiments, 7, (1992) 1564

[6] Zhi-Hui Xu, John Agren, An analysis of piling-up or sinking-in behavior of elastic-plastic materials under a sharp indentation, Philosophical Magazine, 11 August 2004, Vol. 84, No. 23, 2367-2380

[7] RM Pothapragada, RA Mirshams, S Vadlakonda, Effect of pile-up in Nanoindentation of Micro and Nanocrystalline Ni using FEM. Mater. Res. Soc. Symp. Proc. Vol. 880E© 2005 Materials Research Society

[8] S Vadlakonda, R Banerjee, A Puthcode, RA Mirshams, Comparison of incipient plasticity in bcc and fcc metals studied using Nanoindentation, Material Science and Engineering A 426(2006) 208-213

[9] GM Pharr, WC Oliver, FR Brotzen, J Mater Res 1992; 7:613

[10] WD Nix, Mater Sci Eng A 1997; 234-236:37

[11] MM Chaudhary, MJ Winter, Phys D- Appl Phys 1988; 21:370

[12] J Alcala, AC Barone, M Anglada, Acta Mater 2000; 48:3451

[13] DG Flom, R Komanduri, Wear 2002;252:401

[14] M Hollatz, M Bobeth, W Pompe, V Marx, Acta Mater 1996; 44:4149

[15] NI Tymiak, DE Kramer, DF Bahr, TJ Wyrobek, WW Gerberich, Acta Mater 2000;48:29

[16] A Gouldstone, HJ Koh, KY Zeng,AE Giannakopoulus S Suresh Acta Mater 2000;48:29

[17]Y Gaillard, C Tromas, J Woirgard, Acta Mater 2003; 51:1059

[18] J Li, K Vliet Van, Z Ting, S Yip, S Suresh, Nature 2002;418:307

[19] J Chen, SJ Bull, On the relationship between plastic zone radius and maximum depth during Nanoindentation, Surface & Cotings Technology 201 (2006) 4289-4293

[20] JR Tuck, AM Korsunsky, SJ Bull, RI Davidson, On the application of the work of indentation approach to depth sensing indentation experiments in coated systems, Surface & Coatings Technology 137 (2001) 217-224

[21] Yun-Hee Lee, Unbong Baek, Yong-Il Ki, Seung-Hoon Nahm, On the measurement of pile-up corrected hardness based on the early Hertzian loading analysis, Material Letters xx (2007)

[22] KO Kese, ZC Li, B Bergman, Method to account for true contact area in soda lime glass during Nanoindentation with the Berkovich tip, materials science and Engineering A 404 (2005) 1-8

[23] Keith Bowman, Mechanical Behavior of Materials, Wiley 2004, P.50-60

[24] Nanoindenter™ Manual, MTS Corporation

[25] ASM Handbook, Vol. 2

[26] Soer WA, Hosson J Th M De, Material Letters 59 (2005) 3192-3195

[27] Soer WA, K E Aifantis, Hosson J Th M De, Acta Materialia 53 (2005) 4665-4676

[28] Zaafarani N, Raabe D, Singh RN, Roters F, Zaefferer S, Acta Materialia 54 (2006) 1863-1876

[29] ASM Handbook, Vol. 2, 2002

[30] ESEM Manual, FEI Quanta, 2000